Modelling Nature-Based Solutions for Urban Stormwater Management

Auteur : Sadrijaj, Dorentina
Promoteur(s) : Archambeau, Pierre
Faculté : Faculté des Sciences appliquées
Diplôme : Master en ingénieur civil des constructions, à finalité spécialisée en "civil engineering"
Année académique : 2025-2026
URI/URL : http://hdl.handle.net/2268.2/25205

Modelling Nature-Based Solutions for Urban Stormwater Management

---

Sadrijaj Dorentina

Thesis presented to obtain the degree of:
Master of Science in Civil Engineering

Thesis supervisor:
Archambeau Pierre

Jury:
Archambeau Pierre
Champailler Stéphane
Dessers Christophe
Dewals Benjamin

Academic year: 2025 - 2026

Acknowledgement

First of all, I would like to sincerely thank my supervisor, Pierre Archambeau, as well as Benjamin Dewals, for their invaluable guidance and insightful advice throughout the preparation of this thesis. Their expertise and feedback have been essential to the successful completion of this work, and their guidance greatly helped me to structure and refine my research.

I am also very grateful to Christophe Dessers and Stéphane Champailler for their assistance with the computational aspects of this work and for their constructive guidance. Their help in navigating technical challenges and clarifying complex aspects of the simulations has been extremely valuable.

Finally, I would like to thank my family and friends for their constant support throughout this journey. Their encouragement and understanding have been of great help to me. A special thanks goes to my grandparents, who have inspired me to go further and be courageous.

Abstract

This master's thesis focuses on the modelling of Nature-Based Solutions (NbS) at an urban scale for stormwater management. In the context of climate change and the increasing occurrence of urban flooding, alternative solutions are required to complement conventional grey infrastructure. NbS represent a growing research field, as they rely on natural processes to mitigate runoff and partially restore hydrological functions altered by urbanisation.

This work was carried out within the framework of the Water Smart Cities (WSC) project, which aims to develop a software tool to plan and design sustainable stormwater interventions. The main objective of the thesis was to expand the existing library of the WSC solver by implementing and validating new flow control modules (weirs, orifice and perforated riser) through simple tests with predictable outcomes. They were then applied to several case studies derived from the SPW *Référentiel de gestion des eaux pluviales*, allowing the evaluation of their behaviour in more realistic configurations and comparison with traditional Excel-based approaches.

The solver could be a flexible tool that allows users to model their projects requiring a manageable amount of input data while still capturing key hydraulic processes and system interactions. Compared to simplified Excel-based methods, the solver allows a more refined representation of the system and can help limit excessive oversizing. Overall, this work highlights the potential of the WSC solver as an intermediate tool between simple design methods and highly detailed hydraulic models for urban NbS projects.

Contents

Introduction

With the recent floods that have become increasingly common throughout urbanized zones, it is important to consider solutions that can protect cities and, more important, save the lives of their inhabitants. To this end, it is necessary to redesign urban areas in a way that harvests rainwater by implementing Nature-Based Solutions (NbSs). These solutions are ideal for rainwater and stormwater management as they mimic natural hydrological processes. Indeed, they are based on how water would have behaved if it were not urbanized. Urbanization has made it very difficult to promote rainwater infiltration. Rainwater tends to runoff, which can potentially lead to hydro-meteorological disasters, as observed in recent years, and these disasters will be even more intense with climate change in the near future.

Within the University of Liège, in the Argenco department in collaboration with Gembloux Agro-Bio Tech, a team is developing a software that will enable users to apply NbS to a parcel and evaluate whether the solutions meet their intended objectives. The software is designed to be more sophisticated than the Excel-based tools mostly used nowadays, while remaining user-friendly, trying to make users feel comfortable. It allows users to test multiple solutions through a user interface without overwhelming them with complex mathematical equations. Also, it allows the users to design a project rather quickly. Naturally, a software that is very precise tends to increase the time spent on this type of project. The goal is to attract the users to use the software and to facilitate its use.

The aim of this project is to code various modules representing control mechanisms such as weirs, which are commonly used in NbS, adding to a library of modules already implemented in the software. Subsequently, several scenarios will be implemented to validate the functionality of the modules and to put the software into practice.

The project is called Water Smart Cities (WSC) and is developed by the University of Liège. The project focuses on three main areas :

1. Hydraulic: focuses on the movement of water, how rainwater moves in a certain context;
2. Ecosystem services: measures the benefits of what nature brings to people by comparing temperature before and after for example, by examining the ratio of green spaces in an urban area and other;
3. Pollutants: studies on the quantities of pollutants that can potentially be in the water.

This paper will mostly focus on the hydraulic part of the project since it is about the coding of hydraulic modules.

This thesis also aims to be a first, easy guide to user if a user wants to code a hydraulic module. It might facilitate the comprehension and the learning for said user.
First, a definition of NbS has to be made. NbS addresses a wide range of socio-environmental challenges, including water management, biodiversity conservation, and societal issues such as food security, while aiming to be cost-effective.
In the context of this study, it focuses on managing rainwater and/or stormwater. NbS imitates and tries to come as close as possible to the natural hydrological behaviour of the space that is mostly already urbanized. Usually, the grey infrastructures are kept as such and the only change is that they rely on the NbS implementation so that the pipes (typical grey infrastructure) do not overflow. Grey infrastructures are the usual drainage system, pipelines and others that came with urbanization. With climate changes, these grey infrastructures are not enough and tend to overflow. Hence the need to implement NbS. These solutions favour infiltration and storage. However, there is still a percentage of runoff that they try to convey to storage and, as a last resort, to drainage system. Naturally, these types of solutions tend to decrease the percentage of runoff so, the drainage system finds itself relieved.
A few real-life examples are shown in Figures 1, 2, 3 and 4.

Figure 1: Example of green roof in the Swiss Alps [1]

Figure 2: Example of bioretention cell [2]

Figure 3: Example of sponge city in Sanya, Hainan Province, China [3]

Figure 4: Example of vertical green space: "Bosco Verticale" in Milan [4]

NbS can be considered at different scales. It can go from a house to a whole catchment. The WSC project focuses on small areas (not more than 1-2 [km^2]). The main reason is that rainfall is assumed uniform over the considered area. It is actually recommended to implement these solutions in multiple places in the same city.

The plan of the thesis is as follows:

1. A review of the literature in order to gather information on what already exists.
2. An introduction to the control mechanisms that are implemented. To enable the user to create its own module in the best conditions, a summary of coding aspects is provided. It explains what is the GPU compilation, what and how can the JAX library be used since the code is based on that library. It also explains the Object-Oriented Programming (OOP). The solver is based on residual equations, which are also explained.
3. The implemented modules are tested in different ways. Some of these tests are particularly simple but they are necessary in order to verify the code of the modules.
4. Applications that are much more realistic and complete than the verification tests are implemented to validate the modules and also, have an interaction of multiple modules.
5. To finish this report, a conclusion is made to explain, among other things, the perspectives after this thesis.

Chapter 1

Previous Work

In this section, a total of 24 articles are reviewed to provide an overview of the research conducted in recent years. To structure the analysis, the section is divided into several specific topics. Not all topics appear in every articles, the selection was made to ensure that all relevant subjects were adequately covered. At the end of this section, a summary table of all reviewed articles is provided.

The literature uses a broad range of terms to describe Nature-Based Solution (NbS). Low Impact Development (LID) refers to a form of NbS that minimizes the impact of increased impervious surfaces by mimicking natural hydrological processes that existed prior to urbanisation. LID aims to both reduce stormwater volumes and to improve its quality [5]. Terms like Green Stormwater Infrastructure (GSI), Green Infrastructure (GI) and Water Sensitive Urban Design (WSUD) are interchangeable with LID [5]. Rainwater Harvesting (RWH) refers to systems that collect and store rainwater in tanks, reservoirs or other similar structures [6]. Blue-Green Infrastructure (BGI) encompasses systems that store or slow down runoff and those that mimic natural hydrological processes [7]. In this report, the terminology used for each article follows the terms employed in that article. Nonetheless, all these approaches share similar objectives and can be grouped under the broader concept of NbS.

1.1 Reasons for NbS Implementation and Research

Each article was motivated by specific research objectives. Common reasons include investigating methods to prevent flooding, implementing stormwater via NbS, evaluating the impacts of these solutions, and studying the quality of managed stormwater. Many studies made this information publicly available to build a knowledge base and push for further research. Some studies, however, had additional motivations, detailed below.

Some articles addressed the need to protect groundwater resource. Hasibuan et al. [6] investigated the implementation of RWH in a coastal area of North Jakarta, aiming to assess its effects on land subsidence caused by excessive groundwater extraction. The study also analysed water quality to evaluate its potential for alternative uses, providing easier access to water for the local population. Endah et al. [8] highlighted the importance of preventing groundwater depletion.

As briefly mentioned, water quality is another driver for research. For instance, Sirait et al. [9] examined whether harvested water would sufficiently irrigate greenhouse crops, addressing agricultural water scarcity. Narzis et al. [10] explored the positive effects of GSIs on oil refineries and chemical companies that release

toxins in runoff. Waickowski et al. [11] evaluated these solutions to remove nutrients and sediments from the water also considering overall water quality improvement.
These articles assess whether stormwater can be safely used for human or groundwater recharge purposes.

Simulation studies frequently employed the Stormwater Management Model (SWMM). Rosenberger et al. [12] aimed to upgrade the software, while Wu et al. [7] evaluated SWMM coupled with MODFLOW to model surface water-groundwater interactions. Bosco et al.[13] compared three SWMM modules to determine the most suitable for groundwater modelling. Zhang and Valeo [5] explored the consequences of upscaling in Personal Computer Storm Water Management Model (PCSWMM) simulations, which is a tool based on SWMM with additional features, further details on SWMM are provided in the next subsection. Upscaling is a phenomenon that occurs when a typical small-scale model like PCSWMM, is applied for larger catchments, leading to a loss of spatial heterogeneity in the data. This can influence the outcomes.
These studies present an issue and, in some cases, propose a solution, demonstrated through real-world case studies.

Ecosystem services also constitute a critical aspect of NbS research. Bagheri and Davani [14] investigated the reduction of pump operations and associated energy demands. They also looked into Human Toxicity Potential (HTP) as well as Global Warming Potential (GWP). Pace et al. [15] examined the effect of tree coverage on ecosystem services. Cerda et al. [16] focused on long-term hydrological dynamics and economic benefits of SuDS. Rodriguez et al. [17] concentrated their study on Combined Sewer Overflow (CSO) which is a scourge of urbanisation. Naturally, other articles incorporated ecosystem services as secondary considerations while focusing on different primary objectives.

Some articles proposed frameworks to guide the selection of appropriate NbS for specific sites. Boguniewicz-Zabłocka and Łukasiewicz [18] presented initial tools for solution selection. Wu et al. [19] developed a more sophisticated framework emphasizing the design aspect. Cascone and Vitaliano [20] offered an economic assessment framework implemented for green roofs.
All frameworks were applied to real sites to evaluate their efficiency.

Additional motivation for NbS research were brought to explain the reason to conduct a research such as Rosenberger et al. [21] studying the increase of population in parallel with the worsening of climate change in the future, whereas Wu et al. [22] compared three types of green roofs, including an experimental technology incorporating biochar in the substrate layer. Biochar is produced by heating biomass and also in known to improve soil quality and plant health.

1.2 Monitoring

Monitoring in the reviewed studies primarily focused on hydrological aspects, with some investigations extending to water quality, compliance with environmental thresholds, and ecosystem services. These last two aspects are discussed in the next subsection.

Studies from different regions illustrate the effectiveness of NbS. In North Jakarta, a survey was conducted among residents to understand their habits. It showed that, because of the high population density, the water collected by RWH was not enough, indicating a need for additional systems [6].
Bosco et al. [13] monitored swales in Norway and simulated it on SWMM to calibrate the model for application in similar contexts. This is discussed in more detail in another subsection.
In Philadelphia, the Green City Clean Waters program saw an increase of GSIs from 2006 to 2024 and provided

a long-term opportunity to assess their efficiency. Results showed substantial reductions in peak flows, demonstrating the effectiveness in mitigating urban flooding [23].
In Pennsylvania, the monitoring revealed that constructed wetland was able to return 37 % of incoming flow to the water cycle via percolation and evapotranspiration [24].
Finally, in North Carolina, two bioswales (BS2 and BS4) located near highways showed that BS2 exfiltrated 27% of the total inflow and BS4 exfiltrated 74% [11].

Despite these successes, monitoring remains limited and data gaps are common. Several studies reported incomplete data or imperfect assessments [11], [23], [24].

These studies demonstrate the importance and effectiveness of NbS solutions while emphasizing the need for continued monitoring on long periods of time to support wider implementation and model validation.

1.3 Simulation

As noted previously, most studies that included simulation employed SWMM. An overview of the software is provided here. Naturally, it is not feasible to cover all its features.
SWMM is a rainfall-runoff simulation model capable of handling both event-based as well as continuous rainfall. It allows the implementation of hydraulic infrastructures including both grey infrastructure and NbS, and it provides information about the runoff quantity and quality. Users are also required to accurately represent site conditions.

SWMM is typically applied in projects that aim for precise site representation, involving calibration and validation. In contrast, the project WSC does not aim to be this advanced. However, WSC wants to be multi-functional since it studies not only hydraulic and quality as SWMM, but also ecosystem services. Moreover, WSC is more user-friendly, and requires minimal training beforehand.

PCSWMM is based on SWMM but offers a larger variety of functionalities, facilitating work on large and complex stormwater systems.

1.3.1 Limitations of SWMM and Proposed Improvement

The software SWMM, like any modelling software, has some weak points.
Rosenberger et al. [12] identified an issue with the *SWMM Urban-EVA*. To address this, they developed an upgraded version called *SWMM Urban-EVA-Avg Timestep*, which improved the simulation of runoff, evapotranspiration, and infiltration regardless of the reporting time step. The main limitation of *SWMM Urban-EVA* was that to achieve high accuracy and to correctly capture peaks and troughs which, required a very small time step, resulting in large output files. The *SWMM Urban-EVA-Avg Timestep* version was able to be as accurate as the reference model while allowing larger reporting times, producing more manageable file sizes and preserving all hydrological metrics over time. Some limitations arise from the assumptions made by the software. Zhang and Valeo [5] noticed that PCSWMM transforms irregularly shaped catchments into rectangular shapes, leading to a loss of spatial information before simulations begin. The three main sources of variability affecting catchment hydrology were land use, slope, and soil type. Larger scale catchments tend to introduce greater uncertainties in soil heterogeneity and slope. PCSWMM uses an average value across the entire catchment for soil type and slope. However, at smaller scales, the model tends to overexpress the land use artificially, meaning that it gives more heterogeneity to the data than what is actually true.

While SWMM is not without limitations, it is a flexible tool and open to user modifications, allowing for continuous improvement.

1.3.2 Calibration and Validation

In some studies, the authors monitored a site and afterwards modelled it. This allowed to represent the catchment accurately and calibrate it until the simulated data matched the measured data. A separate dataset from a different period was then used to validate the calibration. This process ensures that the catchment is represented realistically, allowing implementation of NbS to yield reliable predictions of various hydrological metrics.

Groundwater levels were measured in Leuven, Belgium, and these data were used both for calibration and validation, demonstrating the effectiveness of coupling SWMM with MODFLOW [7]. Another groundwater-focused study was conducted in Norway, where, this time, groundwater was directly represented within SWMM by comparing three different modules. The authors of this study monitored swales and modelled them in SWMM, finding that only a few parameters controlled groundwater dynamics, which could significantly reduce computational time and cost. During validation, discrepancies were observed in the snow period, likely due to overfitting of the calibration dataset. Additional factors such as soil stabilization and uncertainties regarding snow management by road managers may have affected the accuracy of the validation [13].

This step highlights, once again, the complexity of the software and the necessity of site monitoring. However, there is a lack of monitoring, only a few simulation studies validated their model.

1.3.3 Type of Simulation

The only article that explicitly discussed the motivation for using both design storms and continuous simulation was the article by Cerda et al. [16]. Design storms (or event-based simulations) are used to size NbS and assess whether they can infiltrate and retain specific rainfall events. Continuous simulations, on the other hand, evaluate the long-term performance of the solution and allow comparison of pre- and post-implementation conditions.

Several other studies used both types of simulations to design and then assess their long-term behaviour [15], [16], [22]. For instance, Pace et al. [15] studied extreme events (both dry and wet soil conditions) and also conducted continuous simulations. However, this was not the case for all studies. Zhai et al. [25], for example, relied solely on two event-based rainfalls and a maximum of 5-year return period while assessing a sponge city. This might have been limiting, and continuous simulations could have been valuable given the large scale of the project.

Nevertheless, simulating both types is not always practical. As discussed later in the summary of Wu et al.'s framework [19], running continuous simulations for a large set of candidate solutions, which is the case after that specific framework, would be too time-consuming. For this reason, the authors recommended focusing on rainfall events that are likely to cause flooding.

Both simulation types appear necessary to fully cover the performance of NbS over their lifetime. However, in some cases, continuous simulations may become too time-consuming. Therefore, testing a wide range of design storms can help ensure the functionality of the solution. This approach does not account for the

drainage between rainfalls, which can be critical, especially when successive rainfall events occur in quick succession, decreasing the efficiency of the system.

1.4 Performance of some NbS Infrastructures

Some solutions prove to be more efficient under specific circumstances. This section provides a summary in order to identify the factors that influence their performance. The aim is to present generalized conclusions that can serve as a preliminary guide for understanding the contexts in which the different solutions are most effective.

Rain barrels: They have a great effect on reducing peak flows and runoff volume. The recommended installation is one barrel every 10 m^2. They are particularly efficient during small storm events, while still offering potential benefits during larger events [14].

Bioretention cells: They show a strong adaptative capacity regarding both total discharge and maximum daily discharge under future rainfall scenarios. Overall, they provide great peak outflows reduction. Smaller footprint (below 0.02 km^2) tend to be more effective; however, because they are easily and widely applicable, large scale deployment enhances peak flow reduction. This solution also demonstrated its effectiveness during large storm events. Bioretention cells must be installed in well-drained soils with high infiltration rate and positioned in areas highly vulnerable to flooding [10], [17], [23].

Green roofs: They promote infiltration and evapotranspiration over limited land areas and reduce peak flows during most rainfall events. Green roofs are most efficient for smaller return-period storms, but they also offer storage potential for higher return-period events. Moreover, their engineered soil substrates offer greater infiltration since this technology is better than native soil [21], [23].

Permeable pavements: This solution is particularly suitable in areas with limited open space. They reduce stormwater volumes and peak flows while contributing to stable groundwater recharge. However, these pavements are not appropriate in areas with high stormwater pollutants, as infiltration may transfer contaminants into the soil and groundwater. The effectiveness depends on sub-catchment size and land use, with parking lots identified as favourable locations for implementation. They perform best during low-magnitude rainfalls, since during intense storms, the soil may saturate rapidly, leading to increased runoff. Their performances are improved in flatter areas, where infiltration is enhanced [7], [23], [26].

Constructed (stormwater) wetlands: These solutions are highly effective at reducing peak flows during large rainfall events, as they are designed to be retentive without requiring extensive space. Percolation processes enhance their storage capacity, while surface storage allows evapotranspiration [24]. Figure 1.1 shows pictures of the constructed stormwater wetland studied by McGauley et al. [24].

Figure 1.1: Constructed stormwater wetland in Villanova University [27]

Rain gardens: They are more effective for small, frequent rainfall events. Their performance depends on catchment size, slope characteristic and housing density, with small scale, high density residential areas showed best results. They perform better on permeable soils, since it improves infiltration rates. However, they are generally ineffective for high return-period or high intensity storm events in reducing peak runoff, but there is always a reduction in runoff volume since it offers storage capacity. They are best suited to residential locales areas and small scale applications [26], [28]. FIGURE 1.2 shows an example of a rain garden in Norway.

Figure 1.2: Example of rain garden in Drammen, Norway [29]

Detention ponds: They are effective as larger downstream systems, where they can temporarily store substantial volumes of runoff and reduced peak flows [28]. FIGURE 1.3 shows a picture of the detention pond near the Seveso River catchment where the study by Marchioni et al. took place [28].

Figure 1.3: Detention pond for the Seveso torrent in Milan [30]

Bioswales: Bioswales differ from traditional swales through the layers: bioswale includes a gravel layer and a perforated underdrain. These features enhance infiltration and drainage efficiency, allowing bioswales to reduce peak flows and runoff volumes more effectively than traditional swales for low and high intensity rainfall [11].

A general observation across the studied solutions is the importance of storage. If the solution does not provide sufficient storage capacity on its own, supplementary systems such as tanks or similar structures may be required in order to ensure performance over the storm event duration.
In addition, solutions with smaller footprints tend to be more effective during small rainfall events. From an economic perspective, choosing a solution with a large footprint might not be justified in areas that predominantly experience low-intensity storms.
Multiple solutions must be combined to maximise the performance of NbS within a stormwater management design. However, spatial constraints may limit the possibility of achieving 100% NbS implementation.

1.5 Scale Consideration

The scale of the study can strongly influence the performance of NbS. The following studies have compared different scales and provide valuable insights into how scale affects the results.

Most studies converge to the same conclusions: large scale assessments are generally not ideal for evaluating NbS. In some cases, at larger scale, studies tend to focus on larger solutions such as restoration. However, in this study, the focus remains on solutions that are applicable at smaller scales, since the WSC project covers a limited area.
Simulation studies using PCSWMM have shown great uncertainties when modelling at large scales. LIDs were found to be less effective as catchment size increases [5]. Similarly, in the Philadelphia study, the impact of GSIs was difficult to notice for the large watershed, as their effects appeared diluted [23]. A study in Milan

was conducted at two different scales: community and municipal scales. Both cases showed a reduction in water velocity and depth in flooded areas, delay of flooding onset, reduction of peak flows upstream, and reduction of flooded areas in general. However, these effects were less obvious at the municipal scale, likely because the ratio of NbS and impervious area was too small. It seemed that there were not enough NbS implemented in the catchment to showcase a general tendency. A large scale study should be implementing multiple solutions targeting different objectives [28].

Given the ongoing need for large scale NbS implementation, an ideal solution is to deploy a significant amount of NbS while still analysing performance at sub-catchment level.
Zhai et al. [25] propose a design framework: first, NbS are evaluated at the micro-catchment scale to prevent flooding; if insufficient, they extend to the sub-catchment, and finally, to the entire catchment if necessary. This method ensures that smaller scale is considered within a city scale study. The following subsection discusses sponge city in more detail.

Three aspects should be considered. First, a sufficient number of NbS should be implemented to effectively prevent flooding. Second, dividing the catchment into multiple sub-catchments and analysing each smaller area can provide more accurate insights on the NbS performance. Third, proper connections and interactions between the different scales should be ensured.

1.6 Framework Examples

Several studies have proposed frameworks for selecting or designing NbS implementation. These frameworks are followed by real-life applications to validate their effectiveness.

A study conducted in Chile evaluated five SuDS alternatives using event-based rainfalls. It found that the best solution was the one that addressed multiple aspects: it was designed to perform under both small and large return-period rainfall events, and also considered water quality capture volume [16].

Simpler methods are also commonly used to select the most appropriate solution depending on the context. The Mutli-Criteria Analysis (MCA) is a widely used method, in which a selection of solutions is compared against predefined criteria deemed important. Each criterion is assigned a weighting factor, and the solution with the highest overall score is selected. This method can be subjective and may be limited in certain scenarios. Another approach, the SWOT analysis, involves listing the Strengths, Weaknesses, Opportunities and Threats. It helps focus on context-specific priorities [18].
The use of these methods could have been an opportunity to engage with stakeholders, public authorities, and/or private landowners, since they do not require any calculations or software skills. The combination of local knowledge and professional expertise could have provided an excellent illustrative example.

A specific framework based on the achievement of targets was also proposed in the study. This focuses on achieving reduction in flood damages. The process begins by estimating the volume reduction needed to achieve the target. Multiple scenarios are then simulated using pervious areas, thus without initially implementing WSUD. The first 100 scenarios that meet the target are retained, and WSUD is subsequently applied according to this information. A verification step ensures that the proposed WSUD designs are feasible, for example, regarding the size of bioretention cells. Ultimately, this approach generates a pool of effective options, from which the best solution can be selected using a life-cycle cost-benefit analysis [19].

Finally, the sponge city approach implemented in the Old Town of Hefei, China, was rapidly mentioned

in the previous subsection. It illustrates a bottom-up design method. The catchment is subdivided into sub-catchments, which are further subdivided into micro-catchments. Each micro-catchment is analysed under event-based rainfalls. If flooding occurs at the micro-catchment level, a mechanism of clustering is activated at the sub-catchment level to manage overflow. If this remain insufficient, the entire catchment is considered. This approach ensures that smaller scale efficiency is maintained even when planning at the city scale. By designing block by block, the method allows more practical and manageable implementation compared to designing for the entire city at once [25].

Multiple frameworks have been presented, some more complex than others. Other methods also exist. This highlights the importance of careful planning ahead before implementing any concrete solution in any software.
However, some frameworks may be limited to specific contexts. For instance, Wu et al. [19] applied their framework in a very specific climate, and it has not been tested in different scenarios, so a complete validation of this framework is still missing.

1.7 Climate Impact

1.7.1 Climate Change and Future Scenarios

Around the world, flooding events are becoming more frequent and more intense. This is a direct consequence of climate change, and future projections indicate that these issues will only worsen. Several articles have analysed whether the implementation of NbS will remain sufficient under future climate conditions. In Europe, conservative rainfall projections are derived from the RCP 8.5 scenario of the Euro-Cordex project. Although other projections exist, these were the ones used in the studies assessing climate impacts.

A study in Leuven, Belgium, showed the significant impact that climate change will have on rainfall intensity in all seasons except summer, where more severe dry periods are expected. For this reason, adaptative solutions are essential. However, the study demonstrated that under future scenarios, peak discharge and peak runoff reductions become less effective. As expected, BGIs remain more effective in smaller future storm events than larger ones [7]. In Fehraltorf, Switzerland, it was shown that GIs that are efficient under historic events are not able to offset climate change in future events. Therefore, their implementation must be more substantial in order to better mitigate flooding and reduce the frequency of Combined Sewer Overflows (CSOs), which is a relief mechanism in sewage combining stormwater and wastewater [17]. They prevent the sewage from being overwhelmed during intense rainfall by discharging excess water directly into receiving water bodies. Quagliolo et al. [20] reached similar conclusions, they showed that NbS designed for current storms will not be sufficient under future climate conditions. Flood depths between 2013 and the projected conditions for 2050 are expected to increase by up to 11% without any NbS. Nonetheless, under future climate changes, NbS still provide improvement: flood mitigation increases by 24% for the 10-year return period, 18% for the 50-year, and 16% for the 100-year. Although the proportion of NbS implementation must be increased compared to what is sufficient under present climate conditions, they still offer benefits in future scenarios.

Urbanisation continues to rise, and population growth is expected to intensify this trend. In the district of Moosach in Munich, Germany, a study investigated combined effects of climate change and population increase. It concluded that NbS implementation will become mandatory under future climate conditions due

to increased rainfall intensity and frequency. Otherwise, severe stormwater management issues are expected. An 8 % increase in living space achieved by adding storeys (vertical expansion) and NbS resulted in a 38 % reduction in runoff compared to traditional ground-expansion development [21].

High-rise building architecture has become more common with rapid urbanisation. Moravej et al. [31] introduced and discussed Vertical Green System (VGS). The article did not analyse future scenarios; however, it can be considered as a fitting solution that aligns urban growth, population increase and NbS. VGS consists of vegetated walls on high-rise buildings, which is relevant since dense cities often have more wall area than roof area. The study assessed different storage tank capacities, wall-to-roof ratios and three climates. In humid subtropical climate, stormwater is reduced by maximum 60 % and could even be self-sufficient, meaning that no artificial watering is needed. In oceanic climate, the reduction of stormwater was up to 100 % with the right configuration, and, in Mediterranean climate, it was up to 80 %. In these last two climates, water must be supplied during dry months for maintenance purposes, which is not ideal since these periods already face high water demand. This demand can be reduced by increasing storage capacity or by selecting plant species that are better adapted.

Future climate conditions and population growth must be taken into account in future studies. If these aspects are considered early in the design process, NbS implementation will already be sufficiently robust, avoiding the need for redesign in the future. This offers an opportunity to avoid repeating the mistakes made during the early stages of rapid urbanisation. These solutions must be as adaptative as possible (for both dry and wet periods), avoid adding impervious surfaces, and favouring vertical expansion.

1.7.2 Seasonal Effects and Groundwater Level

Depending on the climate, NbS can be strongly affected by seasonal variations, particularly in relation to groundwater recharge. This subsection summarises studies that analysed changes in groundwater levels.

In Leuven, Belgium (temperate oceanic climate), the simulation of groundwater after the implementation of BGIs showed high groundwater levels in winter and low levels in summer. Although the improvement compared with current conditions is significant, the authors note that further increases in pervious surface (e.g., permeable pavements) would help maintain more stable groundwater levels during extreme droughts [7]. Bosco et al. [13] reached similar conclusions and also demonstrated that, in SWMM, the "aquifer" module represents groundwater level more accurately than the "LID" module. In Pennsylvania, USA (humid continental climate), results similarly indicated that winter groundwater levels were higher, reducing the percolation capacity of wetlands and therefore their storage volume. In contrast, during summer, wetlands can store and infiltrate more water thanks to higher percolation rates [24].

This section highlights the importance of implementing adaptive solutions capable of maintaining their benefits throughout the year. It is also essential to ensure that stormwater quality remains acceptable before infiltration to avoid contaminating groundwater. For groundwater recharge purposes, infiltration solutions should be prioritized.

1.8 Ecosystem Services and Pollutants

The best solution considers multiple aspects. The WSC project aims not only to address hydraulic aspects but also to improve ecosystem services and reduce pollutants.

Hasibuan et al. [6] studied the quality of water collected by RWH infrastructures. They concluded that the quality was sufficient only for sanitation purposes (bathing and washing) and not for consumption. In the latter case, it must be treated before use. This article also examined the quality of other water resources to the inhabitants of Jakarta. Water supplied through pipelines was of good quality, but many households also relied on wells. Water from wells was of lower quality than that from the RWH systems. However, wells were more easily accessible and provided enough water when pipelines were expensive, highlighting a social dimension in water access. In Houston, GSIs removed toxins from water released by the oil refineries and chemical companies [10]. Bioswales in North Carolina improved water quality; however, the concentrations of some pollutants still exceeded acceptable threshold [11].

Most implementations reduced contamination levels, but in some contexts, they were insufficient to clean stormwater for groundwater recharge or human consumption. More treatment facilities should be built to provide drinking water, and the NbS technologies should be improved to allow infiltration of clean water. If this is not possible, NbS designed to enhance infiltration should be avoided.

Ecosystem services can take different shapes. Bagheri and Davani [14] demonstrated that the GWP was reduced by implementing rain barrels, as measured in kg CO_2-Eq. However, regarding HTP, it was insufficient to assert that there has been an improvement. Increasing tree coverage up to 30% across multiple sub-catchments resulted in decreased air temperature and runoff volume [15]. Cerda and Gironas [16] analysed four economic services and monetized two of them, leaving pedestrian accessibility and stability unmonetized. They found that with SuDS implementation, no roads experienced more than 5 hours of flooding per year. These solutions were more efficient for frequent, moderate rainfall events, leading to a 78% reduction in the duration of medium-level pedestrian hazard, while the reduction reached only 30% for high-level pedestrian hazard, highlighting reduced efficiency under more severe flooding conditions. In the substrate layer of green roofs, biochar was introduced and compared to traditional green roofs to assess its effects on ecosystem services. This recycled material, discussed in more detail in the next subsection, showed great potential for building thermal regulation and water retention, surpassing the two other traditional green roof types. Heat mitigation allowed buildings to save energy due to reduced temperatures [22]. In Milan, two ecosystem services were studied at both community and municipal scales: "Water Flow Regulation" and "Water Quality Regulation". NbS implementation was effective for both services. Although, at the municipal scale, the effect on water quality was more limited because spatial coverage was smaller compared to the community scale, as stated previously. The effectiveness is diluted over a larger area [28].

Ecosystem services encompass environmental, human wellbeing, damage control, economical, and other aspects. A good solution is one that addresses multiple ecosystem services simultaneously.

1.9 Materials, Connexions and Techniques

The implementation of NbS is much more efficient when applied in the right location, using appropriate materials and specific techniques. The goal is to maximize their potential and anticipate potential issues by adopting solutions that consider future consequences.

Green roofs (or walls for VGS), rain gardens, and bioretention cells are composed of multiple layers, including, in some cases, a vegetated layer. Their performance depends on the properties of these different layers. When well-designed, these systems enhance water storage and may not require any water supply for maintenance. Thickness is an important parameter to consider. For instance, it is recommended that green roof substrate layers be at least 20 [cm] thick to store a 10-year return period rainfall [10], [21], [31].

The materials used in these infrastructures significantly influence their performances. Rain barrels can affect HTP and GWP, and this effect can be either positive or negative. The study proposed to reuse barrels from restaurants, which could improve sustainability by reusing materials. However, to achieve simultaneous improvements in both HTP and GWP, further simulations or alternative materials may be needed [14]. Green roof substrate layers can also be composed of different materials. Cascone and Vitaliano [22] added biochar which reduced heat absorption, promoted evaporation cooling and enhanced water retention thanks to its porous structure that absorbs and stores moisture effectively. The performance of vegetated layers depends on plant species and their maintenance [22], [31].

Soil saturation strongly affects the retention capacity of NbS. Dry soil improves stormwater mitigation but reduces heat mitigation effectiveness. Conversely, wet soil is more effective for heat mitigation. Depending on the context, additional storage may be needed to buffer against water scarcity. During drought months, vegetation must be maintained, and since saturated soil enhances heat mitigation, watering may be necessary. In smaller NbS such as green roofs and rain gardens, soil saturation has a great influence on their performance: if these systems saturate quickly, their smaller storage capacity fills faster [15], [21].

NbS can be enhanced by adding small hydraulic elements, optimizing connections, or rethinking outlets. Bioswales coupled with check dams showed better runoff mitigation and infiltration than swales without check dams [11]. Figure 1.4 shows the cross-section of a check dam implemented in bioswales in North Carolina [11]. Figure 1.5 shows a picture of a check dam in another project in North Carolina. Connecting runoff from green roofs to sewers through pervious areas actually increased the green roof performances. This simple measure ended up having greater impact than permeable pavements and bioretention cells which is rarely the case [17]. Kwak et al. [23] observed that, between events, GIs sometimes did not have enough time to drain before the next rainfall, limiting the efficiency for the next rainfall. Therefore, proper drainage should be prioritized, especially in areas with frequent rainfalls. A well-designed outlet can improve retention by discharging water slowly downstream (low-release mechanism) while still allowing water in the wetland to percolate or undergo evapotranspiration [24].

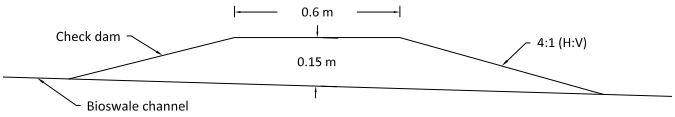

Figure 1.4: Cross section of check dam used in the two bioswales in North Carolina [11]

Figure 1.5: Check dams in Mango Creek, North Carolina [32]

1.10 Benefits-Costs

Most stakeholders and investors are influenced by the cost of implementing NbS. To assess the benefits of installing NbS, one must monetize the problems that arise when no implementation occurs and compare them with the situation where NbS are deployed.

Three studies calculated such benefits and reached interesting conclusions for future real-life projects. In Chile, Cerda et al. [16] examined four ecosystem aspects through continuous simulation and monetized two of them: CSO reduction and transport delays. Reducing CSO recurrence generated economic gains by reducing the diameter of the required pipe. With SuDS implementation, 97% of CSO were under control using only a 300 [mm] pipe instead of the initial 1250 [mm] pipe needed without SuDS. Overall, this resulted in a saving of USD 3,413,061 in construction costs. Transport delays due to flooding were also monetized: delays experienced by cars proved the most costly, leading to a total benefit of 45,536 $/year. Wu et al. [19] conducted a life-cycle cost-benefit analysis and found that targets that are set too low (minimal retention capacity) or too high (retention capacity for rare, extreme events) were not economically viable. In the first case, the system cannot retain great amounts of rainfall, and in the second, the event is so rare that designing for it becomes excessively expensive. When considering NbS implementation, costs are divided into investment costs (a unique payment at the beginning; information derived from CAPEX studies[1]) and maintenance costs (recurring throughout the lifespan; information derived from OPEX studies[2]). One study focused solely on building damage assessment as a benefit and found that, in Rapallo, Italy, NbS implementation generated benefits of 6.1 million €/year, reducing damage costs by 90%. When compared with green roof costs, only low intensity NbS were economically viable from a flood mitigation perspective, since their implementation cost was lower than the avoided damages. This was not the case for medium and high NbS implementation. The issue does not lie in the implementation itself but in the assessment, which addressed only a limited set of benefits: only one benefit was considered. Economically viable NbS must account for multiple benefits [20].

A good NbS implementation considers multiple benefits. This is an outcome consistently demonstrated across the studies presented in this section.

[1]Capital expenditure: costs associated with the design, planning, and construction of NbS [33]
[2]Operating expenses: costs associated with the monitoring, maintenance, and operation of the NbS over its lifespan [33]

Some authors also highlighted the lack of knowledge regarding the life-cycle of WSUD and the costs of certain NbS [19], [20].
Future projects that are actually implemented should report the different cost, and a shared information database should be made available to allow for reliable estimations.

1.11 Critical Assessment

Several missing opportunities and issues were identified across the reviewed articles.

There was a notable lack of information regarding the lifespan of NbS. This aspect was not properly studied and was rarely mentioned. Bagheri and Davani [14] assumed a 20-year lifespan for rain barrels; Wu et al. [19] estimated a 30-year lifespan for bioretention cells; Cascone et Vitaliano ([20]) considered a 40-year lifespan for green roofs. For most other infrastructures, no information was provided. Naturally, lifespan increases when infrastructures are properly maintained.

Many authors mentioned the importance of maintenance, for instance, preventing clogging of the surface layer, avoiding substrate compaction, managing biochar degradation, and so on [13], [22], [26].
However, no study seized the opportunity to analyse system performance under unmaintained conditions. Although the assumption of regular maintenance is common, it would have been relevant to simulate a lack of maintenance to quantify performance loss and potential damage.

In some cases, NbS implementation can reduce certain ecosystem services. For example, Pace et al.[15] noted downside to increasing tree coverage, such as pollen allergy, additional management of tree required...

Some studies might have been overly optimistic about feasible implementation percentages. The study conducted by Quagliolo et al. [20], for instance, assumed that green roofs could be installed on all roofs, which is unrealistic. Even in leading cities such as Toronto or Basel, maximum implementation reached only 40-50%.

Biochar is a material for which large scale availability remains limited. Alternative recycled materials should be explored to avoid supply chain constraints and excessive costs [22]. This consideration is crucial in early research stages, since the inequality that flows from the material production could be erased or at least limited.

In some studies, the monitoring period was far too short, representing a missed opportunity. Longer monitoring would have allowed for seasonal effects study and ensured proper model calibration [24], [22].

The study on VGS used evapotranspiration rates from horizontal surfaces rather than vertical ones. More research on the evapotranspiration rates of vertical surfaces must be done to produce accurate models [31].

Most of these limitations could be addressed through increased research efforts and shared datasets, ultimately improving model accuracy. Current monitoring is insufficient and should be extended. These solutions could enhance the quality of life and prevent future disasters: research is crucial.

Table 1.1: Summary of Reviewed Articles

Ref.	Scale	Main subject(s)	Tool/ Method	NbS implementation	Main result(s)
[6]	Around 12 km²	Hydraulic and Pollutants	Monitoring, Survey and Calculation	RWH technologies (unspecified, probably roof catchments)	• Insufficient water to supply the coastal population • Water quality suitable only for sanitation
[8]	891,87 m²	Hydraulic	Calculation	Roof catchment and 2 underground units storage	A 64 m³ reservoir is sufficient to meet the school building's water needs
[9]	120 m²	Hydraulic and Hydrology	Calculation	Roof catchment and storage tank	Potential to fully meet the greenhouse's water demand
[12]	9,3 ha	Yes	Simulation (continuous)	GR[3], GS[4] and trees	Improvements with SWMM-UrbanEVA-AvgTimestep allow a better representation of infiltration, runoff and evapotranspiration without requiring a small reporting time step (accuracy without extensive data)
[14]	City scale	Hydraulic, Pollutants and LCA[5]	Simulation (continuous)	RB[6]	• Great reduction in runoff and in pump operation • Most pollutants reduced
[17]	82 ha	Hydraulic	Simulation (continuous) and Calculation	BC[7], GR and PP[8]	• GI cannot offset future climate changes • GI have, at most, 48% adaptive capacity
[23]	Around 85 km²	Hydraulic	Monitoring	49 GSIs in 2006; 627 GSIs in 2011; 4628 GSIs in 2023 (mix of BC, GR, PP and more)	• GSI are more effective on smaller watersheds than on larger ones • GSI did not have enough time to drain between rainfall events • Still, GSI effectively suppressed the urban contribution to flooding

[3]Green roofs
[4]Green spaces
[5]Life Cycle Assessement
[6]Rain barrels
[7]Bioretention cells
[8]Permeable pavements

Ref.	Scale	Main subject(s)	Tool/ Method	NbS implementation	Main result(s)
[7]	0,64 km²	Hydraulic and Hydrology	Simulation (continuous)	4 wadis, GR, rainwater tank, buffer bassin with control system (for water level), rain tanks and PP	• BGIs reduce discharge volumes (less effective in the future than in under the present climate) • A seasonal trend exists for BGI scenario when looking at groundwater levels • BGI is effective in maintaining stable groundwater recharge (though more difficult during extreme drought events)
[24]	19,7 ha	Hydraulic and Hydrology	Monitoring and Simulation (continuous)	CSW [9] with specific exit outlet	• Largest peak flows reduction during large storm events (CSW provides large storage, and the outlet configuration helps increase this storage) • CSW effective in the long term • 37% of rainfall was returned to the water cycle
[28]	1,6 km² and 57400 m²	Hydraulic and Ecosystem services	Simulation (continuous and design storms)	3 natural flood storages, PP, RG[10], GR, swales, BC and detention pond	• NbS decreases water velocity and flood depth, delay flooding, and attenuate peak flows • Ecosystem service goals achieved, but more effectively at smaller scales than at large ones (greater NbS coverage needed)
[31]	44000 m²	Hydraulic and Hydrology	Simulation (continuous)	VGS and storage tank	• Depending on the climate type, 60% to 100% annual stormwater was reduced at best • In some cases, additional water is needed during dry months to maintain vegetation (the storage tank may insufficient)
[5]	from 3 km² to 51 km²	Hydraulic and Hydrology	Simulation (continuous) and Calculation	BC	• At large scales, PCSWMM erases information on soil heterogeneity (resulting in higher uncertainties) • PCSWMM uses average values for soil and slope on the entire catchment
[10]	0,3521 km²	Hydraulic, Hydrology and Pollutants	Simulation (continuous)	BC	• BC efficiency depends on its size and layering • Pollutants reduction

[9] Constructed Stormwater Wetland
[10] Rain gardens

Ref.	Scale	Main subject(s)	Tool/ Method	NbS implementation	Main result(s)
[26]	from 0,17 km² to 2,19 km²	Hydraulic and Hydrology	Simulation (continuous) and Survey	RG and PP	• Stakeholders' choices were influenced by maintenance needs, installation costs, and existing infrastructures • PP is most effective in flatter zones across all scales and for small rainfall events (still slightly reduces runoff in larger storms) • RG is most effective in residential zones and at smaller scales for small events (short return periods and low intensity)
[11]	2,12 ha	Hydraulic, Hydrology and Pollutants	Monitoring	2 bioswales (BS2 and BS4) with retrofitted check dams	• BS2: 13 out of 61 events did not produce overflow or underdrain discharge; BS4: 24 out of 53 events • Check dams improve reduction of peak flows and volumes • BS2 exfiltrated 21% of storm events, BS4 exfiltrated 43% • Some pollutant concentration were reduced, but others remained above the allowed threshold
[13]	No info (~1 to 2 ha)	Hydraulic and Hydrology	Simulation (continuous) and Monitoring	Swales	• Possibility to reduce computation time since only a few parameters control groundwater level dynamics • Limitation of SWMM's LID module in representing groundwater levels • SWMM's aquifer module showed the best performance
[25]	No info	Hydraulic	Simulation (design storms)	GR, sunken GS, RG and grasses swales	Landscape approach worked successfully: no flooding for design rainfalls (sub-catchment regulation system activated for one micro-catchment)
[18]	24488 m² and 239,82 m²	Hydraulic, Hydrology and Decision-making methods	Calculation, MCA and SWOT	RG, retentions crates, infiltration swales and infiltration wells	RG: most cost-effective with multi-functional benefits
[21]	6,8 ha	Hydrology	Simulation (event-based)	GR, RG and PP	• RG and GR are limited for high return-period events • Implementation of NbS under projected future climate change is necessary • For 8% increase in living space, NbS achieve a 38% runoff reduction

Ref.	Scale	Main subject(s)	Tool/ Method	NbS implementation	Main result(s)
[16]	1 km²	Hydraulic, Hydrology, Ecosystem services and Economic aspect	Simulation (continuous and design storms)	BC, PP, vegetative swales and 2 retentions pods (with weirs and orifices for control outlets)	• The best SuDS is the one addressing multiple aspects (multi-purpose) • Effectively reduces CSO[11] recurrence, transport delay and pedestrian accessibility and stability
[15]	173,4 km²	Hydrology and Ecosystem services	Simulation (continuous and extreme events)	Tree coverage and bioswales	• High tree coverage improves runoff and temperature mitigation • Dry soil: high storage, resulting in high runoff mitigation • Moist soil: high temperature mitigation
[19]	286,69 ha	Hydraulic, Hydrology, Design framework and Economic aspect	Simulation (design storms) and Cost-benefit analysis	BC	• The presented framework has great flexibility (offers multiple potential solutions) • Most targets were met (target 2: 75% success rate; target 3: 86% success rate) • Extreme targets (very low or very high) are not cost-effective
[20]	435262 m²	Hydraulic, Hydrology, Design framework and Economic aspects	Simulation (design storms) and Cost-benefit analysis	GR	• Future climate (without NbS) shows an 11% increase in flood depth compared to present conditions • NbS under future climate reduce flood depths by 24% for 10-year return period, 18% for 50-year return period, and 16% for 100-year return period • Economic benefits of NbS implementation amount to 6.1 million €/year
[22]	900 m² and 250 m²	Hydrology and Ecosystem services	Monitoring and simulation (continuous)	3 types of GR	The use of biochar in the substrate of GR in Mediterranean climate presents significant advantages in water retention, thermal regulation, and consequently, energy savings

[11] Combined Sewer Overflow

Chapter 2

Fundamental Concepts

2.1 Modules

2.1.1 Swale

A module simulating swales already exists in the software and has been tested by the development team. The test was conducted on the rain garden located in Gembloux, Belgium represented in Figure 2.1. The rain garden consists of a succession of three swales (coloured blue, orange, and green in Figure 2.1a), with any remaining runoff is drained into a detention pond, which includes both a permanent pond and a temporary expansion area. This site is fully monitored, with sensors measuring water levels and flow rates, to quantify infiltration and determine the required storage capacity. The study provides valuable insights for both biodiversity enhancement and the understanding of hydraulic dynamics. More detailed information about this project can be found in [34].

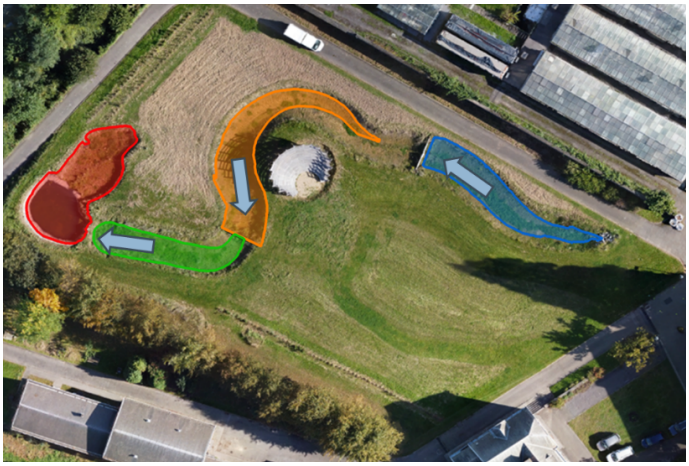

(a) Plan view

(b) Triangular weir as a control mechanism

Figure 2.1: Rain garden in Gembloux [34]

A swale is a shallow ditch (maximum depth between 400 and 600 [mm]) that is filled with vegetation. The side slopes should be below 20-25%. The vegetation slows down the runoff and promotes infiltration depending on the soil. Figure 2.2 schematically shows the principle of a swale.

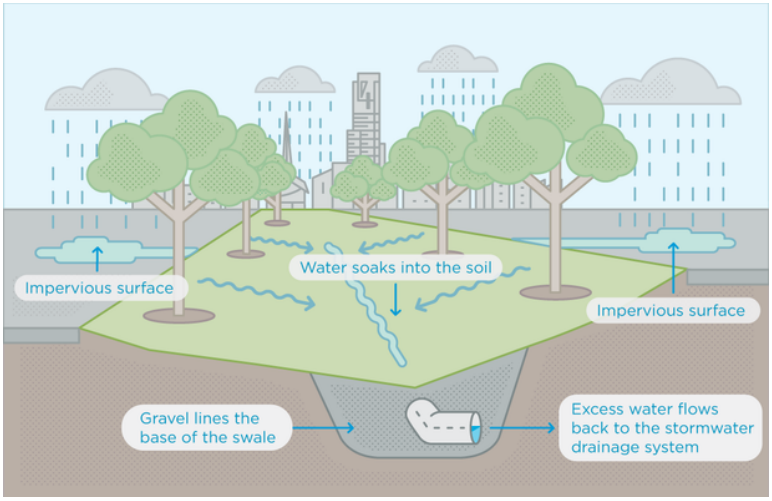

Figure 2.2: Swale principle [35]

Swales can be classified in different ways. A swale can either be dry or wet.
A dry swale has a filter bed with a perforated drain. It provides stormwater treatment and conveys the flow. FIGURE 2.3 depicts the configuration of a dry swale.
A wet swale has a minimum water depth of 150 [mm] and does not contain any underground filter. It provides stormwater treatment through sedimentation and vegetation. It also controls peak flow rates by reducing the flow velocity and promoting infiltration. FIGURE 2.4 shows the general concept of a wet swale.

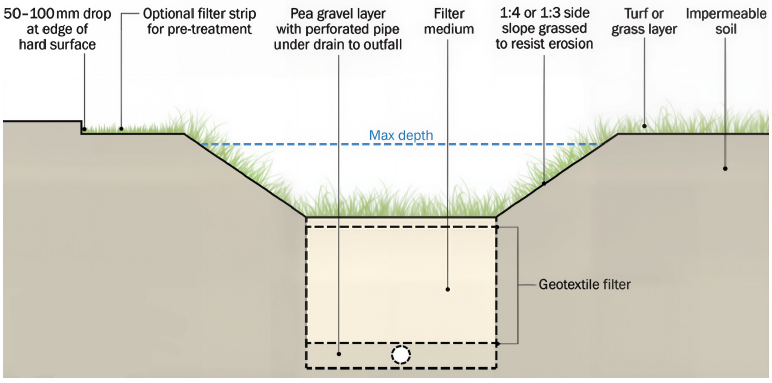

Figure 2.3: Dry swale [36]

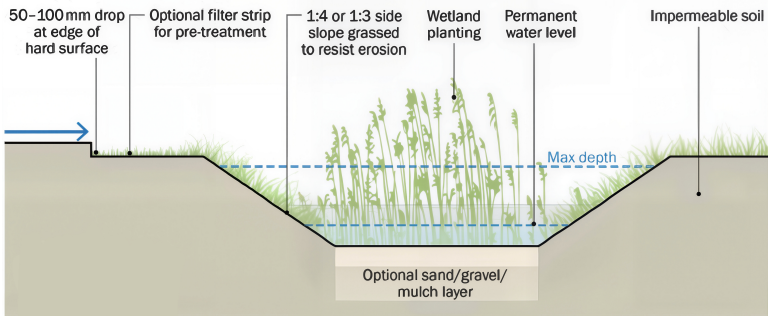

Figure 2.4: Wet swale [36]

Swales can also be classified according to infiltration conditions.
An infiltrating swale promotes infiltration when the soil has sufficient permeability and is not contaminated.

A draining swale primarily serves a storage and conveyance function. This solution is used when the infiltration capacity is insufficient (< 1 [mm/h]) and/or the soil is contaminated. The outflow is regulated and evacuated either through a drain below the swale or along the surface.
A combined swale mixes the two approaches. It is used when the soil has moderate infiltration capacity (between 1 and 20 [mm/h]). In this case, infiltration through the soil is slow, and the outflow regulation can be regulated as described previously.

This module can be modelled thanks to the following equations:

- Conservation of mass:

$$\frac{dV}{dt} = \sum_i Q_{\text{in}}^i(t) - \sum_j Q_{\text{out}}^j(t) - f_{GA} \tag{2.1}$$

  where:

  - V is the total volume in the swale [m^3],
  - Q_{in} are the various inflow rates [m^3/s],
  - Q_{out} are the various outflow rates [m^3/s],
  - f_{GA} is the infiltration discharge according to Green-Ampt [m^3/s].

- Green–Ampt (infiltration):

$$f_{GA} = K_s \cdot A \cdot \frac{\Delta H}{L} \tag{2.2}$$

  where the hydraulic head gradient is defined as:

$$\frac{\Delta H}{L} = 1 + \frac{(h + \psi_f)(\theta_s - \theta_i)}{F} = 1 + \frac{\psi^* \, \Delta\theta}{F}$$

  where:

  - K_s is the saturated hydraulic conductivity [m/s],
  - A is the infiltrating surface [m^2],
  - L is the depth of the wetting front [m],
  - h is the water depth above the soil surface [m],
  - ψ_f is the suction head at the wetting front [m],
  - θ_i is the initial volumetric water content [-],
  - θ_s is the saturated volumetric water content [-],
  - ψ^* is the effective capillary head driving water into the soil [m],
  - F is the cumulative infiltration [m].

2.1.2 Reservoir

A reservoir is a means used to store stormwater to reduce inflows into the sewage systems. If the water meets quality standard, it can be reused to alleviate water scarcity. Otherwise, after the rainfall, it can be released

to the sewage system once the network is no longer overloaded. Reservoirs can come in many different sizes, and they can be buried underground or installed above ground. This is not a NbS per se; however, this module is linked to NbS, impervious areas and grey infrastructures, and used as a buffer zone thanks to its storage capacity.
Reservoirs can be made of different materials, but if the stored stormwater is used for consumption or sanitation, the chosen material has to be closely studied to not contaminate the water. The water can be treated before or after entering the reservoir.

The module *reservoir* in the WSC project is modelled by the following equations:

- Conservation of mass:

$$\frac{dV}{dt} = \sum_i Q_{\text{in}}^i(t) - \sum_j Q_{\text{out}}^j(t) \tag{2.3}$$

  where:

  - V is the total volume in the reservoir [m^3],
  - Q_{in} are the various inflow rates [m^3/s],
  - Q_{out} are the various outflow rates [m^3/s].

- Hydraulic head (or piezometric head):

$$H = h + z \tag{2.4}$$

  where:

  - h is the pressure head [m],
  - z is the elevation head (altitude) [m].

2.1.3 Pipe

A pipe is a simple conduit and not an NbS itself. It is considered part of the grey infrastructure, but it can connect different NbSs and/or grey infrastructures together. In the next section, the pipe module is used extensively; for this reason, the governing equation of this module is presented:

- Unsteady Bernoulli equation without pressure (for a circular conduit):

$$\lambda \frac{dQ}{dt} + \frac{Q \cdot |Q|}{2K} = \gamma \cdot \Delta H \tag{2.5}$$

  where the hydraulic inertia coefficient λ and the hydraulic resistance coefficient γ are defined as:

$$\lambda = \frac{f}{L} \cdot S \quad ; \quad \gamma = \frac{g \cdot D}{L}$$

  where:

  - Q is the discharge [m^3/s],

- K is the hydraulic loss coefficient [m^3],
- ΔH is the hydraulic head difference between the upstream and downstream ends of the pipe [m],
- f is the pipe friction coefficient [-],
- S is the pipe cross-sectional area [m^2],
- L is the pipe length [m],
- g is the gravitational acceleration (9.81 [m/s^2]),
- D is the pipe diameter [m].

2.1.4 Weir

A weir is a structure that discharges an overflow from upstream to downstream. It can serve as a connection between reservoirs, canals, and many other hydraulic systems. It functions as a control structure because it allows water to pass only once a certain upstream level is reached. It maintains water levels within a desired range and prevents excessive flow downstream. A few examples of weirs are shown in Figure 2.5.
From a NbS perspective, a weir can be installed at the entrance and/or exit of a swale, a rain garden, or other green infrastructures. It can also provide additional time for upstream water to infiltrate.

(a) Serrière River weir [37]

(b) Example of weir in a NbS setting [36]

Figure 2.5: Examples of weirs

In the following, two types of weirs are explained: rectangular and triangular weirs. The difference is geometric, and various coefficients, as well as their mathematical expressions, are affected by this difference. This work considers only weirs operating under free-flow conditions, excluding submerged weirs.

2.1.4.1 Rectangular

A schematic diagram of a rectangular weir is shown in Figure 2.6.

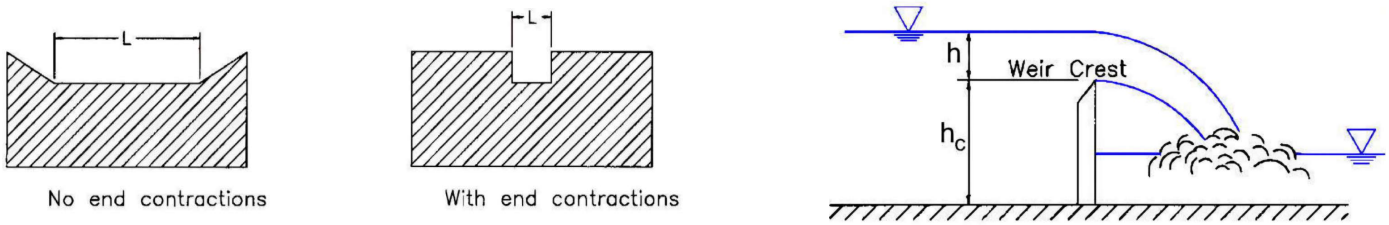

Figure 2.6: Rectangular weir [38]

The rectangular weir is governed by the following equation:

$$Q = C \cdot L \cdot H^{\frac{3}{2}} \tag{2.6}$$

where:

- Q is the discharge over the weir [m^3/s],
- C is the discharge coefficient (inside lies the root square of $(2 \cdot g)$)[[$m^{1/2}/s$]],
- L is the length of the weir [m],
- H is the upstream head above the crest [m],
- g is the gravitational acceleration (9.81 [m/s^2]).

The discharge coefficient for a broad-crested weir can vary between 1.4 and 1.7. The discharge coefficient for a sharp-crested weir is 1.84; however, according to Smith [39], the upper limit is 1.69.

2.1.4.2 Triangular (or V-notch)

A schematic diagram of a triangular weir is shown in FIGURE 2.7.

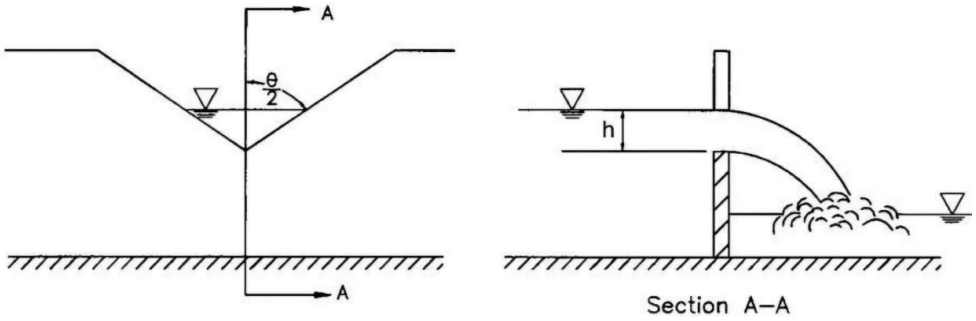

Figure 2.7: Triangular weir [38]

The triangular weir is governed by the following equation:

$$Q = C \cdot \tan(\theta/2) \cdot H^{\frac{5}{2}} \tag{2.7}$$

where:

- Q is the discharge over the weir [m^3/s],
- C is the discharge coefficient (inside lies the root square of $(2 \cdot g)$)[[$m^{1/2}/s$]],
- θ is the angle of the weir [°],
- H is the upstream head above the crest from the lowest point [m].

The discharge coefficient depends on the weir angle and the crest shape. For a 90° V-notch thin plate weir, the discharge coefficient is 1.38. For a broad-crested V-notch weir, this coefficient depends on the weir's shape, and its exact value must be determined experimentally or from design charts.

2.1.5 Standard Orifice

A standard orifice is a simple control structure consisting of a circular opening between two hydraulic systems. It can be an orifice in a plate between two reservoirs or other structures. A schematic diagram of a standard orifice is shown in Figure 2.8.

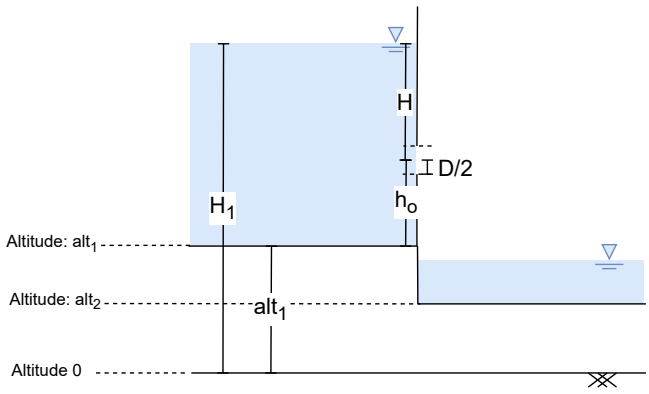

(a) Not submerged case

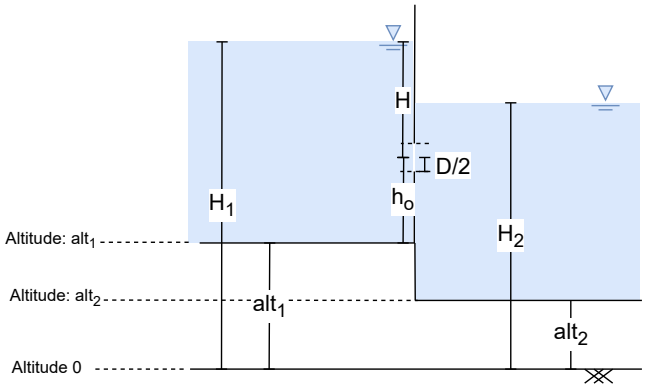

(b) Submerged case

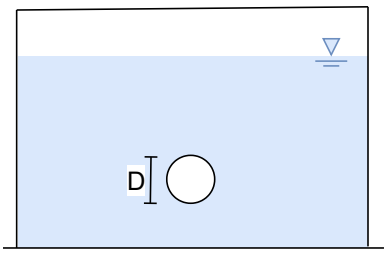

(c) Elevation view

Figure 2.8: Orifice

The standard orifice is governed by the following equation:

$$Q = C \cdot A \cdot \sqrt{H} \tag{2.8}$$

where:

- Q is the discharge through the orifice [m^3/s],

- C is the discharge coefficient (inside lies the root square of $(2 \cdot g)$)[[$m^{1/2}/s$]],
- A is the area of the orifice [m^2],
- H is the head to be considered (double definition explained afterwards) [m].

The discharge Q changes definition depending on the context:

- Case 1: The orifice is not submerged downstream (see Figure 2.8a). The head H is defined by:

$$H = H_1 - alt_1 - h_0$$

  where:

  - H_1 is the upstream head [m],
  - alt_1 is the upstream elevation [m],
  - h_o is the height of the orifice measured from its centre [m].

- Case 2: The orifice is submerged downstream (see Figure 2.8b). The head is defined by:

$$H = H_1 - H_2$$

  where:

  - H_1 is the upstream head [m],
  - H_2 is the downstream head [m].

This mathematical expression (Eq. 2.8) is valid for orifices with a diameter of 300 [mm] or less, provided that the ratio of hydraulic head to diameter satisfies $H/D > 1.5$. For larger diameters or smaller H/D ratios, the analysis should take into account the water levels at the inlet and outlet, as well as pressure losses, as recommended in the *Guide de gestion des eaux pluviales* [40].
The discharge coefficient is typically 0.6 when the plate thickness is smaller than the orifice diameter (which is usually the case) and 0.8 when it is thicker. If the edges are rounded, C is equal to 0.92. These values are given by *The SuDS Manual* [36]. All the values mentioned are not multiplied by $\sqrt{2 \cdot g}$ which must be applied in order to correctly use Eq. 2.8.

2.1.6 Perforated Riser

A perforated riser is a section of pipe with holes. It is usually installed inside a chamber in such a way that rainwater enters the chamber through a designated inlet. The only exit for the water is through the perforated riser, which is connected to a pipe that conveys the rainwater out of the chamber. A schematic diagram of the perforated riser is shown in Figure 2.9.

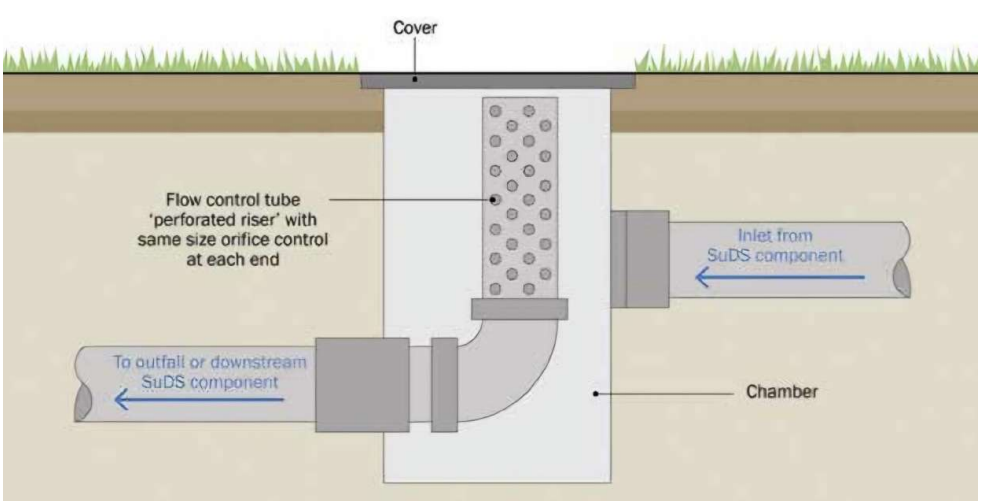

(a) Typical perforated riser configuration [36]

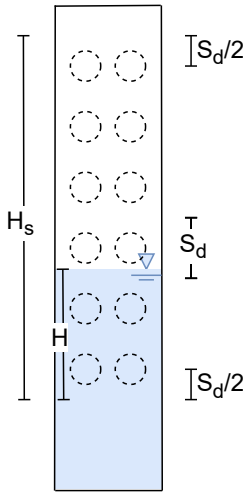

(b) Zoom on module

Figure 2.9: Perforated riser

The perforated riser is governed by the following equation:

$$Q = \frac{2 \cdot A_p \cdot C_p}{3 \cdot H_s} \cdot H^{\frac{3}{2}} \tag{2.9}$$

where:

- Q is the discharge entering the holes [m^3/s],
- C_p is the discharge coefficient (inside lies the root square of $(2 \cdot g)$)[[$m^{1/2}/s$]],
- A_p is the area of all the holes [m^2],
- H_s is the height of the perforated riser [m],
- H is the hydraulic head from a distance $S_d/2$ from the lowest hole (with S_d: distance between two holes) [m].

The discharge coefficient is 0.61 as mentioned in *The SuDS Manual* [36].

2.2 Informatic Methods

2.2.1 CPU-GPU Computation and Jax Library

The software uses JAX, a Python library for high-performance numerical computing. JAX provides most of the functions of the Numpy library (by calling `jax.numpy.` *`"function"`*) and additional features. These features allow code to be executed efficiently on CPUThe main difference is that the CPU[1], and optionally on GPU[2] or TPU[3], allowing efficient parallel computation.

[1]Central Processing Unit
[2]Graphics Processing Unit
[3]Tensor Processing Unit: processor specialized for deep-learning operations, similar to a GPU

The main difference is that the CPU processes tasks serially, whereas the GPU splits the tasks and executes them in parallel. This is possible because the GPU has many more cores (up to thousands), while the CPU has between 2 and 64 cores.

By using the JAX library, the code follows this approach:

1. Before performing any calculations, it goes through all the functions once and translates the pure Python code into an intermediate language called *"jaxpr"* (a JAX expression). This translation is enabled by tracing: each argument of the functions becomes a tracer object, which records the operations executed within the function.

2. From the first to the last iteration, the code follows the *jaxpr* translation and executes exactly the operations recorded, without going back inside the original Python functions.

The translation actually optimises the code, therefore increasing execution speed and reducing memory usage. This optimization is performed by the XLA (Accelerated Linear Algebra) compiler, which compiles the Python functions for efficient execution on CPU, and optionally on GPU or TPU. It is invoked simply by calling `jit_compile` (standing for *just-in-time*), allowing the code to run efficiently in parallel and take full advantage of the available hardware resources.

The main reason for using the JAX library is its automatic differentiation capability, which allows the efficient and accurate computation of the Jacobian matrix required by the Newton-Raphson solver presented later.

This type of coding is purely functional. The returned value is determined solely by the inputs; there are no side effects. This property is called immutability. It means that, although this approach enables advanced optimization techniques, only the returned value of the function can be changed, nothing else. For example, if the user wants to store intermediate information within the function, it must be returned. If the solver does not allow it, another technique has to be used. In some cases, the use of `jax.disable_jit()` may work. This disables JIT compilation and allows the inputs to be modified in the usual Python way; however, the code could run significantly slower.

There are some limitations when using JAX. During the initial function tracing, the code uses tracer to enable the translation of the Python code into *jaxpr*. No actual numerical values are involved in this process. If the code contains "*if...else*" constructs, the tracer does not evaluate any conditions because it represents an abstract computation rather than a concrete value, and therefore cannot perform the translation. This typically results in a *"TraceBoolConversionError"*. There are several ways to bypass this error. The technical documentation of Exoplanet [41] proposes the following solution `jax.numpy.where()`, which can work in some cases. However, in the project presented in this report, the method most commonly used to bypass non-differentiable operations, including boolean branches, is the *sigmoid* function , called via `"jax.nn.sigmoid(x)"` or the *softplus* function , called via `"jax.nn.softplus(x)"`.
This boolean-related limitation is directly linked to the constraint imposed by automatic differentiation in JAX, which requires all functions involved in the computation to be continuously differentiable. These functions are detailed in the following subsection.

2.2.2 Object-Oriented Programming (OOP)

Object-oriented programming is a way to structure code. The code for this project is quite large and, in some aspects, can be repetitive. Therefore, there is a need for structured and efficient programming. OOP is well-suited for this purpose. In this thesis, as mentioned previously, modules are the focus. A module is hydraulic component that can, either by itself or linked to other modules, serve as a green solution for managing stormwater. Although each module represents something different, the implementation is largely similar. It is necessary to define the intrinsic and extrinsic unknowns, the parameters describing the hydraulic structure's shape, the initial conditions, and so on.

OOP is based on classes, which allow the creation of objects. A class groups attributes and methods but does not assign any value yet. This principle is called encapsulation. An object uses the class by assigning values to the attributes and calling its methods. For example, for a swale: a class is created for the swale and every parameter needed to describe it are listed as well as its unknowns and the function to solve the residual equations linked to it. At this point, no specific values are assigned to the attributes. When a test is run, the class is called to create an object, and all values are provided, such as the geometrical parameters, hydrological parameters, and initial conditions.

Therefore, OOP allows the grouping of data and characteristics under the same class. This is indeed the case in this project. When creating a module, the class *"ComputeModule"* is called. An important property of OOP is inheritance: a class can inherit attributes and methods from another class. In this project, each module inherits from the parent class *ComputeModule*. This class actually contains the code structure for all modules, making the process systematic and easier for the user to create new modules.

There are many other pillars of this programming paradigm, such as abstraction, meaning that the implementation details are hidden from the developers allowing them to focus on what an object does rather than how it is implemented. There are other properties and advantages of OOP; however, they are not the main focus of this thesis.

2.2.3 Solver

The solver is based on the Newton-Raphson method. The goal is to solve the following equation:

$$\mathbf{R}(\mathbf{x}) = 0 \tag{2.10}$$

where:

- $\mathbf{x}$ is the vector of unknowns,
- $\mathbf{R}$ is the residual vector.

At each simulation iteration n, the Newton-Raphson solver performs up to m iterations to solve this equation:

$$\mathbf{x}_{m+1} = \mathbf{x}_m - \mathbf{J}_F^{-1}(\mathbf{x}_m)\,\mathbf{R}(\mathbf{x}_m) \tag{2.11}$$

where:

- $\mathbf{x}_{m+1}$ is the solution at iteration $m+1$,
- $\mathbf{x}_m$ is the solution at iteration m,
- $\mathbf{J}_F(\mathbf{x}_m)$ is the Jacobian matrix at iteration m,
- $\mathbf{R}(\mathbf{x_m})$ is the residuals vector at iteration m.

An implicit time integration method is one in which the unknown at the new time step appears on both sides of the equation, meaning the solution depends on the unknown itself. For instance, the discretised conservation of mass (see Eq. 2.3) solved implicitly can be written as:

$$V_{n+1} - V_n = \Delta t \left(\sum_i Q_{\text{in}}^i(t_{n+1}) - \sum_j Q_{\text{out}}^j(t_{n+1}) \right) \tag{2.12}$$

The aim is to find V_{n+1} so that the residual satisfies:

$$R(V_{n+1}) = V_{n+1} - V_n - \Delta t \left(\sum_i Q_{\text{in}}^i(t_{n+1}) - \sum_j Q_{\text{out}}^j(t_{n+1}) \right) = 0 \tag{2.13}$$

As shown in Eq. 2.11, the inverse of the Jacobian matrix must be computed. This motivates further the use of the JAX library, which provides automatic differentiation. However, this requires all functions to be continuous and differentiable. If an equation involves parameters that can take different expressions depending on the context, these must be expressed in a continuous manner. For this reason, the sigmoid function, mentioned briefly before, is used to formulate smoothly such relations. In Python, this function is called `jax.nn.sigmoid(x)` and is defined as:

$$sigmoid(x) = \frac{1}{1 + e^{-x}} \tag{2.14}$$

Figure 2.10 illustrates the graph of the sigmoid. It shows that if x is negative, *sigmoid* approaches zero and if x is positive, *sigmoid* is very close to one.
This provides a continuous solution to express conditional equations, allowing the Jacobian matrix to be correctly defined.
Moreover, it can be used to emulate a *True* or *False* condition, and thus simulates an *if...else*.
This method is not perfect: if x is near zero, the function gives an intermediate value between 0 and 1. However, the steepness of the S-shaped curve can be tightened by multiplying x with a factor, reducing the range of intermediate values, but it does not eliminate them entirely.

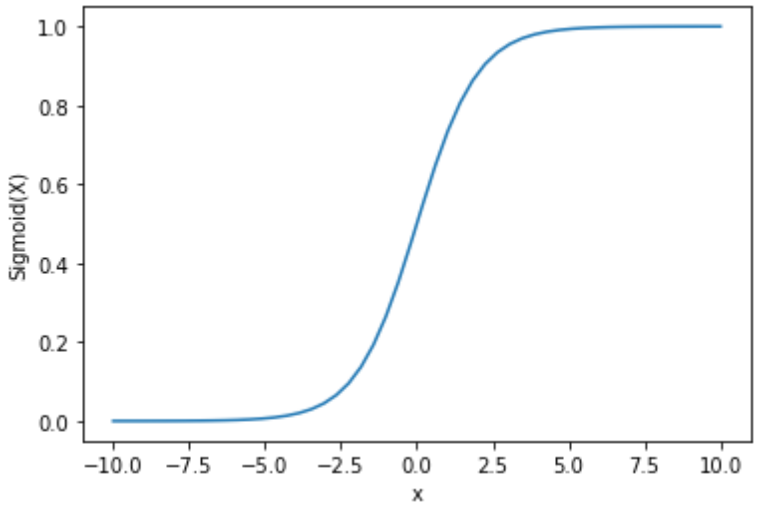

Figure 2.10: Sigmoid

Another alternative to `jax.nn.sigmoid()` is the function `jax.nn.softplus()`. The *softplus* is the primitive of the *sigmoid* and is defined as:

$$softplus(x) = \ln(1 + e^x) \tag{2.15}$$

This function is represented in FIGURE 2.11. As seen in this figure, if x is negative, the function is close to zero, but it never reaches zero exactly. If x is positive, the *softplus* function equals x. This ensures that the parameter x never becomes negative, which can be particularly necessary for hydraulic problems. In the following sections, this function is used to guarantee that the water level never drops below zero, as numerical noise can sometimes produce slightly negative results. Moreover, because this function is continuous, it allow the Jacobian matric to be correctly defined even with conditional equations, just as with the *sigmoid*.

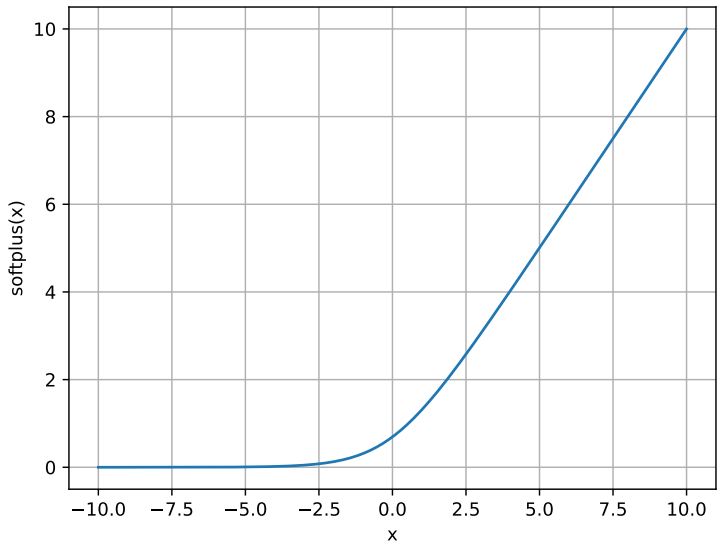

Figure 2.11: Softplus

2.2.4 Residual Equations

When creating the class for a module, the most important part that describes the hydraulic behaviour governed by the module is the residual equations.
The equations for each module are analytical equations, but for numerical implementation, slight modifications may be necessary. For instance, *softplus* is never used in the analytical equations. However, because some parameters are not continuously differentiable, *softplus* is applied to enable their numerical evaluation. Functions and parameters not initially present in the original governing equations may be introduced to allow accurate numerical representation of the modules.

Previously, the concepts of intrinsic and extrinsic unknowns were introduced. An intrinsic unknown is controlled by the module under study, whereas an extrinsic unknown is provided by another module and is not controlled by the considered module. For example, a weir determines the discharge that will exit the module, which is its intrinsic unknown. In contrast, the hydraulic head is received from the previous module, making it an extrinsic unknown.

The number of intrinsic unknowns is the number of expected residual equations. In the previous section, four control mechanisms were introduced. Each mechanism is a module defined by a mathematical equation, its own discharge formula. These four modules each have one intrinsic unknown which is the discharge Q meaning that each only requires one residual equation.

The solver finds a solution for the unknown at each iteration so that the residual is as close as possible to zero. There are two levels of iterations: the Newton-Raphson iterations and simulation iterations. The simulation has N iterations, determined by the time step (Δt) and the total time ($t_f - t_0$). For simulation iteration n, the Newton-Raphson solver performs up to M iterations until the residual falls below the given tolerance (here 10^{-5}) or a maximum of 50 Newton-Raphson iterations is reached, to avoid excessive computation time.

Chapter 3

Module and Verification Tests

In this chapter, each coded module is examined. First, the analytical solution is developed to compare it with the numerical solution and to confirm the correct functioning of the code. Next, multiple simple tests are implemented to ensure that the module has been correctly implemented. Afterwards, the residuals equations are checked to verify that, at each time step, the solver runs smoothly and that the residuals do not exceed a predefined threshold. Finally, the errors for different time steps are plotted to assess the stability of the numerical model.

3.1 Rectangular Weir

3.1.1 Analytical Solution

The outflow from a rectangular weir is given by:

$$Q = -C \cdot L \cdot H^{\frac{3}{2}} \tag{3.1}$$

which can be transformed as:

$$S \cdot \frac{dH}{dt} = -C \cdot L \cdot H^{\frac{3}{2}} \tag{3.2}$$

where:

- S is the plan area of the NbS element upstream of the weir [m²].

The negative sign indicates that the water depth decreases over time because it is an outflow. The equation can be developed as follows:

$$\frac{dH}{H^{\frac{3}{2}}} = -\frac{C \cdot L}{S} dt \tag{3.3}$$

$$\int \frac{dH}{H^{\frac{3}{2}}} = \int -\frac{C \cdot L}{S} dt \tag{3.4}$$

$$-2 \cdot H^{\frac{-1}{2}} = -\frac{C \cdot L}{S} \cdot t + C_1 \tag{3.5}$$

$$H^{\frac{-1}{2}} = \frac{1}{2} \cdot \frac{C \cdot L}{S} \cdot t + \frac{-1}{2} \cdot C_1 \tag{3.6}$$

$$H = 4 \cdot \left[\frac{C \cdot L}{S} \cdot t - C_1 \right]^{-2} \tag{3.7}$$

where:

- C_1 is the integration constant.

The integration constant is found thanks to the initial condition:

$$H(t = 0) = H_0 : \text{initial hydraulic head in NbS element upstream of the weir}$$

$$\Rightarrow C_1 = -2 \cdot H_0^{-\frac{1}{2}}$$

Finally, the analytical solution for the rectangular weir is:

$$H(t) = 4 \cdot \left[\frac{C \cdot L}{S} \cdot t + 2 \cdot H_0^{-\frac{1}{2}} \right]^{-2} \tag{3.8}$$

3.1.2 Verification Tests

All tests follow the same setup: one upstream reservoir (called "Reservoir 1", indicated by subscript 1), one downstream reservoir (called "Reservoir 2", indicated by subscript 2), and both reservoirs are connected by a rectangular weir. Table 3.1 provides all the necessary parameter values for the tests. The definition of volume (V) and plan area (S) are derived from the values in Table 3.1 and do not need to be repeated.
A few assumptions are made for all the tests:

- Reservoir 1 and Reservoir 2 have identical dimensions,
- The tests are conducted so that the downstream water level never exceeds the upstream water level ($h_{\text{upstream}} \geq h_{\text{downstream}}$)

Parameter	Notation	Value	Unit
Length of reservoirs and weir	L	1	m
Width of reservoirs	l	1	m
Height of reservoirs and weir	h_r	2	m
Elevation of reservoir 1	alt_1	0	m
Elevation of weir	alt_w	0	m
Elevation of reservoir 1	alt_1	0	m
Elevation of reservoir 2	alt_2	0	m
Discharge coefficient	C	1.69	$m^{1/2}/s$
Time step	Δt	0.01	s
Final time	t_f	60	s

Table 3.1: Parameter values

There are four verification tests implemented for this module:

- Test 1: The water level in Reservoir 1 is just below the weir's crest.
- Test 2: The water level in Reservoir 1 is the same as the weir's crest.
- Test 3: The volume in Reservoir 1 results in a water level higher than the weir's crest. This test is used to compare the numerical solution with the analytical one, to analyse the residuals, and to study the error for different time steps.
- Test 4: The water level in Reservoir 1 is equal to the weir's crest, and there is an inflow rate entering Reservoir 1 (Q_{in}). The total initial volume of water increases at each time step.

3.1.2.1 Test 1

Table 3.2 provides the initial values for Test 1. The initial hydraulic head and the initial volume in each reservoir are not explicitly mentioned, as they can be derived from the water levels and the elevations given in Table 3.1. This remark applies to all tests afterwards.
A simple diagram representing this test is shown in Figure 3.1.

Parameter	Notation	Value	Unit
Water level in reservoir 1	$h_{1,0}$	1.99	m
Water level in reservoir 2	$h_{2,0}$	0	m
Discharge on the weir	Q_w	0	m^3/s

Table 3.2: Initial conditions for Test 1

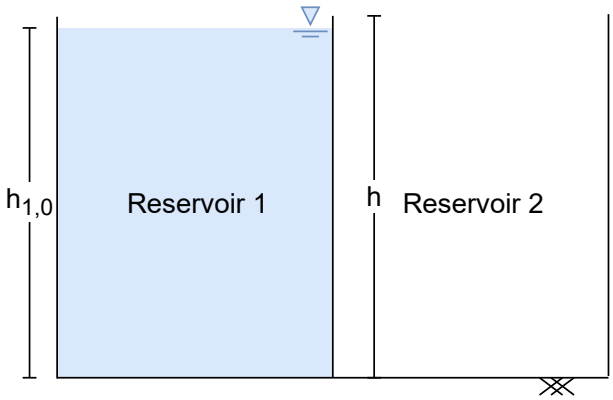

Figure 3.1: Diagram representing Test 1 initially

As shown in FIGURE 3.2, the hydraulic heads in Reservoir 1 remain constant over time. The hydraulic heads at the weir and Reservoir 2 do not increase. This behaviour is expected, since the volume in Reservoir 1 is insufficient to overflow the weir and fill Reservoir 2.

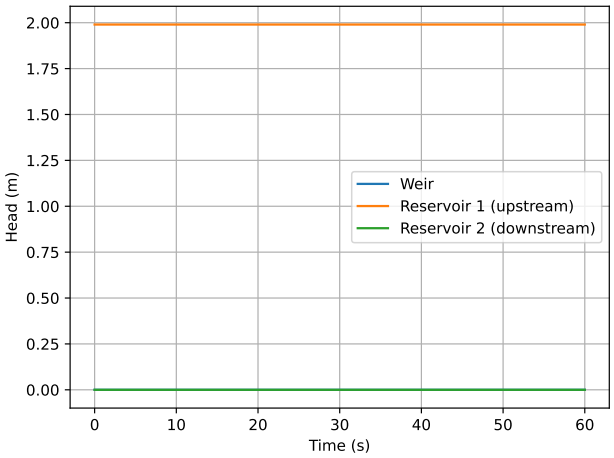

Figure 3.2: Hydraulic heads comparison for Test 1

3.1.2.2 Test 2

TABLE 3.3 provides the initial values for Test 2. A simple diagram representing this test is shown in FIGURE 3.3.

Parameter	Notation	Value	Unit
Water level in reservoir 1	$h_{1,0}$	2	m
Water level in reservoir 2	$h_{2,0}$	0	m
Discharge on the weir	Q_w	0	m^3/s

Table 3.3: Initial conditions for Test 2

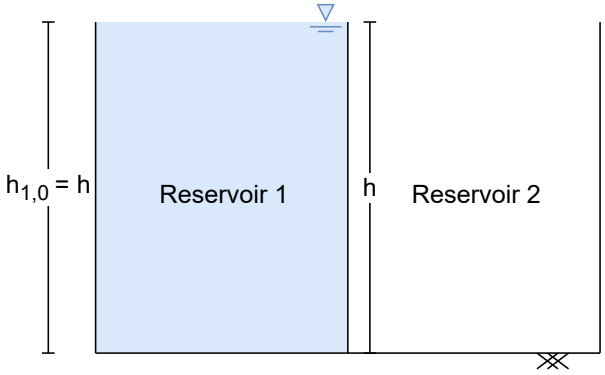

Figure 3.3: Diagram representing Test 2 initially

Since the volume in Reservoir 1 is still insufficient to overflow the weir, the conclusions are the same as for Test 1. However, this test was designed to monitor the threshold between water overflowing the weir and no overflow occurring. In this case, as shown in FIGURE 3.4, Reservoir 1 remains full, no water flows over the weir, and Reservoir 2 stays empty as initially.

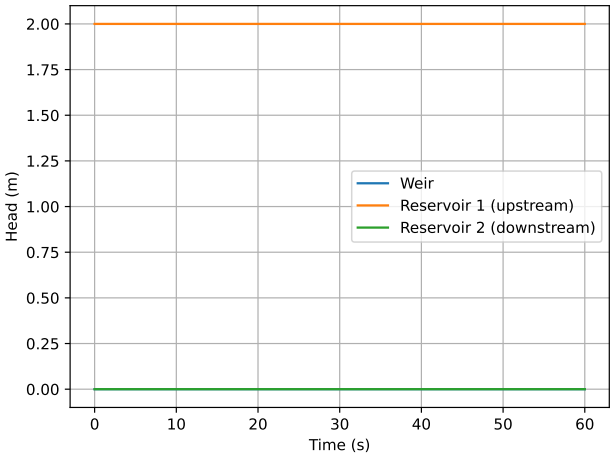

Figure 3.4: Hydraulic heads comparison for Test 2

3.1.2.3 Test 3

TABLE 3.4 provides the initial values for Test 3 and FIGURE 3.5 shows a simple schematic representation of the test at the initial state.

Parameter	Notation	Value	Unit
Water level in reservoir 1	$h_{1,0}$	2.1	m
Water level in reservoir 2	$h_{2,0}$	0	m
Discharge on the weir	Q_w	0	m^3/s

Table 3.4: Initial conditions for Test 3

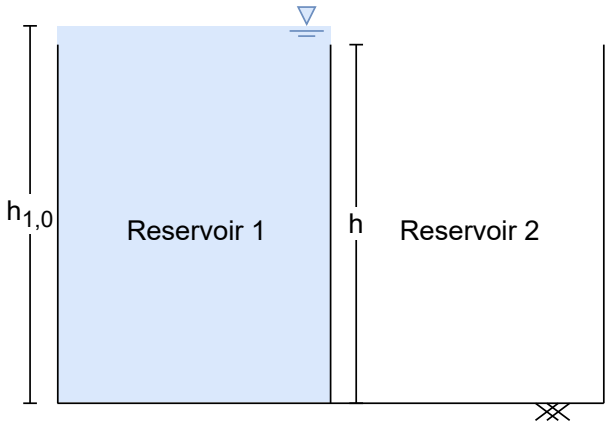

Figure 3.5: Diagram representing Test 3 initially

As illustrated in FIGURE 3.6, the initial volume in Reservoir 1 exceeds its storage capacity. The excess water immediately flows over the weir, filling Reservoir 2 and increasing its hydraulic head. The system quickly reaches a stable configuration, in which the hydraulic heads at the weir and in Reservoir 2 remain constant.

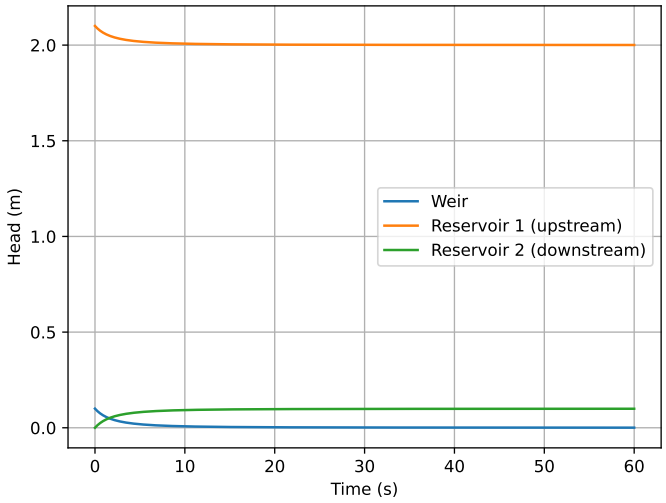

Figure 3.6: Hydraulic heads comparison for Test 3

3.1.2.4 Test 4

TABLE 3.5 provides the initial values for Test 4. The inflow rate (Q_{in}) is 0.05 [m^3/s] and it is injected consistently throughout the entire test. FIGURE 3.7 shows a schematic representation of the test at the initial state.

Parameter	Notation	Value	Unit
Water level in reservoir 1	$h_{1,0}$	1.2	m
Water level in reservoir 2	$h_{2,0}$	0	m
Discharge on the weir	Q_w	0	m^3/s

Table 3.5: Initial conditions for Test 4

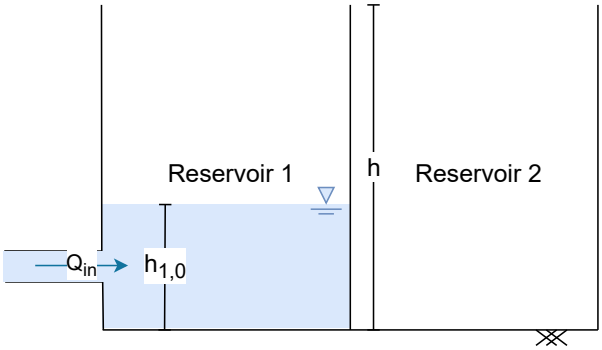

Figure 3.7: Diagram representing Test 4 initially

FIGURE 3.8 shows that, initially, Reservoir 1 does not contain enough water to overflow into Reservoir 2 via the weir. However, due to the constant discharge inflow, Reservoir 1 gradually fills, and around 16 [s], the excess water begins to flow over the weir into Reservoir 2. Reservoir 2 continues to fill until the end of the simulation. Similarly, the hydraulic head at the weir remains constant throughout the simulation.

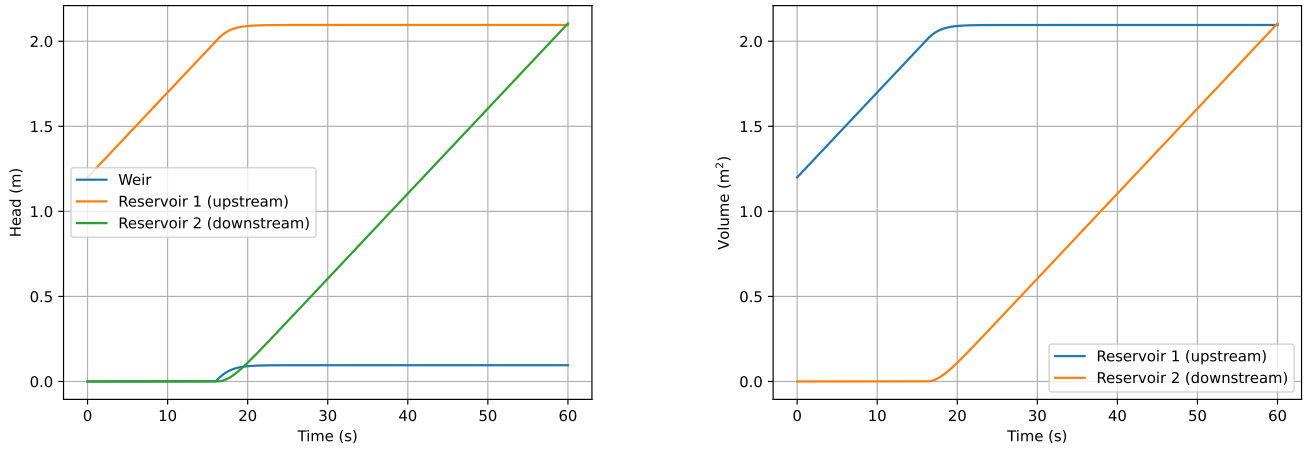

(a) Hydraulic heads comparison

(b) Volumes comparison

Figure 3.8: Results Test 4

By calculation, it is simple:

- Total initial volume: $V_0 = (h_{1,0} \cdot l \cdot L) + (h_{2,0} \cdot l \cdot L) = 1.2\ \text{m}^3$
- Total volume at the end of the test ($t_f = 60\text{s}$): $V_f = V_0 + Q_{in} \cdot t_f = 4.2\ \text{m}^3$

The values computed by the code are as follows: $V_0 = 1.2\ \text{m}^3$ (imposed by the initial conditions) and $V_f = 4.200182\ \text{m}^3$ (numerical solution), which match the expected results. Figure 3.8b shows the evolution of the volume over time. This fourth test confirms that the code appears to be functioning correctly.

3.1.3 Comparison to Analytical Solution

Figure 3.9 compares the numerical solution given by the solver and the analytical solution defined in Eq. 3.8. The analytical solution represents the expected physical behaviour. This means that if the solver finds a solution that closely matches the analytical solution, the numerical results can be considered correct.
The figure shows that the two solutions almost perfectly overlap, indicating that the numerical model accurately represents the behaviour of a rectangular weir and reproduces the evolution over time as predicted by the analytical solution.

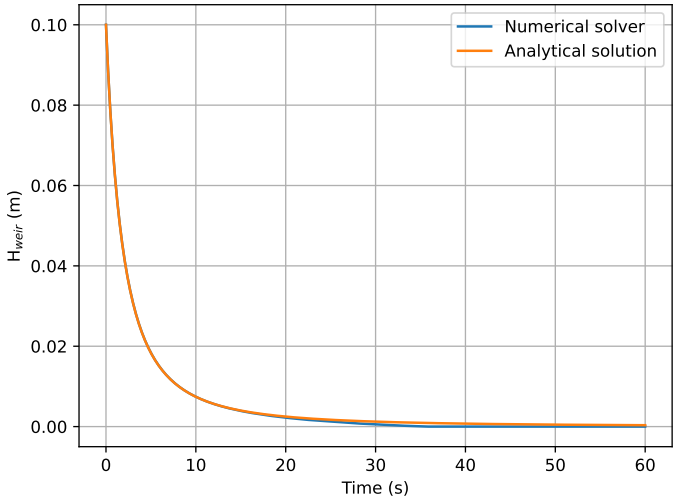

Figure 3.9: Numerical and analytical solutions

3.1.4 Residuals

To ensure that the residuals are converging, the L2 norm is used. It is defined as:

$$\|r\|_2 = \sqrt{\sum_{i=0}^{n} |r_i|^2} \tag{3.9}$$

where:

- r is a residual equation;
- n is the number of residual equations.

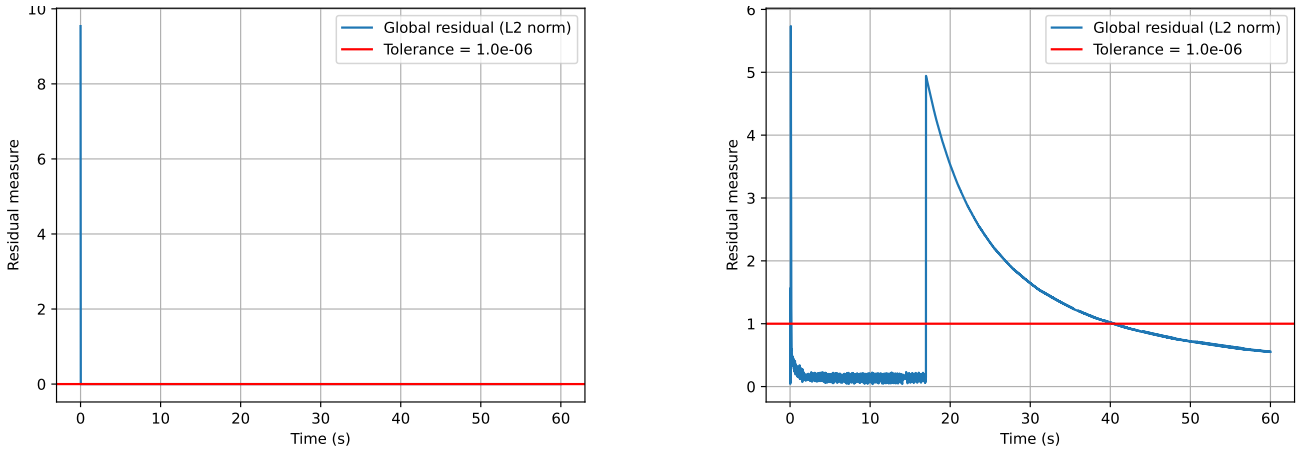

(a) With initial condition value

(b) Without initial conditions value

Figure 3.10: L2 norm of residuals

The chosen tolerance is 10^{-6} throughout the whole report when studying residual errors. As seen in FIGURE 3.10a, the very first value, which corresponds to the imposed initial conditions, is excessively large and is therefore discarded, as shown in FIGURE 3.10b. For the rest of the report, the initial value is removed since it did not originate from the numerical resolution. In FIGURE 3.10b, the norm generally decreases except around 14 [s], where there is a spike. After that spike, the L2 norm decreases again. The first peak might still be a consequence of the initial condition.
Newton-Raphson has indeed converged, so the observed peak is not caused by the solver. This observed peak may arise from the use of the function `jax.nn.softplus`, which was explained in a previous section. When the solution is very close to equilibrium, the difference between iteration i and its predecessor is near zero. In this configuration, the *softplus* function does not exactly equal zero but approaches it (see FIGURE 2.11). This could also explain the first peak.
However, the peak is not excessive; the value is just below $5 \cdot 10^{-6}$, so it can be affirmed that the residuals converge.

3.1.5 Error for Different Time Steps

To ensure that the numerical solution is stable, a study of the error for different time steps is performed. The chosen time steps are:

Δt	0.01	0.02	0.04	0.05	0.08	0.1	0.2	0.4	0.5	1

To analyse the accuracy of the module, two metrics are used: Numerical Standard Errors (NSE) and Root Mean Squared Error (RMSE).
The ideal value for NSE is close to 1. If NSE equals 0, the numerical solution is equal to the mean of the analytical solution, and if it is negative, it is worse than using the mean value. NSE is defined in Eq. 3.10.
The ideal value for RMSE is 0. RMSE is defined in Eq. 3.11.

$$NSE = 1 - \frac{\sum_{i=0}^{n}(R_i - M_i)^2}{\sum_{i=0}^{n}(R_i - R)^2} \tag{3.10}$$

$$RMSE = \sqrt{\frac{1}{n}\sum_{i=0}^{n}(R_i - M_i)^2} \tag{3.11}$$

where:

- n is the total number of iterations;
- R_i is the analytical value at iteration i;
- M_i is the numerical value at iteration i;
- R is the mean of analytical values.

As shown in Figure 3.11a, for all considered time steps, NSE is close to 1, indicating that the numerical solution accurately approximates the analytical solution. As the time step increases, NSE decreases; as expected, smaller time steps yield higher accuracy.
The conclusions for RMSE are similar. Figure 3.11b shows that RMSE remains close to 0 for all time steps, confirming that the numerical solution approaches the analytical solution. Smaller time steps improve accuracy.
It can be concluded that the numerical solver provides a stable and accurate solution.

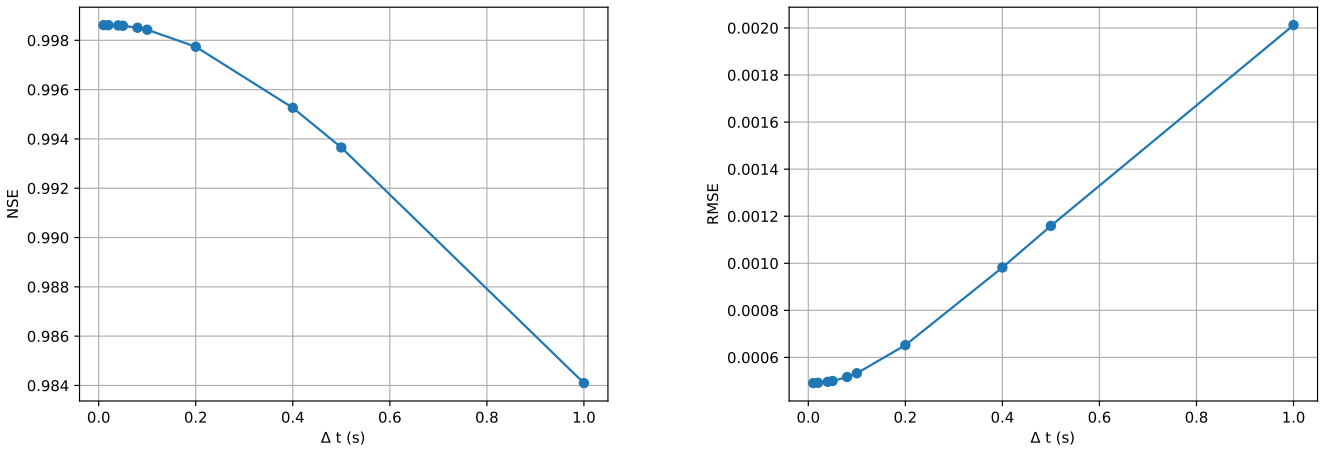

(a) NSE

(b) RMSE

Figure 3.11: Error metrics

3.2 Triangular Weir

3.2.1 Analytical Solution

The outflow from a triangular weir is given by:

$$Q = -C \cdot \tan\frac{\theta}{2} \cdot H^{\frac{5}{2}} \tag{3.12}$$

which can be transformed as:

$$S \cdot \frac{dH}{dt} = -C \cdot \tan\frac{\theta}{2} \cdot H^{\frac{5}{2}} \tag{3.13}$$

where:

- S is the plan area of the NbS element upstream of the weir [m²].

The equation can be developed as follows:

$$\frac{dH}{H^{\frac{5}{2}}} = -\frac{C \cdot \tan\frac{\theta}{2}}{S} dt \tag{3.14}$$

$$\int \frac{dH}{H^{\frac{5}{2}}} = \int -\frac{C \cdot \tan\frac{\theta}{2}}{S} dt \tag{3.15}$$

$$\frac{-2}{3} \cdot H^{\frac{-3}{2}} = -\frac{C \cdot \tan\frac{\theta}{2}}{S} \cdot t + C_1 \tag{3.16}$$

$$H^{\frac{-3}{2}} = \frac{3}{2} \cdot \frac{C \cdot \tan\frac{\theta}{2}}{S} \cdot t + \frac{-3}{2} \cdot C_1 \tag{3.17}$$

$$H = \left[1{,}5 \cdot \left(\frac{C \cdot \tan\frac{\theta}{2}}{S} \cdot t - C_1\right)\right]^{-\frac{2}{3}} \tag{3.18}$$

where:

- C_1 is the integration constant.

The integration constant is found thanks to the initial condition:

$$H(t = 0) = H_0 : \text{initial hydraulic head in NbS element upstream of the weir}$$

$$\Rightarrow C_1 = -\frac{H_0^{-\frac{3}{2}}}{1{,}5}$$

Finally, the analytical solution for the triangular weir is:

$$H(t) = \left[1{,}5 \cdot \left(\frac{C \cdot \tan\frac{\theta}{2}}{S} \cdot t + \frac{H_0^{-\frac{3}{2}}}{1{,}5}\right)\right]^{-\frac{2}{3}} \tag{3.19}$$

3.2.2 Verification Tests

All the tests in this section are exactly the same as those for the rectangular weir, except that here the weir is triangular. The definition of volume (V) and plan area (S) are derived from the values in Table 3.6 and do not need to be repeated.
A few assumptions are made for all the tests:

- Reservoir 1 and Reservoir 2 have identical same dimensions,
- The tests are conducted so that the downstream water level never exceeds the upstream water level ($h_{\text{upstream}} \geq h_{\text{downstream}}$)

Parameter	Notation	Value	Unit
Width of reservoirs	l	1	m
Height of reservoirs and weir	h_r	2	m
Elevation of reservoir 1	alt_1	0	m
Elevation of weir	alt_w	0	m
Elevation of reservoir 1	alt_1	0	m
Elevation of reservoir 2	alt_2	0	m
Discharge coefficient	C	1.38	$m^{1/2}/s$
Angle of the weir weir	θ	1.57	rad
Time step	Δt	0.01	s
Final time	t_f	60	s

Table 3.6: Parameter values

There are four verification tests implemented for this module:

- Test 1: The water level in Reservoir 1 is just below the weir's crest.
- Test 2: The water level in Reservoir 1 is the same as the weir's crest.
- Test 3: The volume in Reservoir 1 results in a water level higher than the weir's crest. This test is used to compare the numerical solution with the analytical one, to study the residuals, and to study the error for different time steps.
- Test 4: The water level in Reservoir 1 is equal to the weir's crest, and there is an inflow rate entering Reservoir 1 (Q_{in}). The total initial volume of water increases at each time step.

3.2.2.1 Test 1

Table 3.7 provides the initial values for Test 1.
A simple diagram representing this test is shown in Figure 3.1.

Parameter	Notation	Value	Unit
Water level in reservoir 1	$h_{1,0}$	1.99	m
Water level in reservoir 2	$h_{2,0}$	0	m
Discharge on the weir	Q_w	0	m^3/s

Table 3.7: Initial conditions for Test 1

As shown in FIGURE 3.12, the hydraulic heads in Reservoir 1 remain constant over time. The hydraulic heads at the weir and Reservoir 2 do not increase. The conclusions are the same as in SECTION 3.1.2.1: the volume in Reservoir 1 does not yet generate significant flow over the weir or into Reservoir 2.

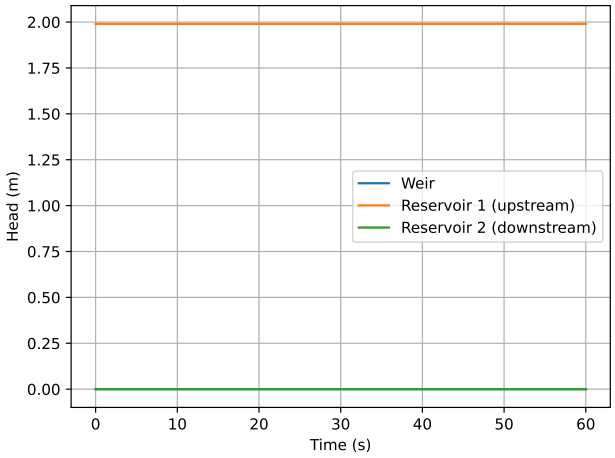

Figure 3.12: Hydraulic heads comparison for Test 1

3.2.2.2 Test 2

TABLE 3.8 provides the initial values for Test 2. A simple diagram representing this test is shown in FIGURE 3.3.

Parameter	Notation	Value	Unit
Water level in reservoir 1	$h_{1,0}$	2	m
Water level in reservoir 2	$h_{2,0}$	0	m
Discharge on the weir	Q_w	0	m^3/s

Table 3.8: Initial conditions for Test 2

The conclusions are the same as in SECTION 3.1.2.2. However, in this case, the hydraulic heads are represented in FIGURE 3.13.

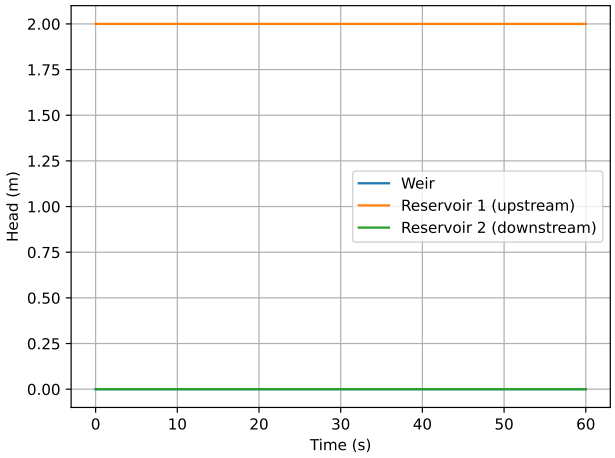

Figure 3.13: Hydraulic heads comparison for Test 2

3.2.2.3 Test 3

Table 3.9 provides the initial values for Test 3. This test is represented in a simple diagram in Figure 3.5.

Parameter	Notation	Value	Unit
Water level in reservoir 1	$h_{1,0}$	2.1	m
Water level in reservoir 2	$h_{2,0}$	0	m
Discharge on the weir	Q_w	0	m^3/s

Table 3.9: Initial conditions for Test 3

The conclusions are the same as in Section 3.1.2.3. The small difference, as shown in Figure 3.14, is that the evolution of the hydraulic heads in all elements does not evolve as smoothly as in the case of the rectangular weir (represented in Figure 3.6). The triangular weir may require slightly more time to reach equilibrium. Reservoir 1 is still overflowing after 60 [s] of simulation, and the hydraulic head at the weir is decreasing and approaching zero.

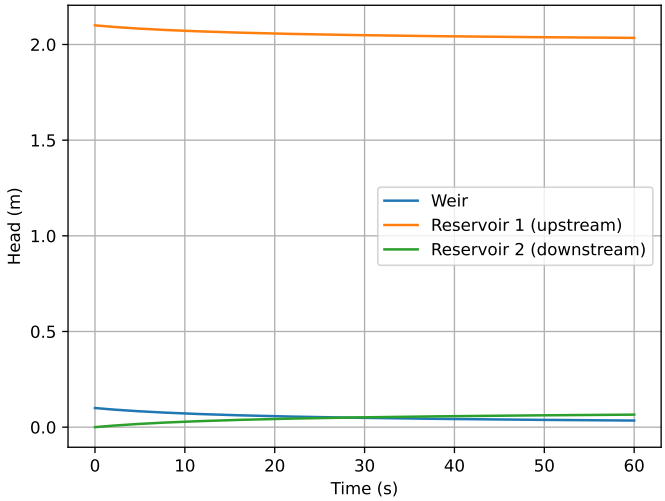

Figure 3.14: Hydraulic heads comparison for Test 3

3.2.2.4 Test 4

Table 3.10 provides the initial values for Test 4. The inflow rate (Q_{in}) is 0.05 [m^3/s] and it is injected consistently throughout the entire test. A simple diagram representing this test is shown in Figure 3.7.

Parameter	Notation	Value	Unit
Water level in reservoir 1	$h_{1,0}$	1.2	m
Water level in reservoir 2	$h_{2,0}$	0	m
Discharge on the weir	Q_w	0	m^3/s

Table 3.10: Initial conditions for Test 4

Figure 3.15 shows that the conclusions of this test are the same as in Section 3.1.2.4. The weir begins to convey the overflow from Reservoir 1 at the same time as the rectangular weir, since the initial conditions are identical. However, once again, the triangular weir is less efficient than the rectangular weir. The hydraulic head at the triangular weir is higher than at the rectangular one (comparison with Figure 3.8a). After 60 [s], the volume in Reservoir 2 for the triangular weir test is lower, since the triangular-shaped weir passes less water than the rectangular-shaped one (see Figure 3.8b).

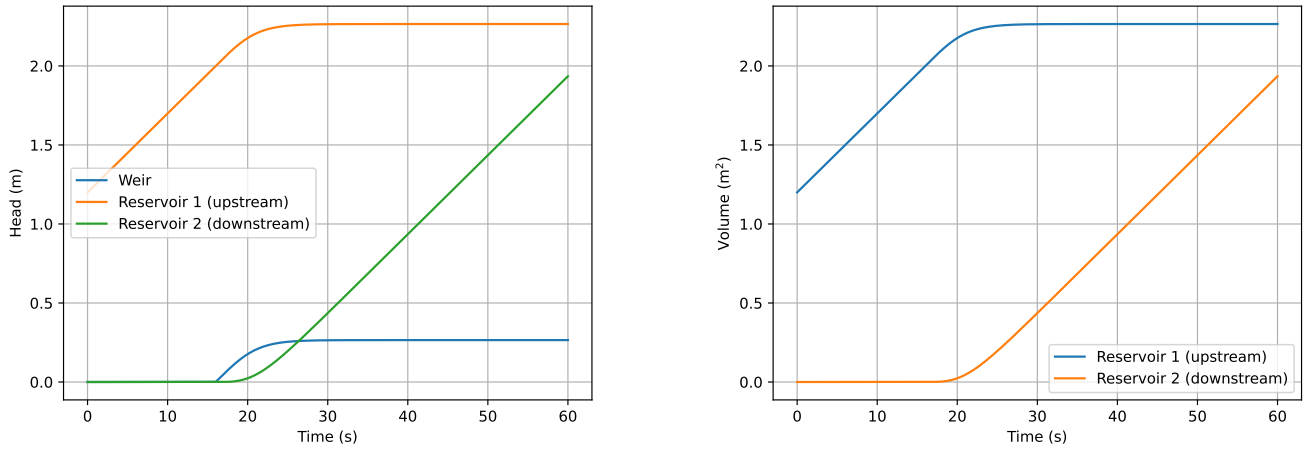

(a) Hydraulic heads comparison

(b) Volumes comparison

Figure 3.15: Results Test 4

By calculation, it is simple:

- Total initial volume: $V_0 = (h_{1,0} \cdot l \cdot L) + (h_{2,0} \cdot l \cdot L) = 1.2\ m^3$
- Total volume at the end of the test ($t_f = 60s$): $V_f = V_0 + Q_{in} \cdot t_f = 4.2\ m^3$

The values computed by the code are as follows: $V_0 = 1.2\ m^3$ (imposed by initial conditions) and $V_f = 4.200277\ m^3$ (numerical solution), which match the expected results. Figure 3.15b shows the evolution of the volume over time. This fourth test confirm that the code appears to be functioning correctly.

3.2.3 Comparison to Analytical Solution

FIGURE 3.16 compares the numerical solution obtained by the solver and the analytical solution defined in EQ. 3.19.
The figure shows that both curves almost perfectly overlap, indicating that the numerical solution correctly models the behaviour of a triangular weir. The solver reproduces the true evolution of the system over time as given by the analytical solution.

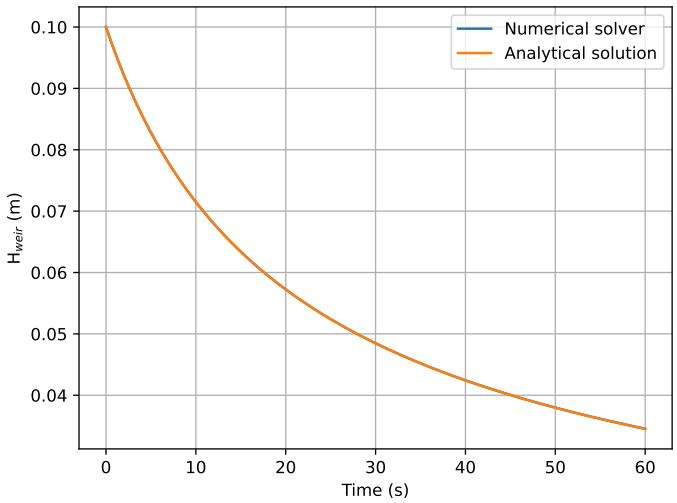

Figure 3.16: Numerical and analytical solutions

3.2.4 Residuals

The study of the residuals for the triangular weir module follows the same methodology as in SECTION 3.1.4. Overall, FIGURE 3.17 shows that the residuals decrease with time with a peak appearing around 54 [s].
Since the Newton-Raphson solver has indeed converged, the peak is not caused by the solver itself. As for the rectangular weir, this behaviour most likely arises from the use of the *softplus* function: the *softplus* must be returning a value very close to zero but not exactly zero, as would occur in reality.
The overall behaviour is somewhat oscillatory throughout the simulation. However, the peak remains very small as it is below $5.5 \cdot 10^{-6}$, and the rest of the residuals stays below this threshold. Therefore, the residuals can be considered to converge.

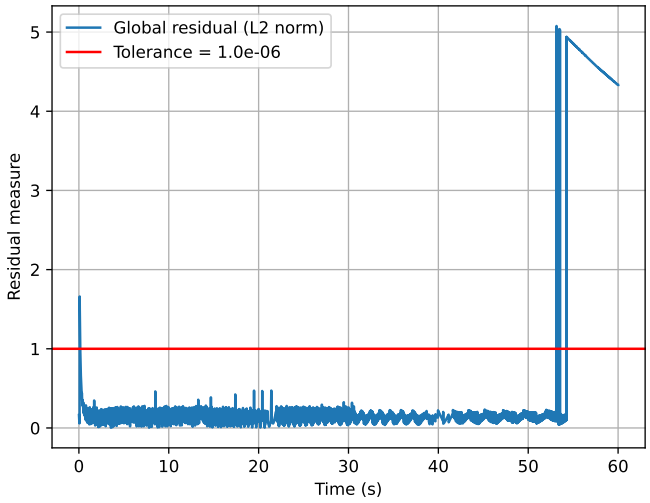

Figure 3.17: L2 norm of residuals (without initial condition value)

3.2.5 Error for Different Time Steps

The time steps selected are the same as for the rectangular weir (see Section 3.1.5), and the methodology is identical.

Figure 3.18 shows the error metrics obtained for the different time steps. As illustrated in Figure 3.18a, for all time steps, NSE remains close to 1. Similarly, in Figure 3.18b, for all time steps, RMSE is close to 0. In both cases, the numerical solution closely matches the analytical one.
Smaller time steps yield a more accurate solution than larger ones. Overall, the numerical solution can be considered stable.

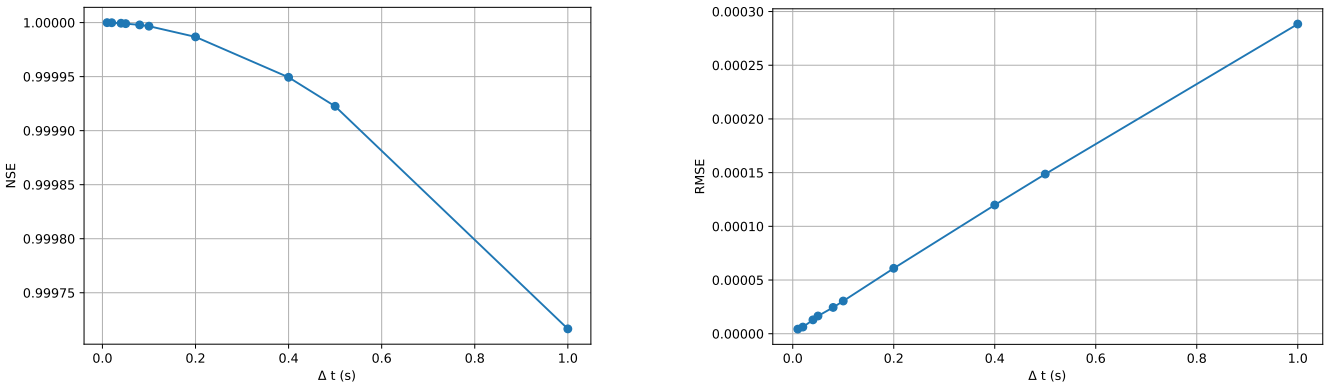

(a) NSE

(b) RMSE

Figure 3.18: Error metrics

3.3 Standard Orifice

3.3.1 Analytical Solution

The outflow from a standard orifice is given by:

$$Q = -C \cdot A \cdot \sqrt{H} \tag{3.20}$$

which can be transformed as:

$$S \cdot \frac{dH_1}{dt} = -C \cdot A \cdot \sqrt{H_1 - H_2} \tag{3.21}$$

$$\frac{dH_1}{dt} = -\frac{C \cdot A}{S} \cdot \sqrt{H_1 - H_2} \tag{3.22}$$

where:

- S is the plan area of the NbS element upstream of the orifice [m²],
- H_1 is the hydraulic head upstream [m],
- H_2 is the hydraulic head downstream [m].

The equation becomes:

$$\frac{dH}{\sqrt{H}} = -2 \cdot \frac{C \cdot A}{S} dt \tag{3.23}$$

$$\int \frac{dH}{\sqrt{H}} = \int -2 \cdot \frac{C \cdot A}{S} dt \tag{3.24}$$

$$2 \cdot \sqrt{H} = -2 \cdot \frac{C \cdot A}{S} \cdot t + C_1 \tag{3.25}$$

$$\sqrt{H} = \frac{-1}{2} \cdot \frac{2 \cdot C \cdot \tan\frac{\theta}{2}}{S} \cdot t + \frac{1}{2} \cdot C_1 \tag{3.26}$$

$$H = \left[\frac{1}{2} \cdot \left(\frac{-C \cdot \tan\frac{\theta}{2}}{S} \cdot t + C_1\right)\right]^{-\frac{2}{3}} \tag{3.27}$$

where:

- C_1 is the integration constant.

The integration constant is found thanks to the initial condition:

$$H(t = 0) = H_0 : \text{initial hydraulic head in NbS element upstream of the orifice}$$

$$\Rightarrow C_1 = 2\sqrt{H_0}$$

Finally, the analytical solution for the standard orifice is:

$$H(t) = \left(\frac{-C \cdot A}{S} \cdot t + \sqrt{H_0}\right)^2 \tag{3.28}$$

3.3.2 Verification Tests

All tests have the same setup: one upstream reservoir (called "Reservoir 1", indicated by subscript 1), one downstream reservoir (called "Reservoir 2", indicated by subscript 2), and both reservoirs are connected by an orifice with a height h_o. TABLE 3.11 provides all necessary parameter values for the tests. The definition of volume (V), plan area (S) and orifice area (A_o) are derived from the values in TABLE 3.11 and do not need to be repeated.
A few assumptions are made for all the tests:

- Reservoir 1 and Reservoir 2 have the exact same dimensions,
- The tests are conducted so that the downstream water level never exceeds the upstream water level ($h_{\text{upstream}} \geq h_{\text{downstream}}$)

Parameter	Notation	Value	Unit
Length of reservoirs and weir	L	1	m
Width of reservoirs	l	1	m
Height of reservoirs	h_r	4	m
Height of orifice	h_o	0.5	m
Elevation of reservoir 1	alt_1	0	m
Elevation of orifice	alt_o	0	m
Elevation of reservoir 2	alt_2	0	m
Discharge coefficient	C	3.1	$m^{1/2}/s$
Orifice radius	r	0.1	m
Time step	Δt	0.01	s
Final time	t_f	60	s

Table 3.11: Parameter values

There are seven verification tests implemented for this module:

- Test 1: The water level in Reservoir 1 is just below the orifice height. Reservoir 2 is initially empty.
- Test 2: The water level in Reservoir 1 is equal to the orifice height. Reservoir 2 is initially empty.
- Test 3: The initial volume in Reservoir 1 produces a water level above the orifice height. Reservoir 2 is initially empty. This test is used to compare the numerical solution to the analytical one, to study the residuals and to analyse the error for different time steps.
- Test 4: The initial water level in Reservoir 1 is above the orifice height. The orifice is submerged on the downstream side, meaning Reservoir 2 is no longer empty and its initial hydraulic head is above h_o. The hydraulic head in Reservoir 1 remains higher than in Reservoir 2. This test is also used to compare the numerical solution to the analytical one, to study the residuals and to analyse the error for different time steps.
- Test 5: Same configuration as Test 4, except that the initial hydraulic heads in Reservoir 1 and Reservoir 2 are equal.

- Test 6: The water level in Reservoir 1 is above the orifice height. An inflow (Q_{in}) enters Reservoir 1, and Reservoir 2 is initially empty. The total volume of water increases with time.
- Test 7: Same configuration as Test 6, except that Reservoir 2 is not empty initially (the orifice is submerged downstream).

3.3.2.1 Test 1

Table 3.12 provides the initial value for test 1 and Figure 3.19 illustrates the test setup.

Parameter	Notation	Value	Unit
Water level in reservoir 1	$h_{1,0}$	0.4	m
Water level in reservoir 2	$h_{2,0}$	0	m
Discharge at the orifice	Q_o	0	m³/s

Table 3.12: Initial conditions for Test 1

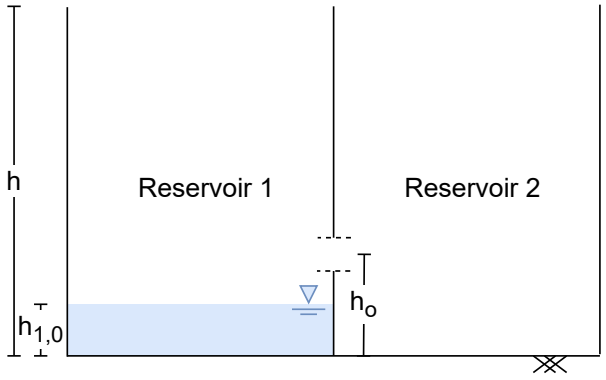

Figure 3.19: Diagram representing Test 1 initially

The reservoir module incorporates a factor η, which represents a drying factor. This factor was introduced to ensure that an empty reservoir does not result in a negative water level. The water level h is defined using the *softplus* function of η, which guarantees a positive value for h. However, this can sometimes lead to hydraulic head values that appear unusual. The hydraulic head is defined as:

$$H_i = \eta_i + \text{altitude}_i$$

In such cases, these anomalies simply indicate that the η-factor is negative, resulting in a negative hydraulic head, as observed in Reservoir 2 in Figure 3.20a.
The water level shown in Figure 3.20b indicates that the water levels in Reservoir 1 remain constant over time, while the water levels of Reservoir 2 do not increase. The conclusions are consistent with those drawn in Section 3.1.2.1: the volume in Reservoir 1 is insufficient to initiate flow through the orifice and fill Reservoir 2.

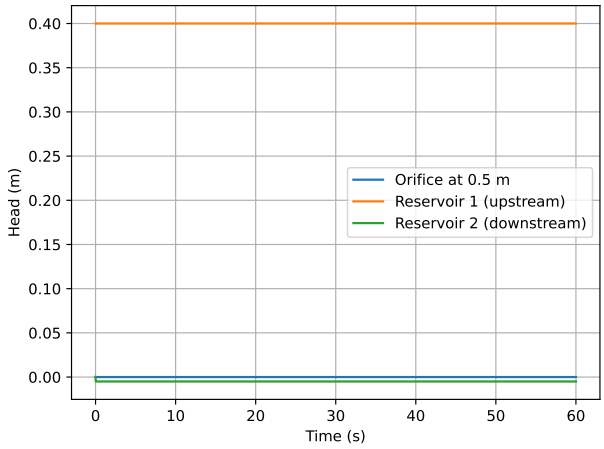

(a) Hydraulic heads comparison

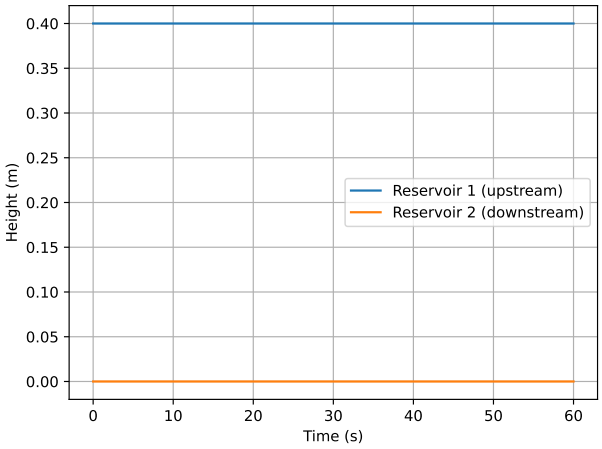

(b) Water levels comparison

Figure 3.20: Results Test 1

3.3.2.2 Test 2

TABLE 3.13 provides the initial values for Test 2 and FIGURE 3.21 illustrates the test setup.

Parameter	Notation	Value	Unit
Water level in reservoir 1	$h_{1,0}$	0.5	m
Water level in reservoir 2	$h_{2,0}$	0	m
Discharge at the orifice	Q_o	0	m^3/s

Table 3.13: Initial conditions for Test 2

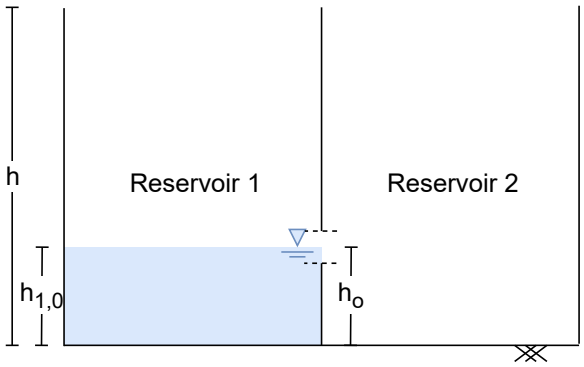

Figure 3.21: Diagram representing Test 2 initially

The conclusions are the same as in SECTION 3.1.2.2. However, in this case, the hydraulic heads are represented in FIGURE 3.22.

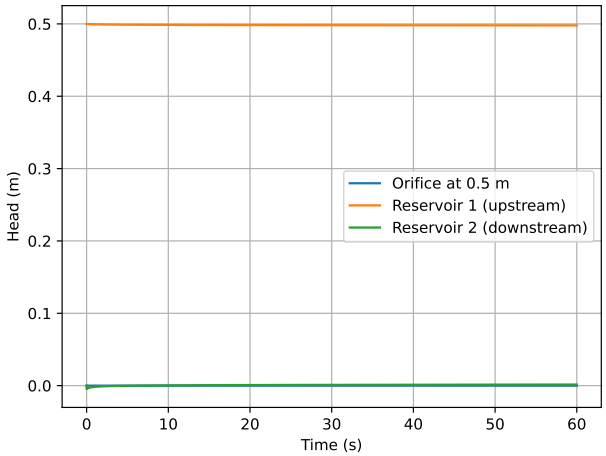

Figure 3.22: Hydraulic heads comparison for Test 2

3.3.2.3 Test 3

Table 3.14 provides the initial values for Test 3 and Figure 3.23 illustrates the test setup.

Parameter	Notation	Value	Unit
Water level in reservoir 1	$h_{1,0}$	1.1	m
Water level in reservoir 2	$h_{2,0}$	0	m
Discharge at the orifice	Q_o	0	m^3/s

Table 3.14: Initial conditions for Test 3

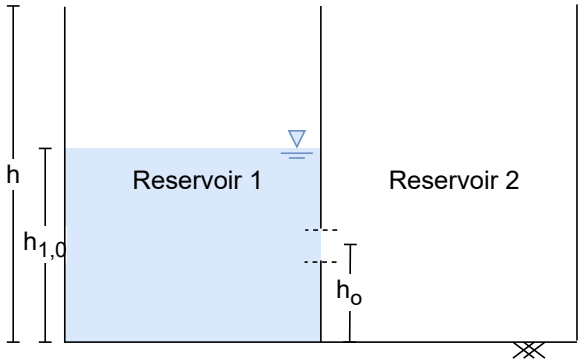

Figure 3.23: Diagram representing Test 3 initially

As shown in Figure 3.24, the hydraulic head in Reservoir 1 decreases while that in Reservoir 2 increases. Reservoir 2 fills up due to the discharge flowing through the orifice. After approximately 12 [s] of simulation, the two reservoirs reach equilibrium since the hydraulic head in Reservoir 1 is equal to that in Reservoir 2. Consequently, the hydraulic head at the orifice approaches zero, indicating that there is no longer a driving head difference across the orifice.
A change in slope is also observable. When the water level in Reservoir 2 reaches the elevation of the orifice (h_o), the hydraulic head for the orifice changes because the switches from a "non-submerged" orifice to a "downstream-submerged" orifice.

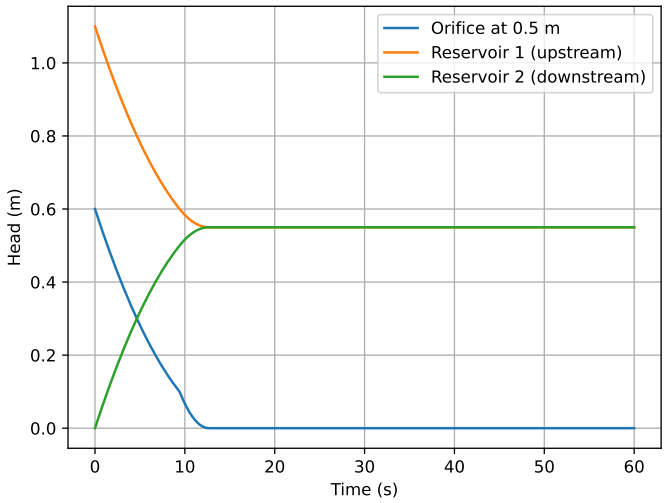

Figure 3.24: Hydraulic heads comparison for Test 3

3.3.2.4 Test 4

Table 3.15 provides the initial values for Test 4 and Figure 3.25 illustrates the test setup.

Parameter	Notation	Value	Unit
Water level in reservoir 1	$h_{1,0}$	4	m
Water level in reservoir 2	$h_{2,0}$	2	m
Discharge at the orifice	Q_o	0	m³/s

Table 3.15: Initial conditions for Test 4

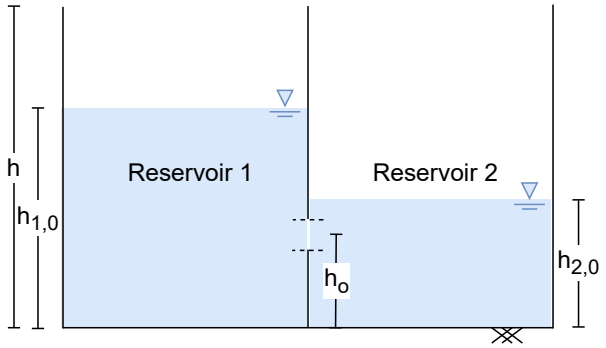

Figure 3.25: Diagram representing Test 4 initially

As shown in FIGURE 3.26, Reservoir 1 discharges water into Reservoir 2 through the orifice. In this case, there is no change in slope since the orifice is submerged throughout the simulation. Once the hydraulic heads in both reservoirs are equal, equilibrium is reached and the flow ceases.

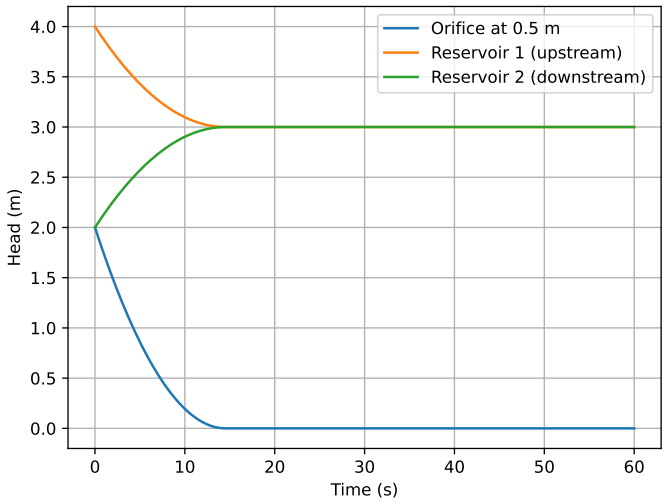

Figure 3.26: Hydraulic heads comparison for Test 4

3.3.2.5 Test 5

TABLE 3.16 provides the initial values for Test 5 and FIGURE 3.27 illustrates the test setup.

Parameter	Notation	Value	Unit
Water level in reservoir 1	$h_{1,0}$	2	m
Water level in reservoir 2	$h_{2,0}$	2	m
Discharge at the orifice	Q_o	0	m³/s

Table 3.16: Initial conditions for Test 5

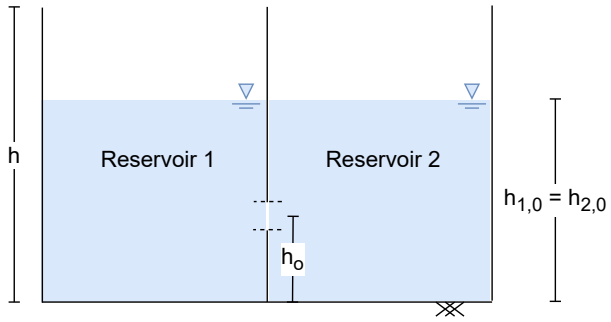

Figure 3.27: Diagram representing Test 5 initially

FIGURE 3.28 shows that the system remains unchanged over time. The reservoirs are already at equilibrium from the initial state, and no flow occurs between them since they share the same hydraulic head.

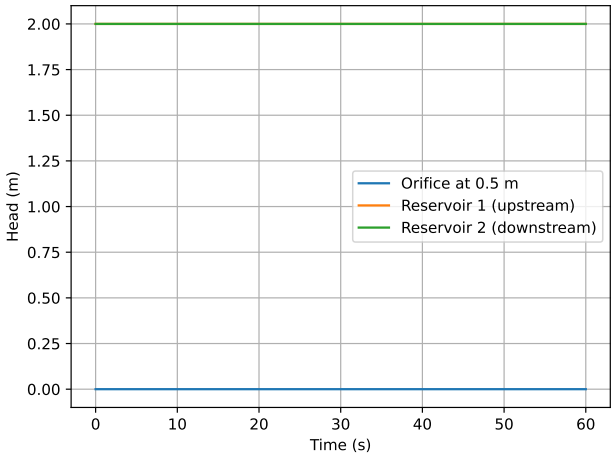

Figure 3.28: Hydraulic heads comparison for Test 5

3.3.2.6 Test 6

TABLE 3.17 provides the initial values for Test 6. The inflow rate (Q_{in}) is 0.05 [m^3/s] and it is injected consistently throughout the entire test. FIGURE 3.29 illustrates the test setup.

Parameter	Notation	Value	Unit
Water level in reservoir 1	$h_{1,0}$	2	m
Water level in reservoir 2	$h_{2,0}$	0	m
Discharge on the weir	Q_w	0	m^3/s

Table 3.17: Initial conditions for Test 6

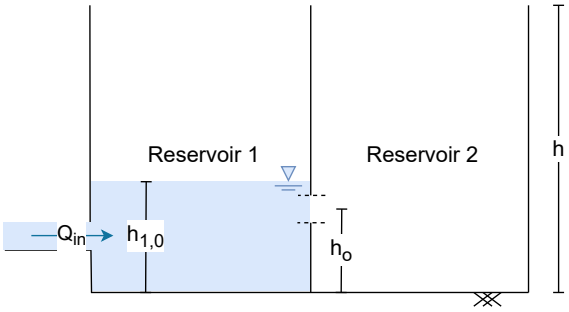

Figure 3.29: Diagram representing Test 6 initially

FIGURE 3.30a shows the evolution of hydraulic heads, which is expected. At the beginning, the orifice conveys most of the flow. Once it is submerged, the slope changes. After a while, an equilibrium is achieved (around 30 [s]), and the hydraulic head at the orifice stabilizes.

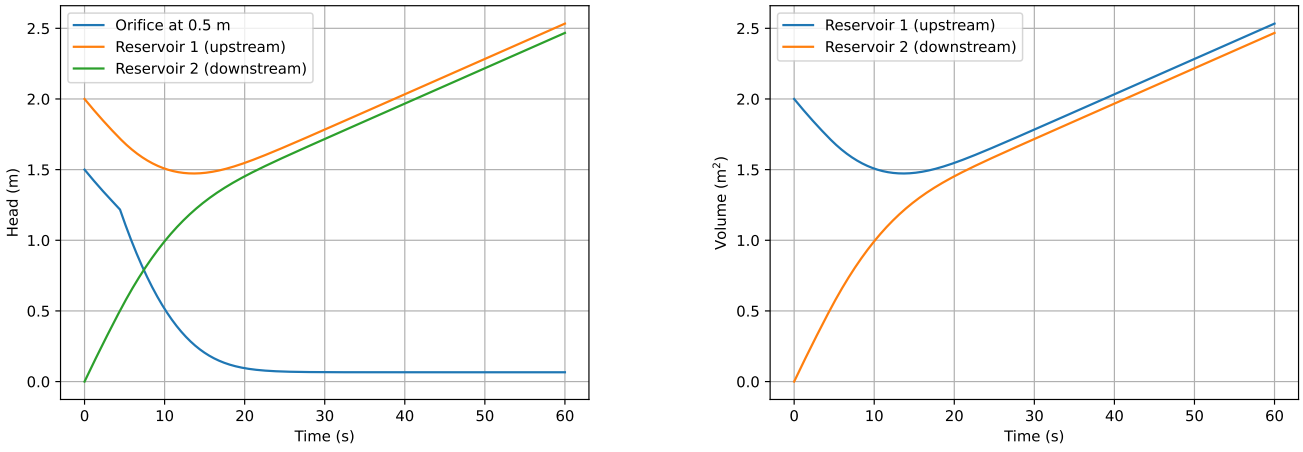

(a) Hydraulic heads comparison

(b) Volumes comparison

Figure 3.30: Results Test 6

By calculation, it is simple:

- Total initial volume: $V_0 = (h_{1,0} \cdot l \cdot L) + (h_{2,0} \cdot l \cdot L) = 2\ \text{m}^3$
- Total volume at the end of the test ($t_f = 60\text{s}$): $V_f = V_0 + Q_{in} \cdot t_f = 5\ \text{m}^3$

The values for the volumes found by the code are as follows: $V_0 = 2\ \text{m}^3$ (imposed by initial conditions) and $V_f = 5.001014\ \text{m}^3$ (numerical solution), which match the expected values. FIGURE 3.30b shows the evolution of the volume over time. Test 6 confirms that the code appears to be functioning correctly.

3.3.2.7 Test 7

TABLE 3.18 provides the initial values for Test 7. The inflow rate (Q_{in}) is 0.05 [m^3/s] and it is injected consistently throughout the entire test. FIGURE 3.31 illustrates the test setup.

Parameter	Notation	Value	Unit
Water level in reservoir 1	$h_{1,0}$	2	m
Water level in reservoir 2	$h_{2,0}$	0.9	m
Discharge on the weir	Q_w	0	m^3/s

Table 3.18: Initial conditions for Test 7

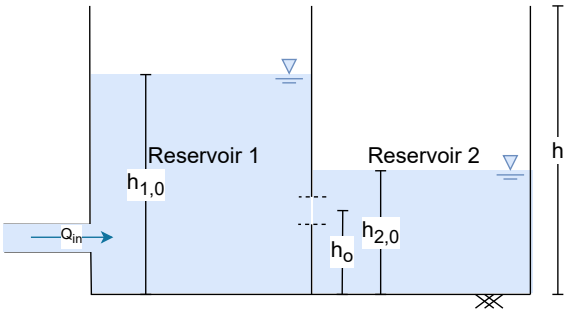

Figure 3.31: Diagram representing Test 7 initially

As shown in FIGURE 3.32a, the hydraulic head at the orifice corresponds to the "submerged downstream" case. After some time, the hydraulic head at the orifice remains constant until the end of the simulation.

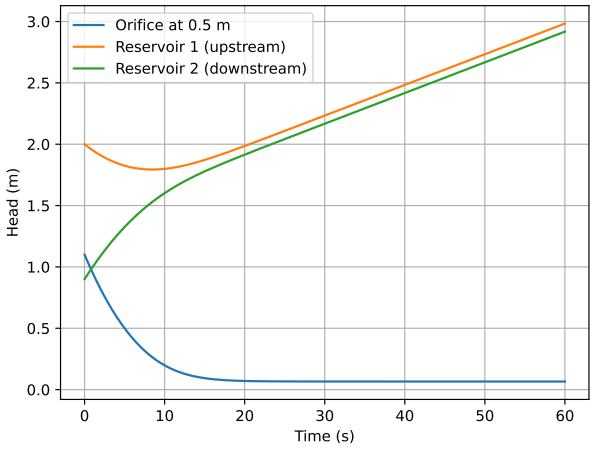

(a) Hydraulic heads comparison

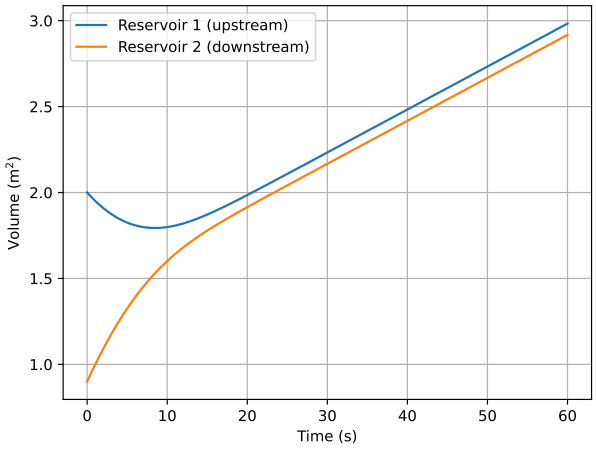

(b) Volumes comparison

Figure 3.32: Results Test 7

By calculation, it is simple:

- Total initial volume: $V_0 = (h_{1,0} \cdot l \cdot L) + (h_{2,0} \cdot l \cdot L) = 2.9\ \text{m}^3$
- Total volume at the end of the test ($t_f = 60\text{s}$): $V_f = V_0 + Q_{in} \cdot t_f = 5.9\ \text{m}^3$

The values for the volumes found by the code are as follows: $V_0 = 2.9$ m^3 (imposed by initial conditions) and $V_f = 5.9010105$ m^3 (numerical solution), which match the expected values. FIGURE 3.32b shows the evolution of the volume over time. Test 7 confirms that the code appears to be functioning correctly.

3.3.3 Comparison to Analytical Solution

FIGURE 3.33 shows the numerical solutions for Tests 3 and 4 and compares them with the analytical solution given by EQ. 3.28.
Two analytical solutions are considered. Both use the same fundamental equation, but the initial condition (H_0) differs. The main difference arises from the definition of the hydraulic head in the orifice discharge law: one represents the non-submerged orifice case, while the other represents the submerged orifice case.

In FIGURE 3.33a, it shows that, for the first 10 [s] of the simulation, the numerical solution overlaps with the analytical solution for the non-submerged orifice. Test 3 was designed to ensure that this case is properly represented, which this figure confirms. After the first 10 [s], the numerical solver finds that the orifice is submerged by the downstream water, and the non-submerged analytical solution is no longer valid. The slope of the numerical solution as it transitions to the submerged case appears roughly parallel to the analytical solution for the submerged orifice. While this observation is not a formal proof, it is with noting.

Test 4 was included to validate the submerged case against its analytical solution. FIGURE 3.33b shows that the numerical solution closely matches the analytical solution.
These comparisons confirm the verification of the numerical solver for both the non-submerged and submerged orifice cases, demonstrating that the solver correctly reproduces these scenarios.

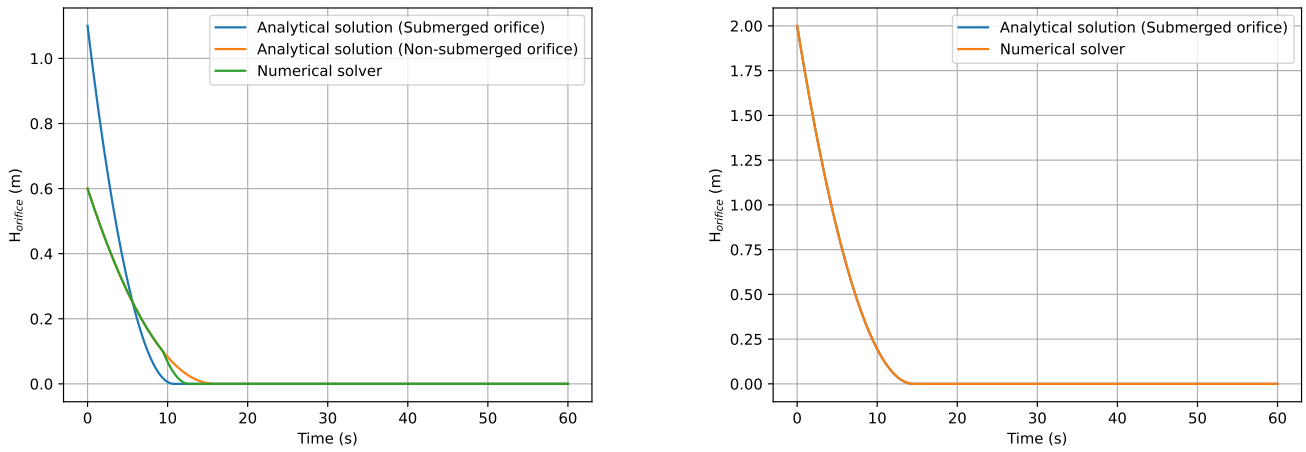

(a) Test 3

(b) Test 4

Figure 3.33: Numerical and analytical solutions

3.3.4 Residuals

The methodology used to study the residuals for the standard orifice module is the same as in SECTION 3.1.4. In general, FIGURE 3.34 shows that the residuals decrease over time, with a peak appearing around 13 [s] and 15 [s] for Test 3 and Test 4, respectively. A second, smaller peak for Test 3 appears around 9 [s].

The peak at $t = 1$ for Test 3 may still be a consequence of the initial conditions.
Newton-Raphson was verified and indeed converged, so the peak can not be caused by the solver. The largest peaks observed in both tests are most likely due to the use of the function `safe_sqrt()`. The orifice module is governed by an equation proportional to the square root of H (see Eq. 2.8). When this expression is differentiated to form the Jacobian matrix, it results in an expression proportional to $H^{-1/2}$. Numerical noise may generate slightly negative values of H, which fall outside the domain of the square root. This issue is addressed by the function `safe_sqrt()`, which also resolves the issue of $H = 0$. Mathematically, the Jacobian would tend toward infinity for this residual, since $\frac{1}{H^{1/2}} \to \infty$ as $H = 0$. The function `safe_sqrt()` enforces a finite value by forcing the output to zero instead of allowing divergence. These largest peaks may also be influenced by the use of the *softplus* function.
The smaller peak observed in Test 3 occurs during a change in slope in the simulation, which corresponds to a modification in the definition of the hydraulic head. As a result, the solver transitions from one definition to another, resulting in a small transient peak in the residuals. This change in definition is implemented through the *softplus* function.
Both tests present a peculiar behaviour: after the peak, the residual decreases and remains on a plateau. However, the spike remains limited: the largest peak stays below $2 \cdot 10^{-5}$, while the smaller in Test 3 remains below 10^{-5}, and below $3 \cdot 10^{-5}$ for Test 4. The plateaus are still below $0.25 \cdot 10^{-5}$ for Test 3 and below 10^{-5} for Test 4, a behaviour that might be specific to this test. Consequently, the residuals can be considered converged.

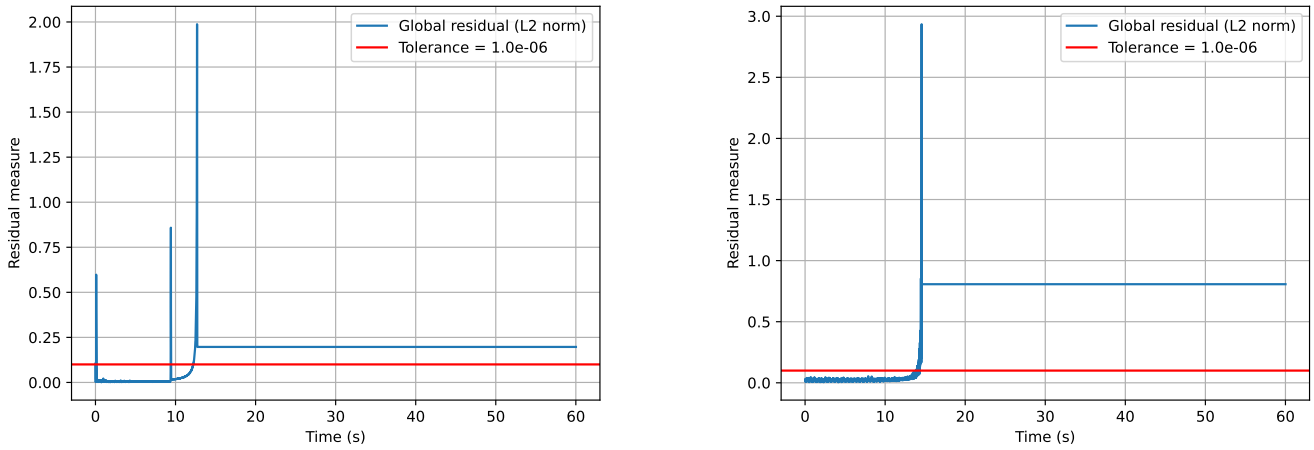

(a) Test 3

(b) Test 4

Figure 3.34: L2 norm of residuals (without initial conditions)

3.3.5 Error for Different Time Steps

The methodology used to study the errors for different time steps is the same as in Section 3.1.5.
For both Figures 3.35a and 3.36a, the NSE values for each time step are close to 1. In Figures 3.35b and 3.36b, the RMSE values, for all time steps, are close to 0. Both metrics indicate that the numerical solver closely approximated the analytical solution
In both cases, smaller time steps yield higher accuracy in the numerical model. Consequently, the numerical solver can be considered stable.

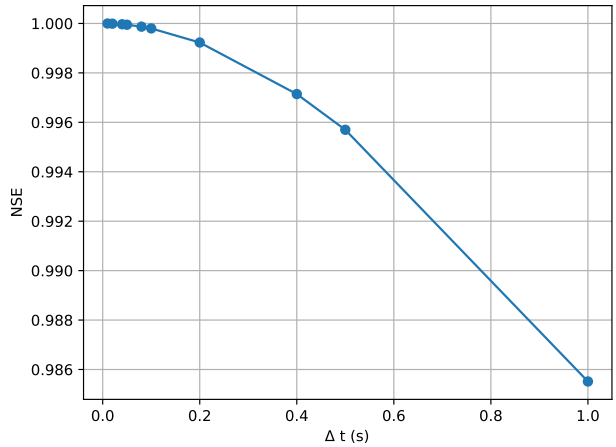

(a) NSE

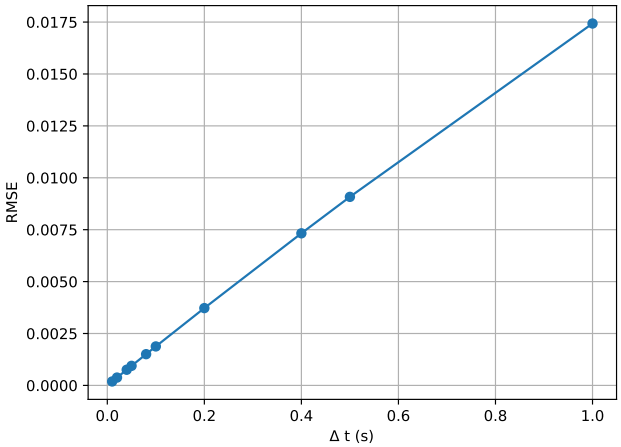

(b) RMSE

Figure 3.35: Error metrics for Test 3

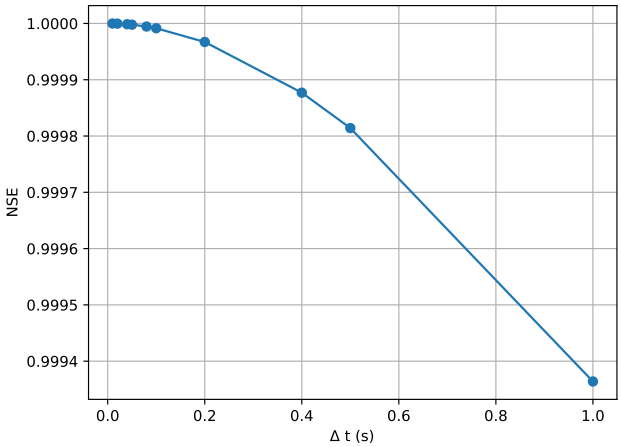

(a) NSE

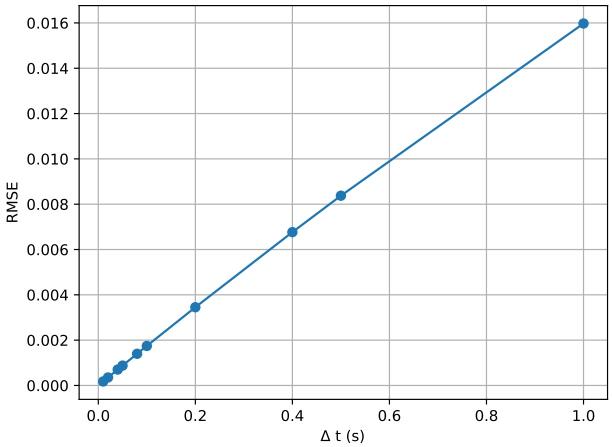

(b) RMSE

Figure 3.36: Error metrics for Test 4

3.4 Perforated Riser

3.4.1 Analytical Solution

The outflow from a perforated riser is given by:

$$Q = -\frac{2 \cdot A_p \cdot C_p}{3 \cdot H_s} \cdot H^{\frac{3}{2}} \tag{3.29}$$

which can be transformed as:

$$S \cdot \frac{dH}{dt} = -\frac{2 \cdot A_p \cdot C_p}{3 \cdot H_s} \cdot H^{\frac{3}{2}} \tag{3.30}$$

where:

- S is the plan area of the chamber [m²].

The equation can be developed as follows:

$$\frac{dH}{H^{\frac{3}{2}}} = -\frac{2 \cdot A_p \cdot C_p}{3 \cdot H_s \cdot S} dt \tag{3.31}$$

$$\int \frac{dH}{H^{\frac{3}{2}}} = \int -\frac{C \cdot L}{S} dt \tag{3.32}$$

$$-2 \cdot H^{\frac{-1}{2}} = -\frac{2 \cdot A_p \cdot C_p}{3 \cdot H_s \cdot S} \cdot t + C_1 \tag{3.33}$$

$$H^{\frac{-1}{2}} = \frac{1}{2} \cdot \frac{2 \cdot A_p \cdot C_p}{3 \cdot H_s \cdot S} \cdot t + \frac{-1}{2} \cdot C_1 \tag{3.34}$$

$$H = 4 \cdot \left[\frac{2 \cdot A_p \cdot C_p}{3 \cdot H_s \cdot S} \cdot t - C_1 \right]^{-2} \tag{3.35}$$

where:

- C_1 is the integration constant.

The integration constant is found thanks to the initial condition:

$$H(t = 0) = H_0 : \text{initial hydraulic head in the chamber}$$

$$\Rightarrow C_1 = -2 \cdot H_0^{-\frac{1}{2}}$$

Finally, the analytical solution for the perforated riser is:

$$H(t) = 2 \cdot \left[\frac{A_p \cdot C_p}{3 \cdot H_s \cdot S} \cdot t + H_0^{-\frac{1}{2}} \right]^{-2} \tag{3.36}$$

3.4.2 Verification Tests

The tests are carried out as follows: a perforated riser is placed inside a chamber, and this riser is linked to a reservoir outside the chamber. The chamber is filled with water, and depending on the water level, a

discharge may or may not enter the perforated riser.
The parameter values required to describe the tests are shown in Table 3.19, and Figure 3.37 illustrates some of these parameters on a simple close-up diagram of a perforated riser.
A few assumptions are made for all the tests:

- Reservoir and chamber have the exact identical dimensions,
- The tests are conducted so that the downstream water level never exceeds the upstream water level ($h_{\text{upstream}} \geq h_{\text{downstream}}$)

Parameter	Notation	Value	Unit
Length of chamber and reservoir	L	1	m
Width of chamber and reservoir	l	1	m
Height of chamber and reservoir	h_r	5	m
Height of perforated riser	H_s	3	m
Elevation of reservoir	alt_1	0	m
Elevation of chamber	alt_2	0	m
Discharge coefficient	C	2.7	$m^{1/2}/s$
Orifices radius	r	0.1	m
Number of orifices (on 1 row)	n_o	6	/
Number of rows	n_r	3	/
Distance between 2 holes	S_d	0.5	m
Time step	Δt	0.01	s
Final time	t_f	60	s

Table 3.19: Parameter values

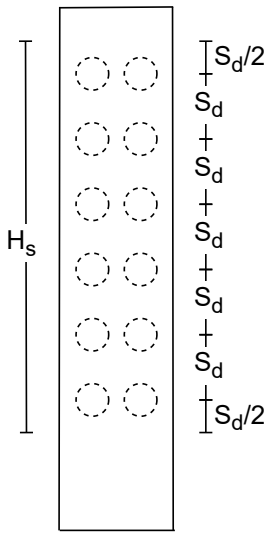

Figure 3.37: Detail of perforated riser

There are four verification tests implemented for this module:

- Test 1: The water level in the chamber is just below the perforated riser's height.
- Test 2: The water level in the chamber is equal to the perforated riser's height.
- Test 3: The chamber contains a volume of water that produces a water level above the perforated riser's height. This test is used to compare the numerical solution to the analytical solution, to study the residuals, and to evaluate the error for different time steps.
- Test 4: The water level in the chamber is equal to the perforated riser's height, with an additional inflow rate entering the chamber (Q_{in}). The total volume of water increases at each time step.

3.4.2.1 Test 1

Table 3.20 provides the initial values for Test 1 and Figure 3.38 illustrates the test setup.

Parameter	Notation	Value	Unit
Water level in chamber	$h_{1,0}$	1.5	m
Water level in reservoir	$h_{2,0}$	0	m
Discharge at the riser	Q_o	0	m^3/s

Table 3.20: Initial conditions for Test 1

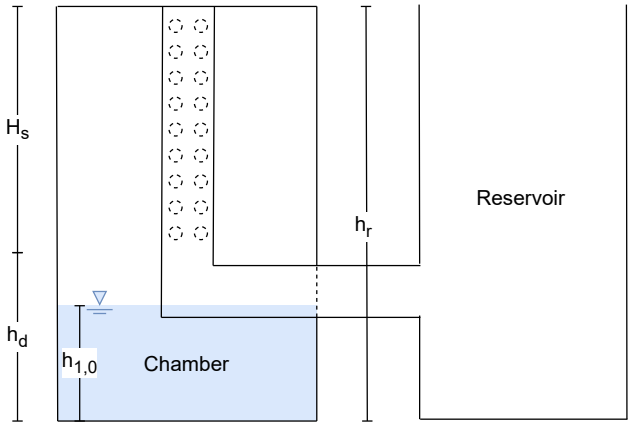

Figure 3.38: Diagram representing Test 1 initially

As shown in FIGURE 3.39, no flow occurs between the hydraulic structures. Indeed, the volume in the chamber is insufficient to activate the perforated riser.

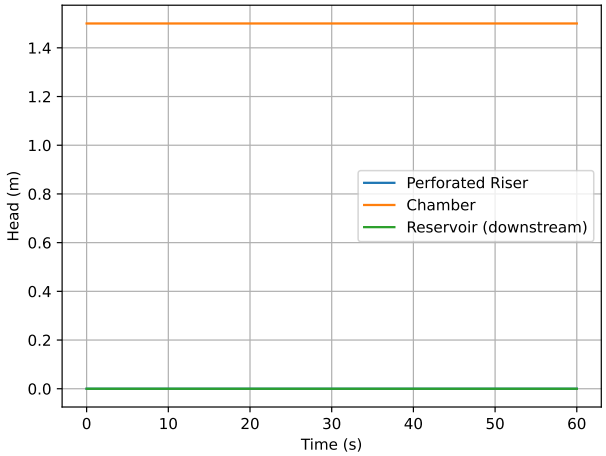

Figure 3.39: Hydraulic heads comparison for Test 1

3.4.2.2 Test 2

TABLE 3.21 provides the initial values for Test 2 and FIGURE 3.40 illustrates the test setup.

Parameter	Notation	Value	Unit
Water level in chamber	$h_{1,0}$	2	m
Water level in reservoir	$h_{2,0}$	0	m
Discharge at the riser	Q_o	0	m^3/s

Table 3.21: Initial conditions for Test 2

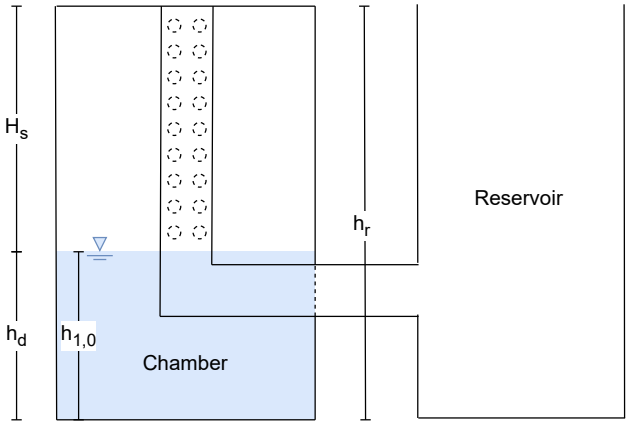

Figure 3.40: Diagram representing Test 2 initially

FIGURE 3.41 shows that when the hydraulic head in the chamber reaches the threshold of the perforated riser entry, no flow occurs. This confirms that the control mechanism behaves correctly at the activation limit.

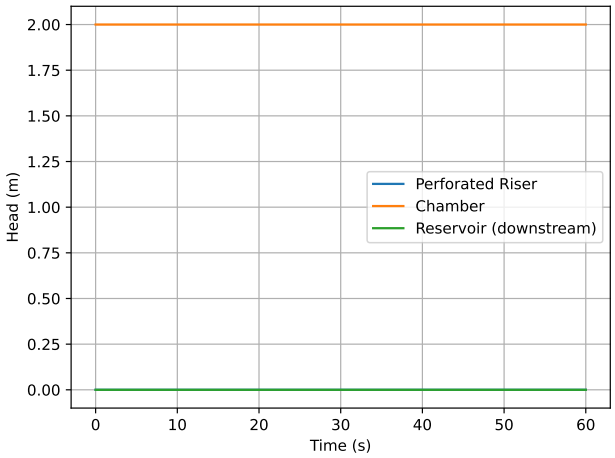

Figure 3.41: Hydraulic heads comparison for Test 2

3.4.2.3 Test 3

TABLE 3.22 provides the initial values for Test 3 and FIGURE 3.42 illustrates the test setup.

Parameter	Notation	Value	Unit
Water level in chamber	$h_{1,0}$	2.5	m
Water level in reservoir	$h_{2,0}$	0	m
Discharge at the riser	Q_o	0	m^3/s

Table 3.22: Initial conditions for Test 3

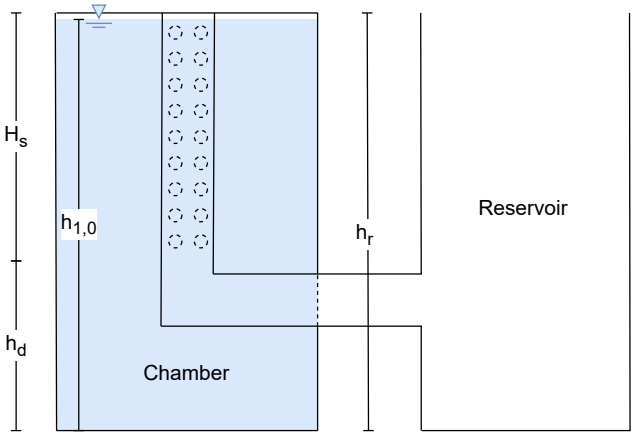

Figure 3.42: Diagram representing Test 3 initially

In FIGURE 3.43, the evolution of hydraulic heads in all hydraulic elements is shown. As expected, the volume in the chamber is sufficient to be captured by the perforated riser, producing a discharge that reaches the reservoir. Around 30 [s], the perforated riser has emptied the chamber down to the bottom of the riser. By the end of the simulation, the reservoir's hydraulic head equals the initial hydraulic head at the riser, verifying the functioning of the module.

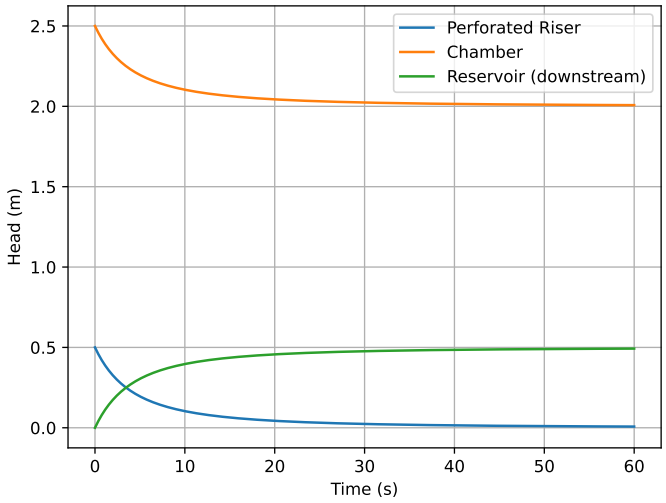

Figure 3.43: Hydraulic heads comparison for Test 3

3.4.2.4 Test 4

TABLE 3.23 provides the initial value for Test 4. The inflow rate (Q_{in}) is 0.05 [m^3/s] and it is injected consistently throughout the entire test. 3.44 illustrates the test setup.

Parameter	Notation	Value	Unit
Water level in chamber	$h_{1,0}$	1.25	m
Water level in reservoir	$h_{2,0}$	0	m
Discharge at the riser	Q_o	0	m^3/s

Table 3.23: Initial conditions for Test 4

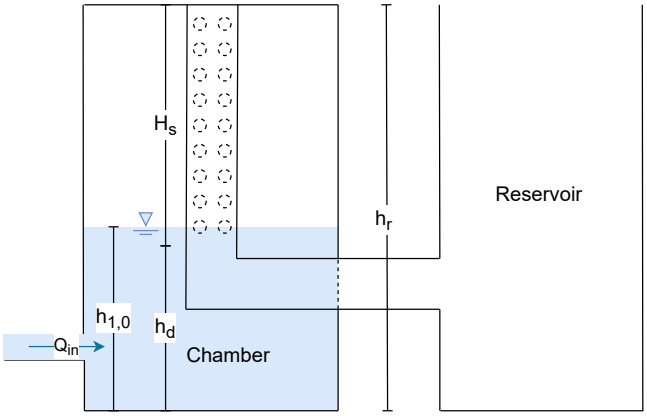

Figure 3.44: Diagram representing Test 4 initially

In FIGURE 3.45a, it can be observed that no flow occurs until the hydraulic head in the chamber reaches 2 [m]. Thereafter, the hydraulic head at the riser increases, reaching a maximum of approximately 0.3 [m].

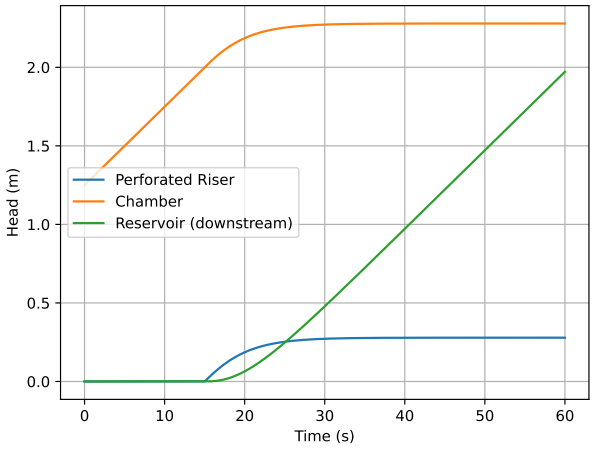

(a) Hydraulic heads comparison

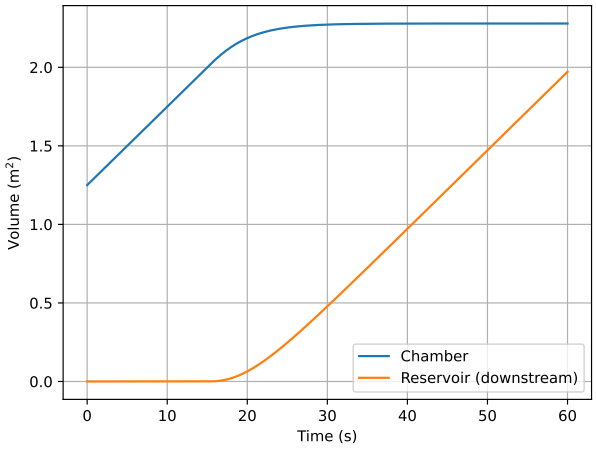

(b) Volumes comparison

Figure 3.45: Results Test 4

By calculation, it is simple:

- Total volume initially: $V_0 = (h_{1,0} \cdot l \cdot L) + (h_{2,0} \cdot l \cdot L) = 1{,}25\ \text{m}^3$
- Total volume at the end of the test ($t_f = 60\text{s}$): $V_f = V_0 + Q_{in} \cdot t_f = 4{,}25\ \text{m}^3$

The values for the volumes found by the code are as follows: $V_0 = 1.25\ \text{m}^3$ (imposed by initial conditions) and $V_f = 4.2504244\ \text{m}^3$ (numerical solution) which match the expected values. Figure 3.45b shows the evolution of the volume over time. This fourth test confirm that the code appears to be functioning correctly.

3.4.3 Comparison to Analytical Solution

Figure 3.46 illustrates the comparison between the numerical solver and the analytical solution, the latter being computed using Eq. 3.36. The figure shows that both solutions overlap closely, demonstrating the correct operation of the module.

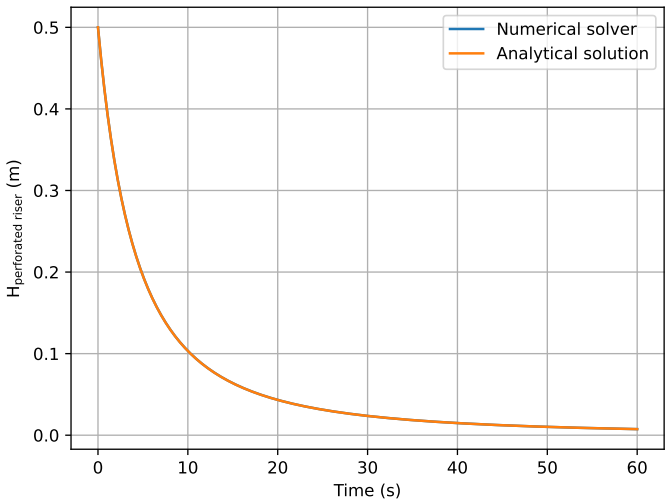

Figure 3.46: Numerical and analytical solutions

3.4.4 Residuals

The methodology used to study the residuals for the perforated riser module is the same as in Section 3.1.4.

In general, Figure 3.47 shows that the residuals decrease over time, with a peak appearing around 50 [s]. The very first peak may still be a consequence of the initial conditions.
The solver was verified, and the Newton-Raphson method indeed converged, so the solver is not responsible for this spike. Like the other modules, the perforated riser was defined using the *softplus* function, which may explain the occurrence of the peak.
The overall behaviour is oscillatory throughout the simulation. Nevertheless, the peak remains below $5.5 \cdot 10^{-6}$, and the rest of the residuals stay below the threshold. The residuals can be considered converged

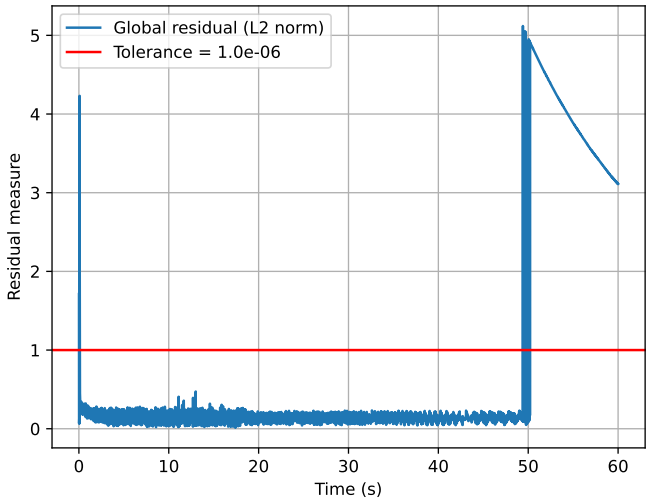

Figure 3.47: L2 norm of residuals (without initial condition value)

3.4.5 Error for Different Time Steps

The methodology used to study the errors for different time steps is the same as in Section 3.1.5.

The NSE values shown in Figure 3.48a are close to 1 for all time steps, and the RMSE values shown in Figure 3.48b are closed to 0 for all time steps. In both cases, this indicates that the numerical solution closely matches the analytical solution. Moreover, both metrics show that smaller time steps lead to higher accuracy. Therefore, the numerical solution can be considered stable.

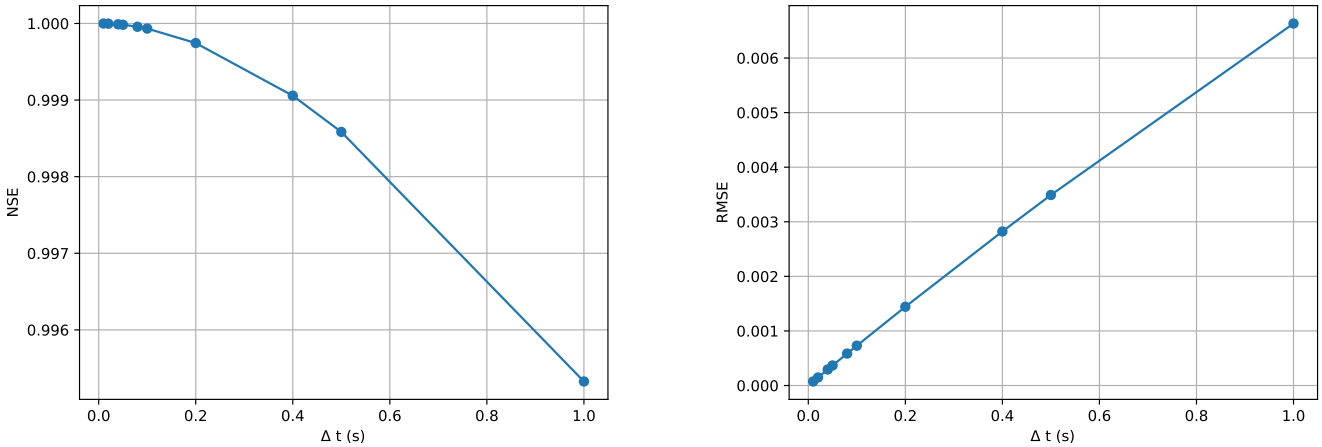

(a) NSE

(b) RMSE

Figure 3.48: Error metrics

Chapter 4

Applications

In this chapter, four applications from the technical guide *Référentiel : Gestion durable des eaux pluviales* published by the SPW ([42], hereafter referred to as the SPW Technical Guide) are modelled using the WSC solver. These applications were initially implemented in an Excel sheet, and the results are available in the SPW Technical Guide. Here, the numerical outputs from the solver are compared with those obtained from the Excel to highlight the added value of a numerical solver over a spreadsheet-based approach.
The information provided for each applications were limited, as the Excel sheet does not require additional details. This tool intended to provide a rough approximation of possible designs. Requirements in terms of storage capacity are often overestimated due to the ease of use, which can lead to a lack of precision; consequently, significant safety factors are implicitly included. The present solver offers a more realistic representation, and therefore demands more detailed input data. As a result of the limited information available, several assumptions were required to implement the applications in the solver.
Furthermore, the Excel sheet provides very limited information regarding components interactions. Its results are steady-state, implying the infiltration rate is constant and the timing of peak volumes is unknown. In contrast, the WSC solver produces unsteady results, allowing the analysis and the representation of the actual temporal evolution of flows and infiltration rates, among others.

4.1 Initial Conditions

Before presenting the applications, a few explanations regarding the initial conditions are required. This step is crucial because poorly defined initial conditions may prevent the solver from converging to meaningful results.
The coefficient η represents the drying effect within the reservoir or swale, and the hydraulic head becomes $H = \eta +$ altitude. In the different modules where η is treated as an intrinsic unknown, the residuals are defined using the `softplus` function, such that $h = \frac{1}{\beta} \cdot \texttt{softplus}(\beta \cdot \eta)$, where β is a constant. The initials conditions are defined as follows:

- Drying effect coefficient: $\eta_0 = 0.0$;
- Water level: $h_0 = \frac{1}{\beta} \cdot \texttt{softplus}(\beta \cdot \eta_0)$;

- Hydraulic head: $H_0 = h_0$ + altitude, where the altitude depends on the module and is usually obtained from WalOnMap;
- Volume: $V_0 = h_0 \cdot S_m$ with S_m being the plan area of the module;
- Cumulative infiltration: $F_0 = 2$ [m] (explanations in the next subsection);
- Infiltration discharge: $f_0 = K_s \cdot A \cdot \left(1 + \frac{\psi^* \cdot \Delta\theta}{F_0}\right)$ (more explanations in Eq. 2.2 about Green-Ampt);
- Discharge for pipes (unsteady Bernoulli): $Q_{0,pipe} = \left[2 \cdot \gamma \cdot \frac{(H_{0,in} - H_{0,out})}{\lambda}\right]^{1/2}$
  where:
  - $H_{0,in}$ is the hydraulic head at the entry of the pipe;
  - $H_{0,out}$ is the hydraulic head at the exit of the pipe;
  - $\gamma = 9.81 \cdot \frac{D_{\text{pipe}}}{L_{\text{pipe}}}$;
  - D_{pipe} is the diameter of the pipe;
  - L_{pipe} is the length of the pipe;
  - $\lambda = \frac{f_{\text{pipe}}}{D_{\text{pipe}}} \cdot \left[\pi \cdot \left(\frac{D_{\text{pipe}}}{2}\right)^2\right]$;
  - f_{pipe} is the friction factor.
- Discharge for weirs (discharge law): $Q_{0,weir} = C \cdot K \cdot H_0^n$
  where:
  - C is the discharge coefficient;
  - K is the constant that is different depending on the discharge law (presented in Eq. 2.6, 2.7, 2.8 and 2.9);
  - n is the exponent that is different depending on the discharge law (presented in Eq. 2.6, 2.7, 2.8 and 2.9);
  - H is the hydraulic head difference which definition depends on the control mechanism used.

4.2 Example 1

4.2.1 Context

The first application is located in Neupré, Belgium. It comprises one large rooftop, a smaller rooftop, an impervious area surrounding the larger building, and a vegetated area. The total surface of this site amounts to 614 [m²]. To manage stormwater, an 80 [m²] swale and an infiltration well with a diameter of 1.5 [m] were implemented.
The infiltration well intercepts precipitation from the front of the larger building as well as from a portion of its rooftop, whereas the swale collects runoff from the remaining portion of the larger rooftop in addition to the smaller rooftop. FIGURE 4.1 depicts the location plan provided in the SPW Technical Guide.
The SPW Technical Guide also specifies the contributing areas corresponding to each NbS device. Moreover, the plan location allows to measure the distances between the infrastructures. These values are reported in the following table:

Type of area	Runoff coefficient	Gross area [m²]	Runoff area [m²]	Elevation[1] [m]	Pipe length [m]
Impervious (well)	0.9	20	18	262	8
Rooftop (well)	1	57	57	267.5	8.8
Rooftop 1 (swale)	1	31.6	79	265	16
Rooftop 2 (swale)	1	47.4	79	265	4

[1] Found on WalOnMap

Figure 4.1: Example 1 location plan

The SPW Technical Guide makes the following assumptions:

- The vegetated area (shown in green in FIGURE 4.1) directly infiltrates rainfall;
- The impervious area located behind the larger building drains into the vegetated area.

In the WSC solver, only the swale and the infiltration well are modelled, as the SPW Technical Guide focused exclusively on these devices. Consequently, the vegetated area is not considered in the model. The runoff areas therefore correspond only to the impervious surfaces and rooftops.

Due to the lack of available information, additional assumptions were required to model the system in the WSC model. The following assumptions are adopted:

- As the distribution of runoff between the two rooftop areas is not explicitly provided, it is assumed that the swale receives $0.4 \cdot 79 = 31.6$ [m²] from the larger building and 47.4 [m²] from the smaller building;
- All pipes have a diameter of 0.05 [m] and are made of PVC, with a Manning roughness coefficient of 0.009 [43];
- Runoff from the rooftops is conveyed to the bottom of the building through a rectangular weir with a discharge coefficient $C = 1.69$ [$m^{1/2} \cdot s^{-1}$] and a crest length $L_{crest} = D_{pipe} = 0.05$ [m];
- Longitudinal head losses in vertical pipes (through the weir) are neglected, whereas head losses in horizontal pipes are fully accounted for;
- All horizontal pipes are assigned a minimum slope of 3%;
- The infiltration rate considered by the SPW Technical Guide is assumed constant over time; however, the WSC model relies on the Green-Ampt formulation, which allows infiltration to vary temporally. In the following section, a calibration is performed to identify the soil type and initial saturation level that best reproduces the SPW Technical Guide value. As the SPW Technical Guide consistently adopts an infiltration rate of $5 \cdot 10^{-6}$ [m/s] in the other examples, the soil parameters yielding the closest results are selected and applied to the remaining simulations in order to enable a comparison between the WSC model and the Excel-based calculations.

Parameter	Value	Unit
Length	9	m
Width	2	m
Height	0.23	m
Angle	30	°
Infiltration surface	18	m²
Return period	25	years
Rainfall duration	6h10’	/
Elevation	261.77	m

Table 4.1: Parameters for swale

Parameter	Value	Unit
Diameter	1.5	m
Height	2	m
Infiltration surface	11.19	m²
Return period	25	years
Rainfall duration	10h	/
Elevation	260	m

Table 4.2: Parameters for infiltration well

4.2.2 Type of Soils (Swale Scenario)

As mentioned previously, the SPW Technical Guide does not specify the soil type, although an infiltration rate is provided. The objective of this subsection is therefore to identify the soil type and initial soil conditions that yield results as close as possible to those obtained with the SPW Technical Guide. Once identified, these

soil parameters are applied to all applications, as the SPW Technical Guide consistently adopts the same infiltration rate.

For the parcel located in Neupré, the interactive map provided by WalOnMap (`https://geoportail.wallonie.be/walonmap`) indicated that the site is underlain by an Aha soil type, corresponding to a silty soil with relatively poor natural drainage. As drainage performance is a key aspect of stormwater management, the swale and the infiltration well may have been locally reworked so that they are constructed in soils with more favourable infiltration properties.

The present analysis relies on Green-Ampt parameters provided in the *HEC-RAS Hydraulic Reference Manual* [44], which summarises typical parameters values for various soil types.

Figure 4.2 is obtained using a cumulative infiltration depth of $F = 2$ [m], indicating that the soil is already highly saturated, in agreement with the assumptions of the SPW Technical Guide system. The figure suggests that the original loam soil was likely not retained in its natural state and that the soil properties tend instead toward those of a sandy loam or a silt loam, as the resulting peak volumes are close to the SPW Technical Guide outcome.

Table 4.3 compares the results obtained for these two soil types with those of the Excel-based calculations. The silt loam option is discarded, as the drainage time ($t_{drainage}$) is significantly longer than that reported in the SPW Technical Guide. For the remainder of this chapter, the simulations therefore rely on the Green-Ampt parameters associated with sandy loam as listed in Table 4.4.

Method	V_{peak} (m^3)	$t_{drainage}$ (s)
Excel sheet (SPW)	3.3	20h22’
WSC solver (sandy loam)	3.1	20h03’
WSC solver (silt loam)	3.3	28h38’

Table 4.3: Results comparison between the SPW Excel sheet and the WSC solver for sandy loam and silt loam soils

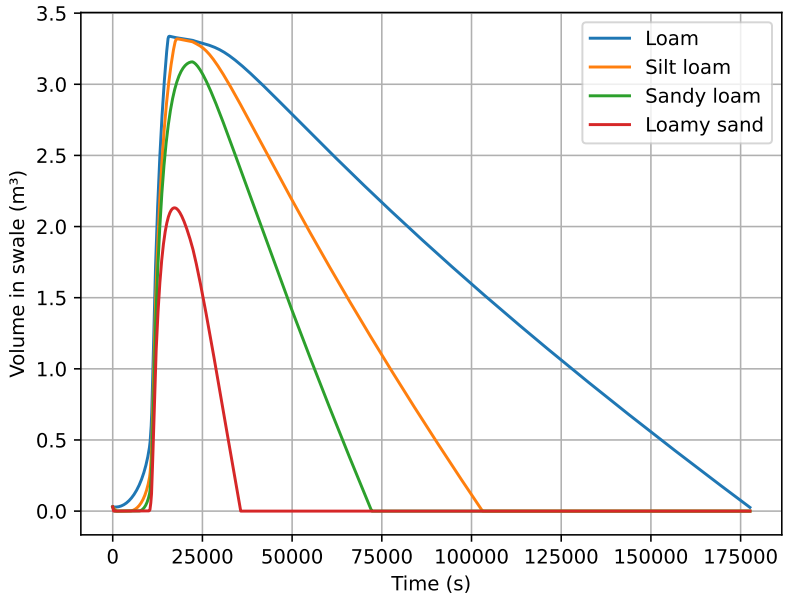

Figure 4.2: Swale volume for different types of soil

Soil	K_s (m/s)	$\Delta\theta$ (-)	ψ^* (m)	F (m)
Sandy loam	$3.028 \cdot 10^{-6}$	0.4615	0.11015	2

Table 4.4: Green-Ampt parameters for sandy loam

FIGURE 4.4 presents the cross-section of the swale scenario in Example 1, while FIGURE 4.3 illustrates each modules created to model this scenario in the WSC model.

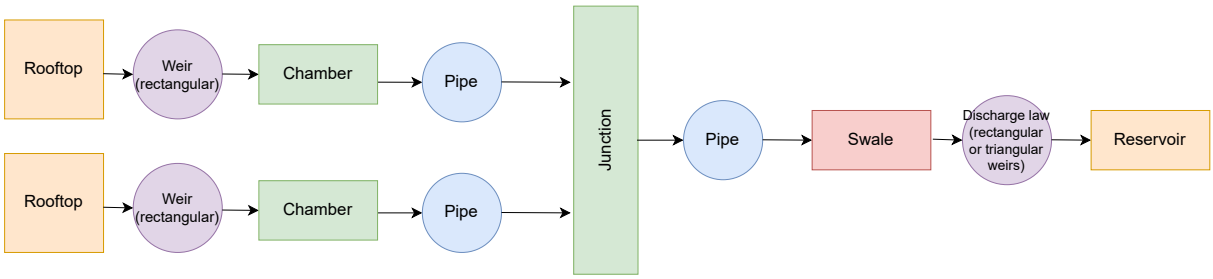

Figure 4.3: Flow diagram (swale scenario)

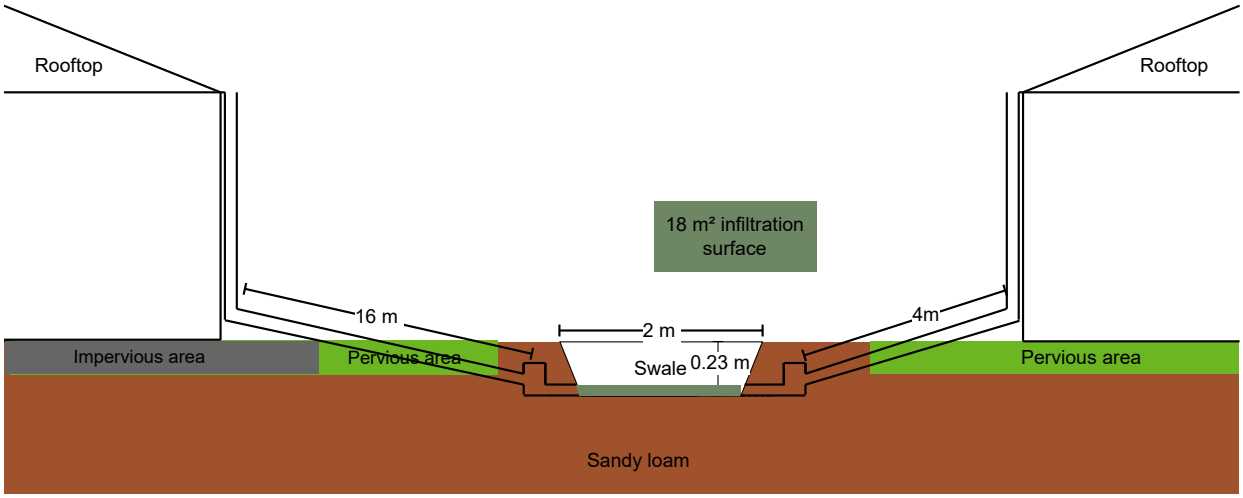

Figure 4.4: Cross section of Example 1 (swale scenario)

4.2.3 Comparison of Different Connections (Well Scenario)

Initially, the connections between the impervious area and the infiltration well was modelled using a single underground pipe. In practice, the configuration is more complex: runoff from the impervious area is first conveyed to the sewer system through a vertical pipe and then transported to the well via a horizontal pipe with a minimum slope of 3%, which collects drainage from both the rooftops and the impervious area. In this model, the vertical pipe is represented by a rectangular weir with a discharge coefficient $C = 1.69$ [$m^{1/2} \cdot s^{-1}$] and a crest length equal to the pipe diameter ($L_{crest} = D_{pipe} = 0.05$ [m]).
This subsection compares these two modelling approaches in order to assess whether the increased level of detail leads to noticeable differences in the results.

FIGURE 4.5 indicates that, at the scale of this application, no major differences are observed between the two configurations. However, the discharge shown in FIGURE 4.5d exhibits a slightly lower peak for the "Weir

+ Pipe" scenario. In the "Pipe" scenario, the steeper effective slope accelerates runoff conveyance toward the well, resulting in a higher peak discharge.
Conversely, as illustrated in FIGURE 4.5b, the reduced discharge in the "Weir + Pipe" configuration leads to an increase in peak stored volume. Water therefore accumulates over a longer period, resulting in a larger volume within the well for this scenario.

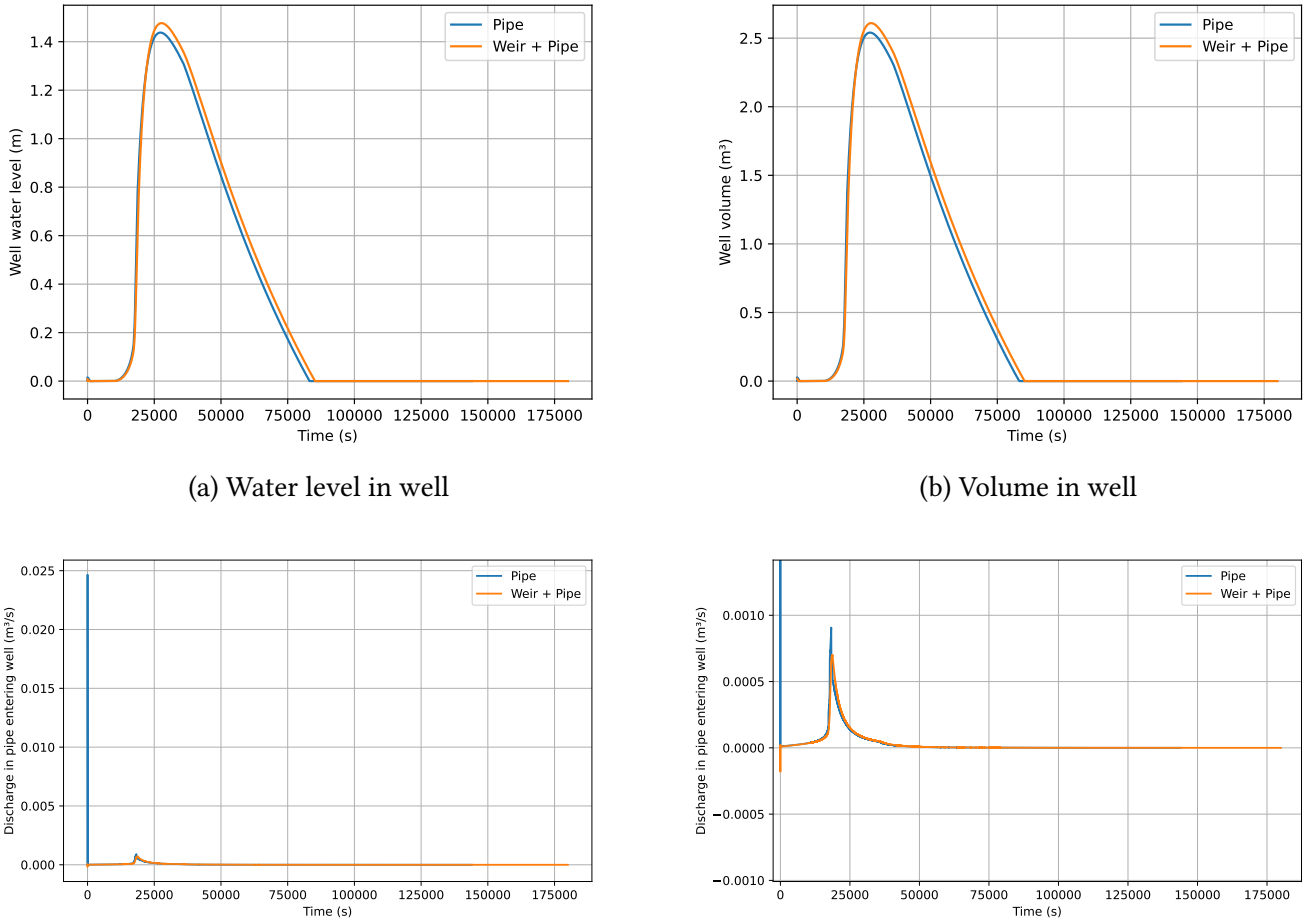

(a) Water level in well

(b) Volume in well

(c) Discharge

(d) Zoom on discharge peaks

Figure 4.5: Comparison of connections between impervious area and well

From this point onward, the connection between the impervious area and the implemented NbS follows the "Weir + Pipe" configuration. FIGURE 4.7 presents the final cross-section of Example 1, while FIGURE 4.6 highlights the modules used in the WSC model. The drawings in the cross-section are not up to scale, they are provided solely as a schematic representation to facilitate the visualization of the system and to gather the necessary information for modelling the example.

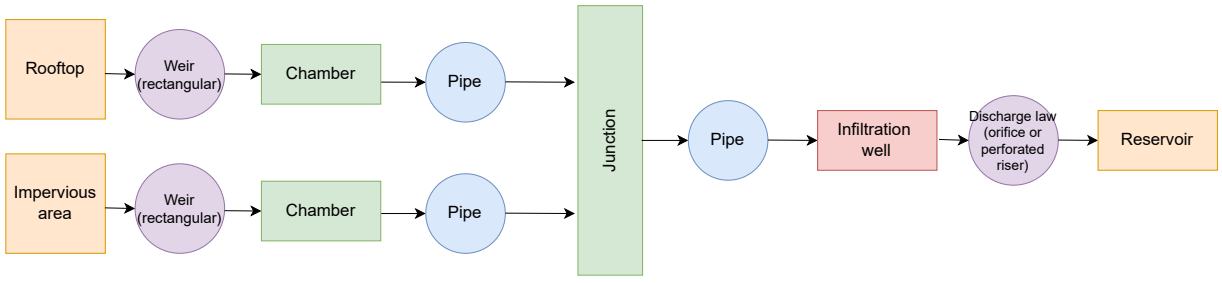

Figure 4.6: Flow diagram (well scenario)

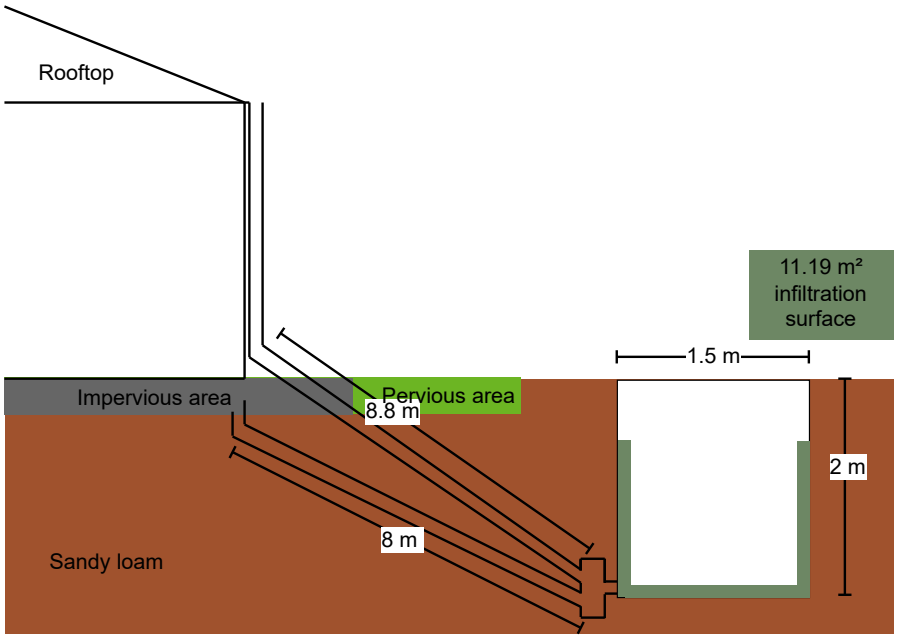

Figure 4.7: Cross section of Example 1 (well scenario)

4.2.4 Results with the solver

4.2.4.1 Swale

As shown in FIGURE 4.8 and as mentioned previously, the values obtained with the solver are very similar to those calculated using the Excel sheet. The solver results are slightly lower, which can be attributed to the tendency of the Excel sheet, due to its lower precision, to overestimate both the drainage time and the required storage capacity. Given the small scale of the application, the differences between the Excel sheet and the solver remain minor, as highlighted in TABLE 4.5. It can therefore be assumed that the dimensions of the swale are sufficient for a 25-year return period rainfall, as the swale does not overflow from a 6h10' rainfall event in Neupré and is fully drained in under 24 hours with the swale.
FIGURE 4.9 shows the hyetograph for this 6h10' rainfall event in Neupré with a 25-year return period.

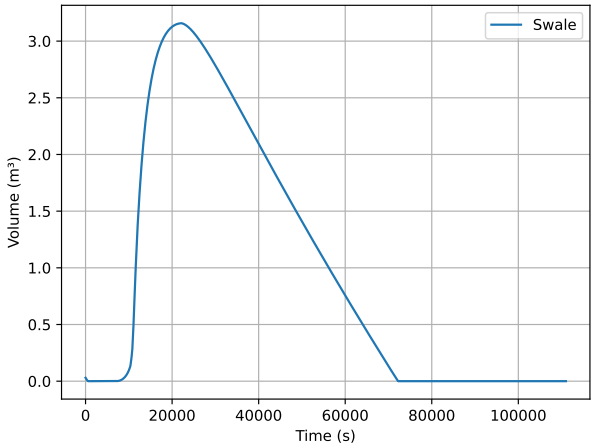

Figure 4.8: Volume in swale (25-year return period)

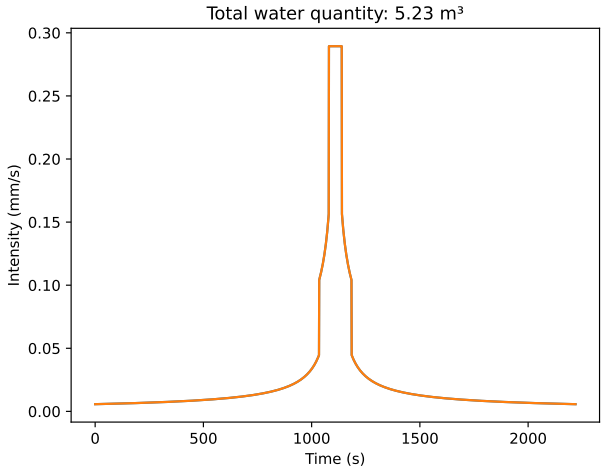

Figure 4.9: Hyetograph (25-year return period)

Method	V_{peak} (m^3)	$t_{drainage}$ (s)
Excel sheet (SPW)	3.3	20h22’
WSC solver	3.1	20h03’

Table 4.5: Results comparison between the SPW Excel sheet and the WSC solver

4.2.4.2 Well

As shown in FIGURE 4.10 and TABLE 4.6, the peak volume estimated by the Excel sheet is significantly higher than that calculated by the solver, and the same applies to the drainage time.
In this case, the results obtained with the solver should be interpreted with caution. The solver assumes infiltration occurs onyl vertically, whereas in reality, the infiltration surface extends beyond the horizontal bottom of the well. A portion of the vertical walls also contributes to infiltration. Since the solver is technically designed for vertical infiltration only, lateral contributions are not properly accounted for. As a result, the computed infiltration rates and volumes may overestimate the actual contribution from the vertical surfaces.
FIGURE 4.11 shows the hyetograph used by the SPW Technical Guide and the WSC model for the well, corresponding to a 10-hour rainfall event. The total volume collected by the runoff surface and the well is 5.2 m^3.

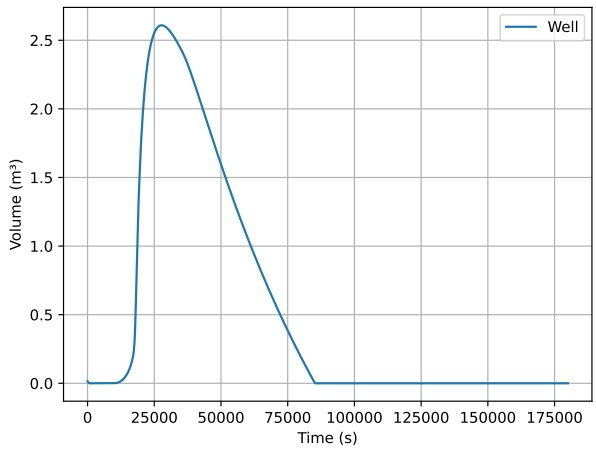

Figure 4.10: Volume in well (25-year return period)

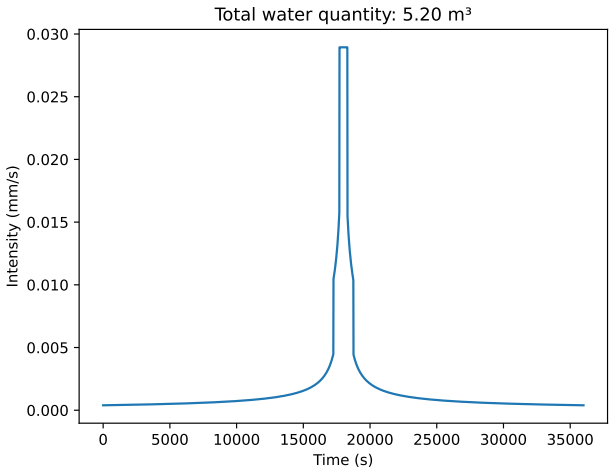

Figure 4.11: Hyetograph (25-year return period)

Method	V_{peak} (m^3)	$t_{drainage}$ (s)
Excel sheet (SPW)	3.5	32h59’
WSC solver	3.1	25h41’

Table 4.6: Results comparison between the SPW Excel sheet and the WSC solver

4.2.5 Influence of Parameters for Different Discharge Laws (100-year Return Period)

In this section, a 100-year return period rainfall event is modelled. Under these conditions, a storage tank is installed at the end of the swale or well to retain the overflow within the system rather than allowing it to

discharge into the surrounding area. The control mechanism between the swale/well and the end reservoir are those previously modelled, tested, and verified in the earlier section. To identify the optimal configurations, the parameters for each control mechanism were varied.
The swale is evaluated using rectangular and triangular weirs, which are compared in a later section. Similarly, the well is assessed with both an orifice and a perforated riser, with a comparison presented in the next section.

The main objectives in selecting the best parameters are as follows:

- Prioritize infiltration over storage wherever possible;
- Ensure that leakage flow does not exceed the maximum between 5 [L/s/ha] and 0.1 [L], if possible, as recommended by [45];
- Maintain drainage times below 24 hours for a rainfall event shorter than 10 hours, and below 48 hours for rainfall equal to or exceeding 10 hours (but less than 48 hours).

4.2.5.1 Rectangular Weir

Eq. 2.6 shows that the discharge through a rectangular weir depends on the discharge coefficient (C), the crest length (L) and the weir height (h_w, included in the hydraulic head H). The influence of each parameters is studied to quantify its effect on the peak outflow discharge ($Q_{\text{out, peak}}$) and the drainage time (t_d).
The volume in the swale or well indicates when the system is fully drained (volume equals zero), while the outflow discharge peaks approximately at the times of peak rainfall.

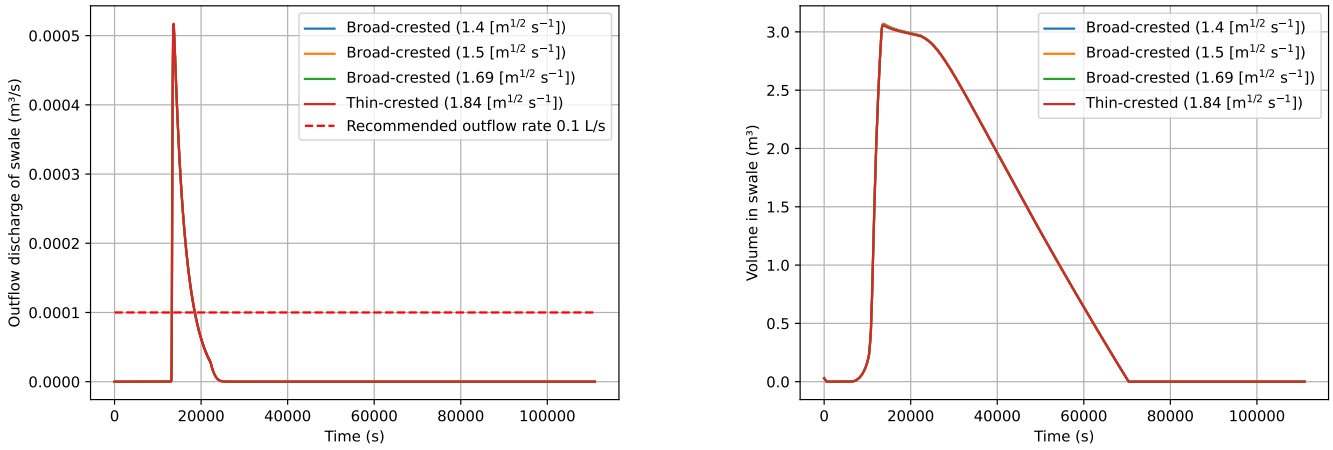

(a) Outflow discharge of swale

(b) Volume in swale

Figure 4.12: Different discharge coefficient values ($L_{\text{crest}} = 0.5$ [m] and $h_w = 0.2$ [m])

Figure 4.12 illustrates that variations in the discharge coefficient have a limited effect on either $Q_{\text{out, peak}}$ or t_d. The lowest $Q_{\text{out, peak}}$ is observed for a broad-crested weir with $C = 1.4$ [m$^{1/2}\cdot$ s^{-1}]. The difference in t_d between $C = 1.4$ [m$^{1/2}\cdot$ s^{-1}] and $C = 1.84$ [m$^{1/2}\cdot$ s^{-1}] is only of a few seconds, with the thin-crested weir having the smallest drainage time.
The coefficient discharge value selected for the remainder of the study is $C = 1.4$ [m$^{1/2}\cdot$ s^{-1}] because it prioritizes infiltration and results in the lowest peak discharge.

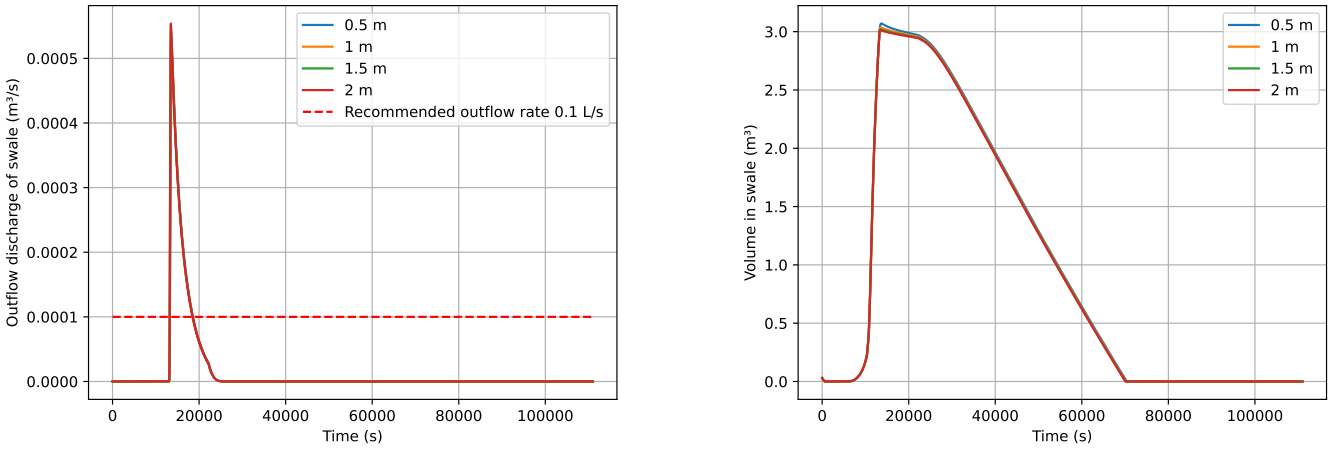

(a) Outflow discharge of swale

(b) Volume in swale

Figure 4.13: Different crest length values ($C = 1.4$ [$m^{1/2} \cdot s^{-1}$] and $h_w = 0.2$ [m])

FIGURE 4.13 shows the influence of the crest length. The impact on system dynamics is minor. The smallest $Q_{\text{out, peak}}$ occurs at $L_{\text{crest}} = 0.5$ [m], but this slightly increases t_d. The difference between the shortest and longest drainage times is only a few minutes. Therefore, $L_{\text{crest}} = 0.5$ [m] is retained for the rest of the study.

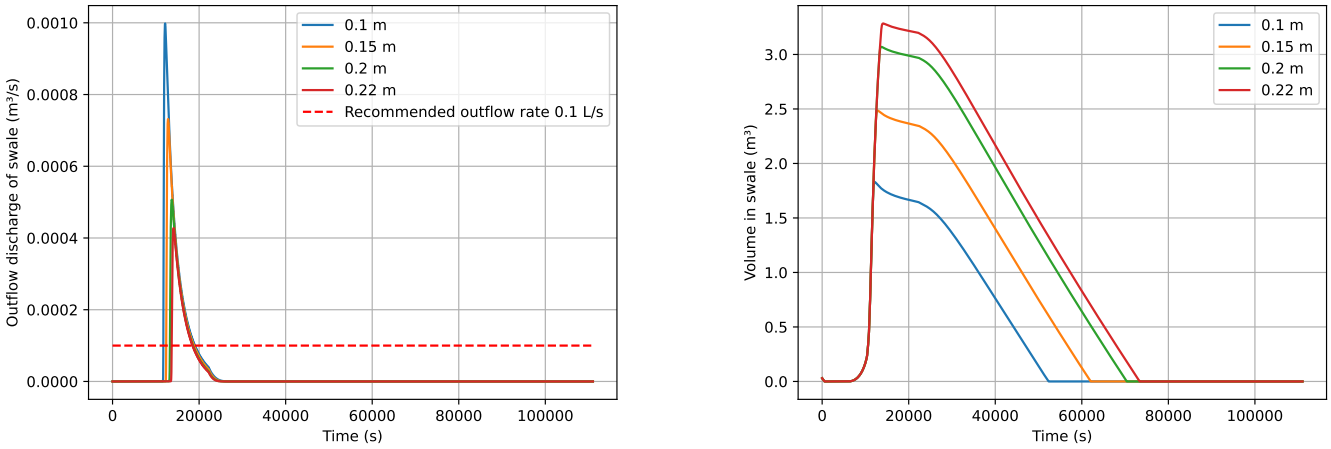

(a) Outflow discharge of swale

(b) Volume in swale

Figure 4.14: Different weir height values ($C = 1.4$ [$m^{1/2} \cdot s^{-1}$] and $L_{\text{crest}} = 0.5$ [m])

FIGURE 4.14 illustrates the effect of the weir height. The weir height has a more significant impact: increasing h_w reduces $Q_{\text{out, peak}}$, but it increases t_d. The value chosen for the remaining study is $h_w = 0.2$ [m], as it provides a lower peak while keeping the drainage time below 24 hours. The swale height is 0.23 [m], choosing $h_w = 0.22$ [m] would result in a weir height of only 1 [cm], which can be considered too small relative to the overall swale height.

4.2.5.2 Triangular Weir

EQ. 2.7 shows that the discharge through a triangular weir depends on the discharge coefficient (C), the weir angle (θ) and the weir height (h_w, included in the hydraulic head H). The influence of each parameters is studied to quantify its effect on the peak discharge outflow ($Q_{\text{out, peak}}$) and the drainage time (t_d).

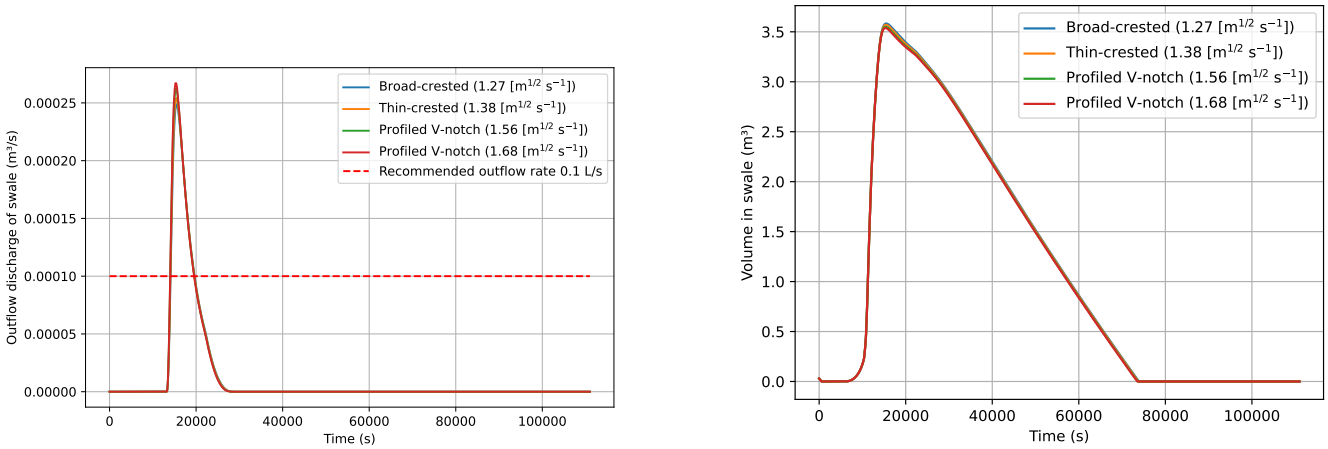

(a) Outflow discharge of swale

(b) Volume in swale

Figure 4.15: Different Discharge Coefficient Values ($\theta = 30[^\circ]$ and $h_w = 0.2$ [m])

The conclusions regarding the discharge coefficient are similar to those found for the rectangular weir. C has little influence on the system dynamics. Smaller discharge coefficient results in a slightly lower $Q_{\text{out, peak}}$, but a slightly higher t_d. Since the difference in drainage time is only a few minutes, $C = 1.27$ [$\text{m}^{1/2} \cdot \text{s}^{-1}$] is retained for further analysis.

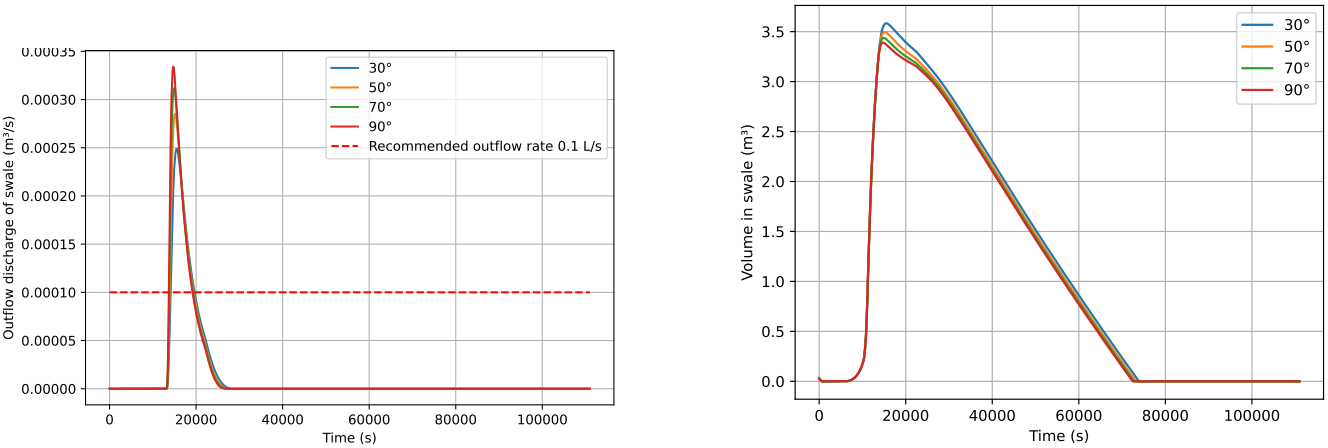

(a) Outflow discharge of swale

(b) Volume in swale

Figure 4.16: Different Weir Angle Values ($C = 1.27$ [$\text{m}^{1/2} \cdot \text{s}^{-1}$] and $h_w = 0.2$ [m])

FIGURE 4.16 illustrates the effect of the weir angle. The angle has some impact on both $Q_{\text{out, peak}}$ and t_d. For all angles studied, the drainage time remains below 24 hours. However, the peak discharge exceeds the recommended threshold for all angles, with $\theta = 30$ [$^\circ$] being closest to the limit. Therefore, the value selected is $\theta = 30[^\circ]$.

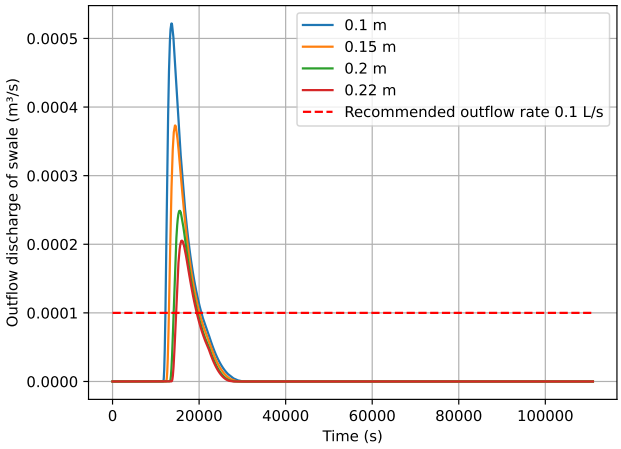

(a) Outflow discharge of swale

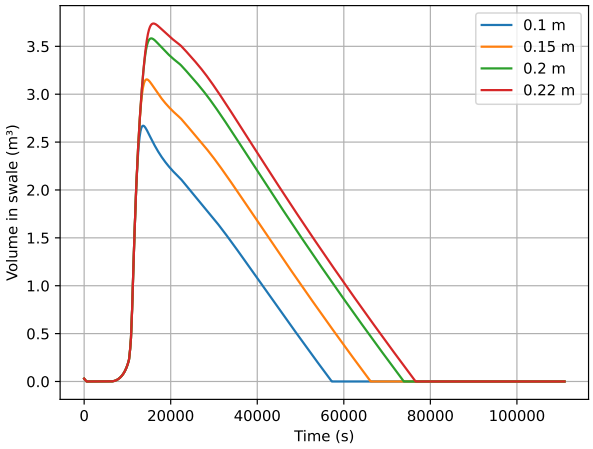

(b) Volume in swale

Figure 4.17: Different Weir Height Values ($C = 1.4$ [$m^{1/2} \cdot s^{-1}$] and $\theta = 30$ [°])

FIGURE 4.17 shows the influence of the weir height. The weir height significantly affects both $Q_{\text{out, peak}}$ and t_d. A lower weir height produces a higher peak discharge but a shorter drainage time (less than 17 hours for $h_w = 0.1$ [m]). To enhance infiltration and minimize storage requirements, $h_w = 0.2$ [m] is chosen. This keeps the drainage time below 24 hours and brings the peak discharge close to the recommended threshold. A higher values, such as $h_w = 0.22$ [m], is avoided for the same reason as with the rectangular weir: a 1 [cm] weir would be too small relative to the swale height.

4.2.5.3 Orifice

EQ. 2.8 shows that the orifice discharge depends on the discharge coefficient (C), the orifice diameter (d_o), and the orifice height (h_o, included in the hydraulic head H). The influence of each of each parameter was studied to quantify its effect on the peak outflow discharge ($Q_{\text{out, peak}}$) and the drainage time (t_d).

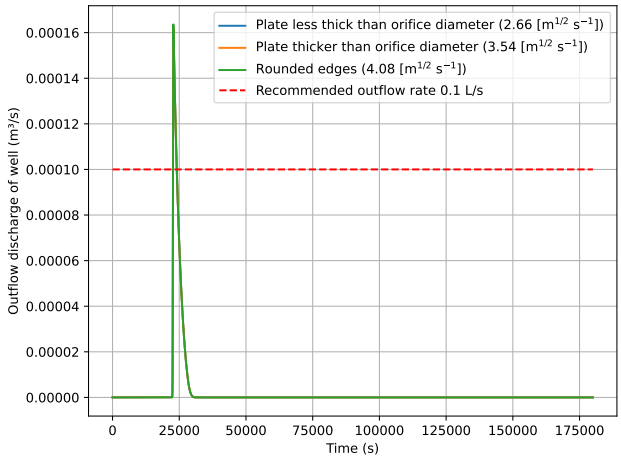

(a) Outflow discharge of well

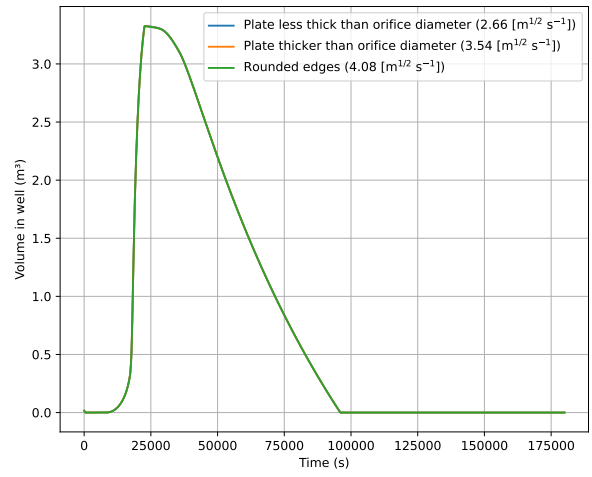

(b) Volume in well

Figure 4.18: Different discharge coefficient values ($d_o = 0.1$ [m] and $h_o = 1.89$ [m])

FIGURE 4.18 shows that, as with the weirs, variations in the discharge coefficient have little effect on the system dynamic. The lowest $Q_{\text{out, peak}}$ occurs for a plate thinner than the diameter ($C = 2.66$ [$m^{1/2} \cdot s^{-1}$]). The

difference in drainage time between the possibilities is minor, only a few minutes.

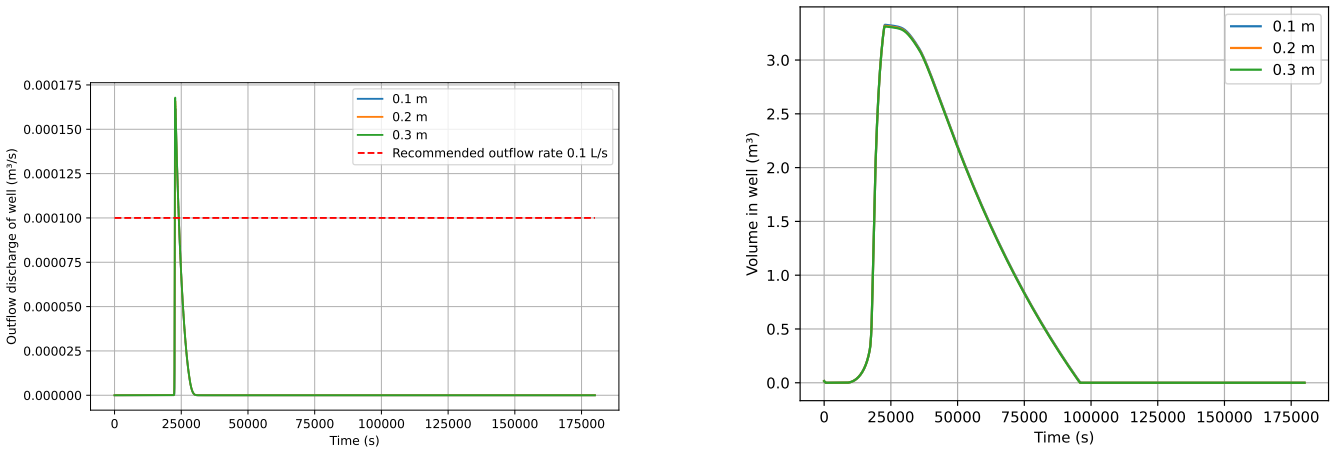

(a) Outflow discharge of well

(b) Volume in well

Figure 4.19: Different orifice diameter values ($C = 2.66$ [$m^{1/2} \cdot s^{-1}$] and $h_o = 1.89$ [m])

Figure 4.19 illustrates the effect of the orifice diameter. The diameter has minimal influence on the system, and $d_o = 0.1$ [m] is chosen, since it is closest to the discharge threshold, even though the differences are small.

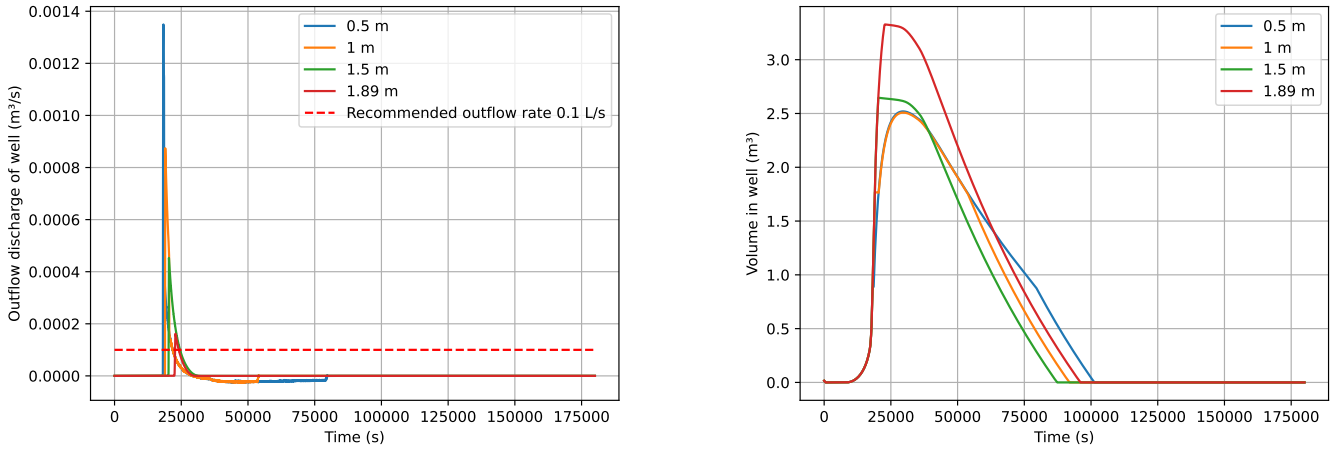

(a) Outflow discharge of well

(b) Volume in well

Figure 4.20: Different weir height values ($C = 2.66$ [$m^{1/2} \cdot s^{-1}$] and $d_o = 0.1$ [m])

Figure 4.20 shows the influence of the orifice height. The orifice height has a significant impact on both $Q_{\text{out, peak}}$ and t_d. Two heights, $h_o = 0.5$ [m] and $h_o = 1$ [m], produces anomalous results, with negative outflow indicating that water flows from the storage reservoir back into the well. This behaviour is undesirable and likely represents a solver limitation or numerical implementation; these values are therefore rejected.
The value retained is $h_o = 1.89$ [m], as it fully utilizes the well volume, as seen from the peak volume in Figure 4.20b. This configuration produces the highest peak of all the possibilities. The drainage time is relatively long but remains below the maximum allowed, at approximately 26 hours, staying within the target limit of 48 hours.

4.2.5.4 Perforated Riser

Eq. 2.9 shows that the perforated riser depends on the discharge coefficient (C_p), the diameters of the holes (d_p, included in the total holes area A_p), the number of holes per row (n_h, included in A_p), the number of rows (n_r, included in A_p), and the height of the riser (H_s). Since the diameter and discharge coefficient have already been studied for the orifice, and the perforated riser is conceptually similar to multiple orifices, this study focuses on the number of holes per row (n_h) and the number of rows (n_r). The riser height depends on the number of holes and the spacing between them, set at $S = 0.3$ [m] to align with the holes diameter ($d_o = 0.1$ [m], as for the orifice).

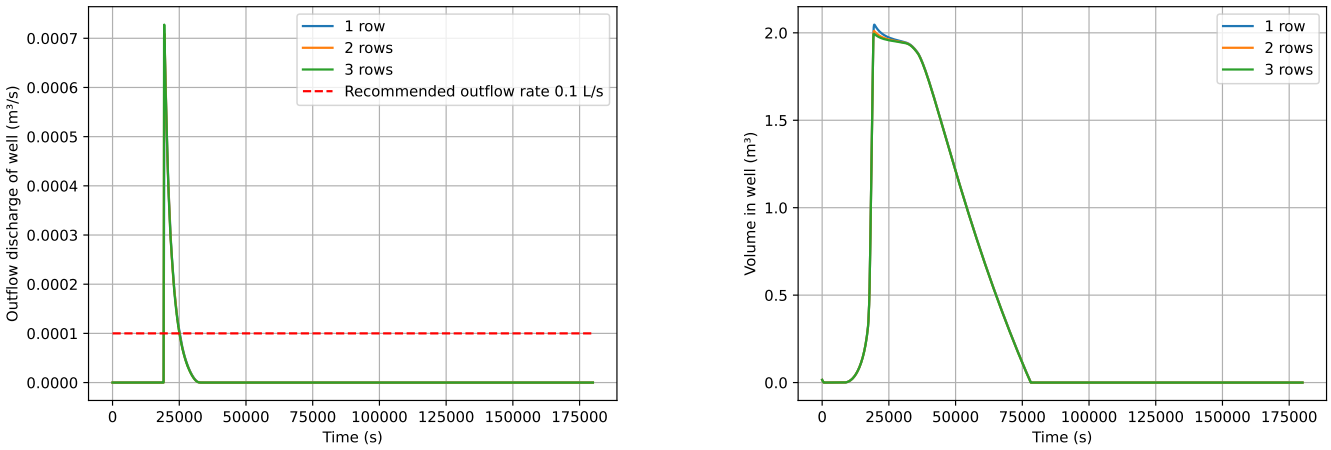

(a) Outflow discharge of well

(b) Volume in well

Figure 4.21: Different number of rows ($n_h = 2$)

Figure 4.21 shows that the number of rows has little impact on $Q_{\text{out, peak}}$ and t_d. To illustrate the difference between this multi-hole system with the single-hole orifice studied previously, the number of rows is chosen as 2.

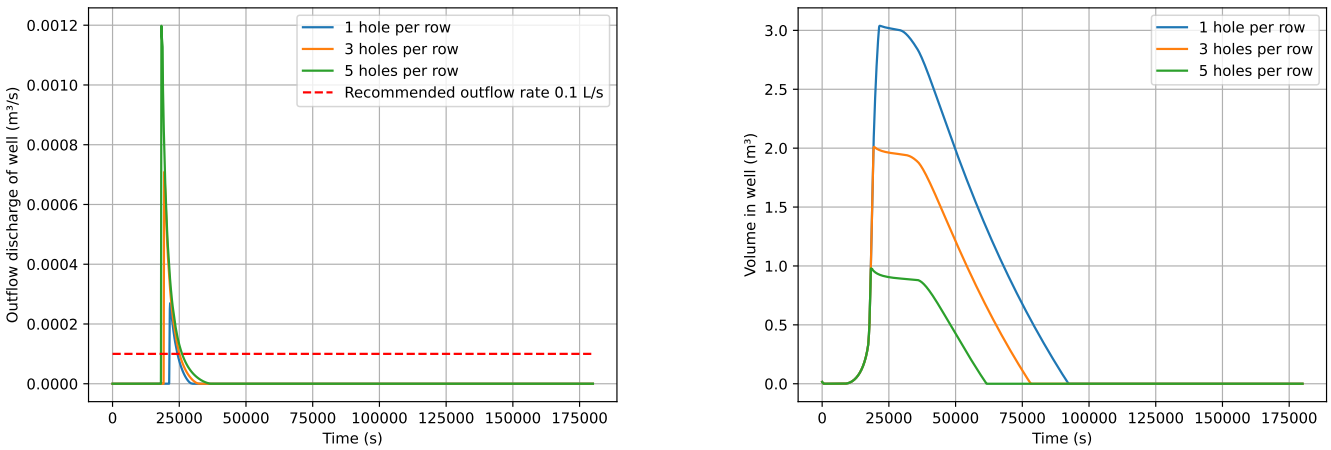

(a) Outflow discharge of well

(b) Volume in well

Figure 4.22: Different number of holes per row ($n_r = 2$)

Figure 4.22 demonstrates that the number of holes per row significantly affects the system behaviour. Again, to showcase the difference between the standard orifice with the perforated riser, the number of holes per row is set to 2. This value represents a good compromise between hydraulic performance of a perforated riser and infiltration efficiency.

4.2.6 Return Periods of 50-year and 100-year

4.2.6.1 Swale

TABLE 4.7 summarises the parameters selected for the rectangular and triangular weirs in the swale.

Weir	C ($m^{1/2} \cdot s^{-1}$)	L_{crest} (m)	θ (°)	Height (m)
Rectangular	1.4	0.5	/	0.2
Triangular	1.27	/	30	0.2

Table 4.7: Parameters chosen for each weirs

For a 50-year return period rainfall, FIGURE 4.23c shows that the swale overflows with both weirs since it needs an additional storage tank. FIGURE 4.23a and FIGURE 4.23b allow a comparison between the rectangular and triangular weirs. The triangular weir produces a lower discharge peak and requires less storage volume. It promotes infiltration in the swale and respects the discharge threshold of 0.1 [L/s]. The rectangular weir, by contrast, accelerates drainage and allows a smaller swale to be designed.
In this case, the triangular weir appears to be the best solution with respect to the main selection objectives. However, for other sites, soil types, or spatial constraints, the optimal solution may differ.

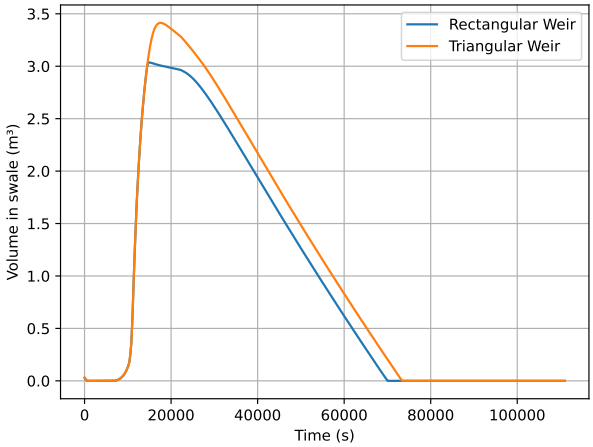

(a) Volume in swale

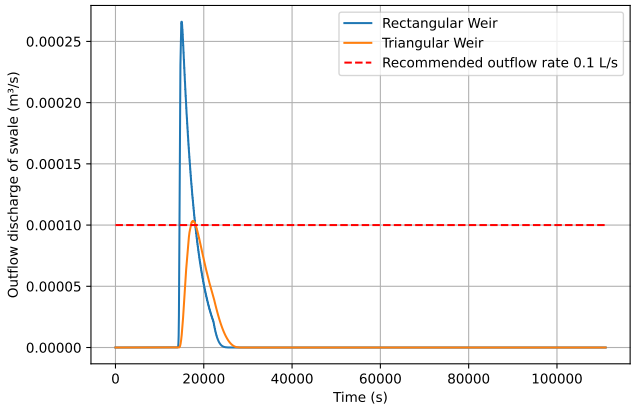

(b) Swale outflow discharge

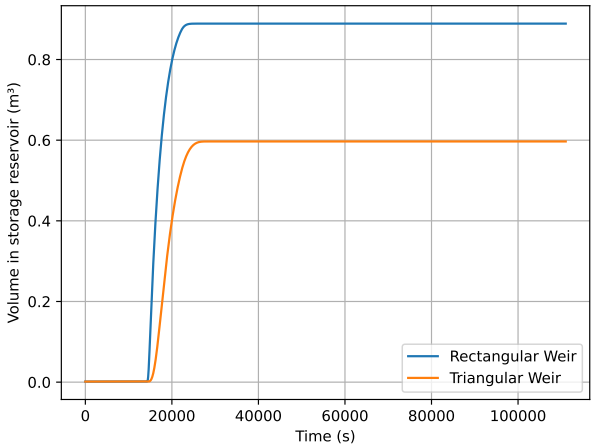

(c) Storage reservoir

Figure 4.23: Comparison rectangular and triangular weirs (50-year return period)

For the 100-year return period, FIGURE 4.24 compares the two weirs. The conclusions are similar, but the discharge threshold is exceeded even with the triangular weir.

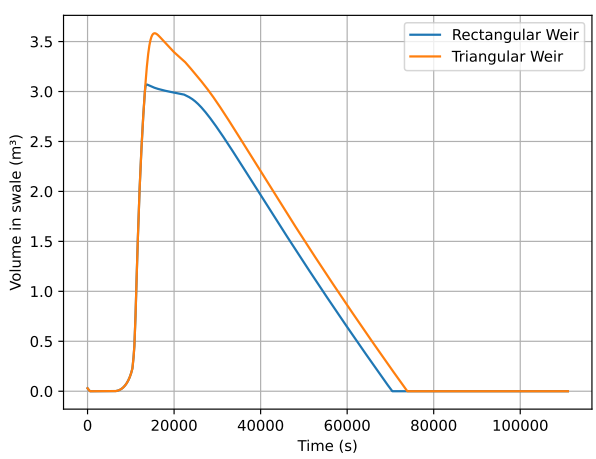

(a) Volume in swale

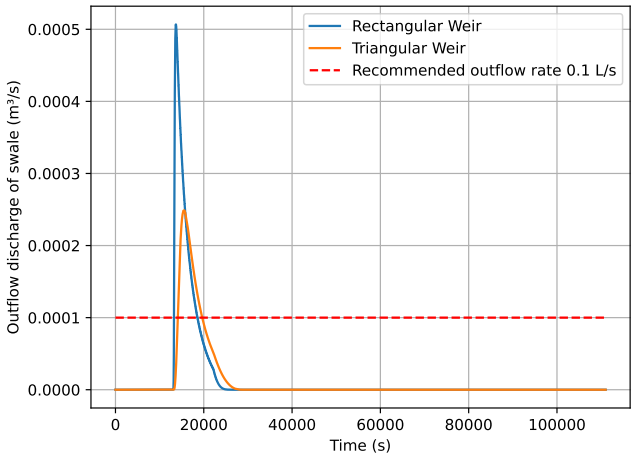

(b) Outflow discharge of swale

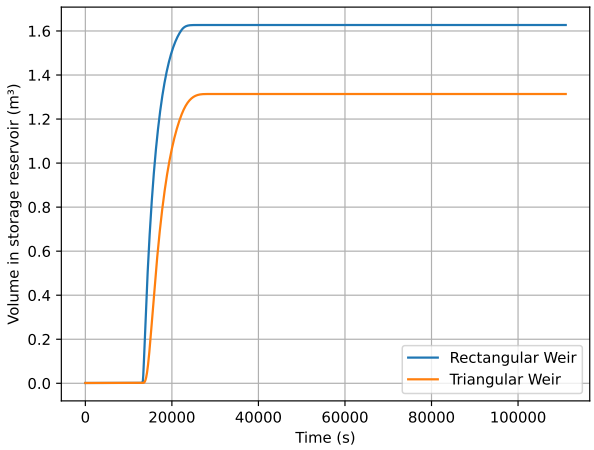

(c) Storage reservoir

Figure 4.24: Comparison rectangular and triangular weirs (100-year return period)

The following table summarises the main results for the rectangular and the triangular weirs for the 50-year and 100-year return periods:

	Return Period	$Q_{\text{out, peak}}$ (m³/s)	$V_{\text{out, peak}}$ (m³)	t_d (s)
Rectangular weir	50	$2.7 \cdot 10^{-4}$	3	19h27'
Triangular weir	50	10^{-4}	3.4	20h23'
Rectangular weir	100	$5.1 \cdot 10^{-4}$	3.1	19h34'
Triangular weir	100	$2.5 \cdot 10^{-4}$	3.4	20h32'

4.2.6.2 Well

TABLE 4.8 summarises the parameters chosen for the orifice and perforated riser used in the well.

Weir	C ($m^{1/2} \cdot s^{-1}$)	Diameter (m)	Number of rows	Number of holes	Height (m)
Orifice	2.66	0.1	/	/	1.89
Perforated riser	2.7	0.1	2	2	0.6 (S=0.3 [m])

Table 4.8: Parameters chosen for each control mechanism

For the 50-year return period, FIGURE 4.25 shows that the water level in the well always remains below its height (2 [m]), and the end reservoir remains empty. Therefore, the study focuses on the 100-year return period.

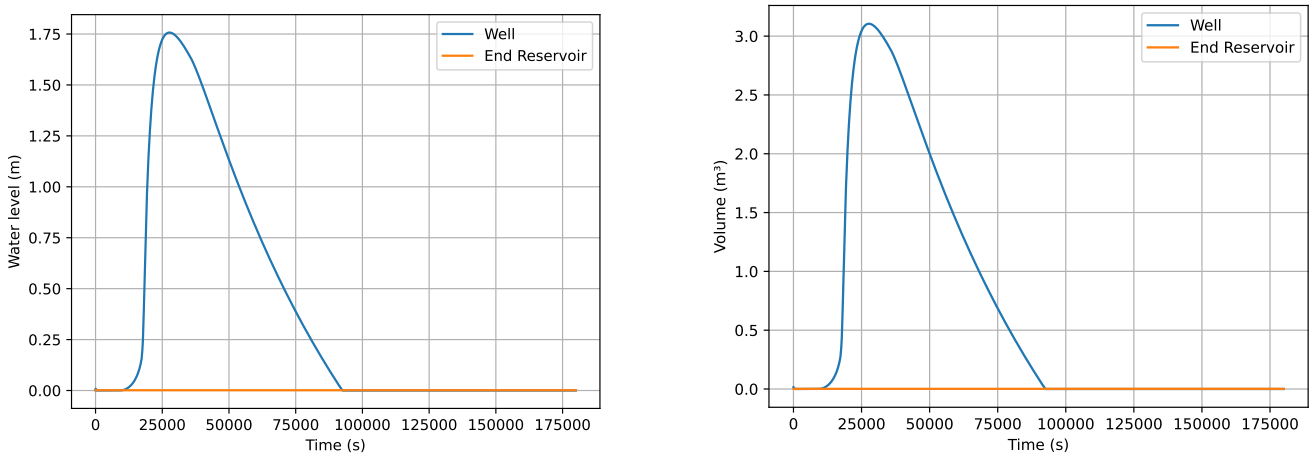

(a) Water level in well and in end reservoir

(b) Volume in well and in end reservoir

Figure 4.25: 50-year return period

FIGURE 4.26 shows that, for a 100-year return period, the orifice prioritizes infiltration, producing an outflow discharge near the threshold of 0.1 [L/s] and a larger peak volume, fully utilizing the well capacity. The perforated riser, by contrast, accelerates drainage, minimizing t_d.

The following table summarises the main information comparing the orifice and the perforated riser for a 100-year return period:

	Return period	$Q_{\text{out, peak}}$ (m^3/s)	$V_{\text{out, peak}}$ (m^3)	t_d (s)
Orifice	100	$1.6 \cdot 10^{-4}$	3.3	26h41’
Perforated riser	100	$4.8 \cdot 10^{-4}$	2.5	23h44’

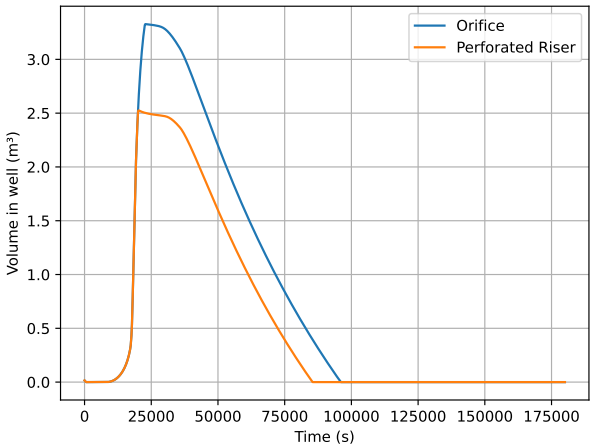

(a) Volume in well

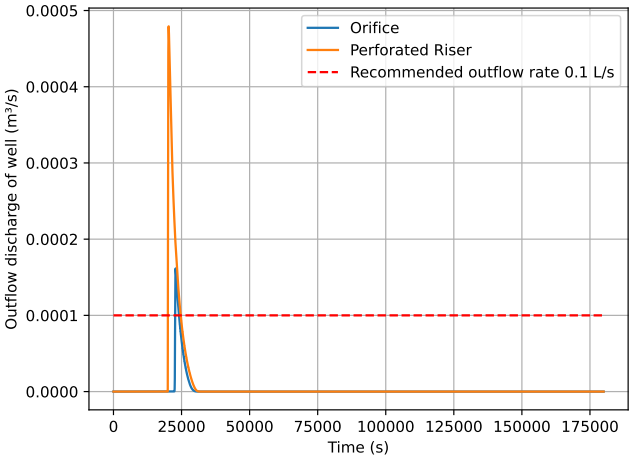

(b) Outflow discharge of well

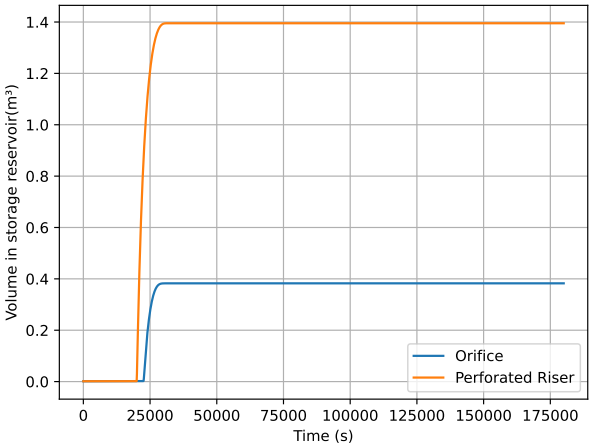

(c) Storage reservoir

Figure 4.26: Comparison orifice and perforated riser (100-year return period)

4.3 Example 2

4.3.1 Context

This example considers a reservoir with a surface area of 5019 [m²] located beneath a parking in Dison, Belgium. The top of the reservoir could be made of Ultra-Lightweight Honeycomb Structures, expanded clay, or gravel 20/60, but the exact material was not specified. Since the reservoir height depends on the material used according to the SPW Technical Guide, expanded gravel was chosen. Figure 4.27 shows the location plan from the SPW Technical Guide system. Table 4.9 summarises the main parameters for the reservoir. The SPW Technical Guide also provides the areas to consider for each NbS device runoff zones, summarised in the following table:

Type of area	Runoff coefficient	Gross area [m²]	Runoff area [m²]	Elevation[1][m]	Pipe length [m]
Impervious	0.9	88.37	79.53	290	9.4
Rooftop	1	142.98	142.98	300	9.4

[1] Found on WalOnMap

Figure 4.27: Example 2 location plan

The SPW Technical Guide assumptions are as follows:

- The pervious area (represented in green in Figure 4.27) directly infiltrates rainwater;
- Runoff from the impervious area and the rooftop is directed to the reservoir.

Because the site area exceeds the current solver capacity, a reduction factor was applied to all lengths and surfaces. Additional modelling assumptions include:

- All pipes have a diameter of 0.05 [m] and are made of PVC which has a Manning roughness coefficient of 0.009 [43];

- Rainwater from the rooftop is conveyed to the bottom of the building via a rectangular weir with a discharge coefficient $C = 1.69$ [$m^{1/2} \cdot s^{-1}$] and a crest length $L_{crest} = D_{pipe} = 0.05$ [m];
- Longitudinal head losses in vertical pipes (through the weir) are neglected, whereas horizontal pipe losses are fully accounted for;
- All horizontal pipes have a minimum slope of 3%;
- Only runoff from the parking above the reservoir is considered, not infiltration;
- Original lengths and areas were divided by 10 and 100, respectively, to fit the solver; recalculated values were used in the Excel sheet;
- The reservoir is assumed rectangular for modelling purposes, keeping the same surface;
- Soil is sandy loam to maintain comparability with the SPW Technical Guide system (see TABLE 4.4 for parameter values).

Parameter	Value	Unit
Length	7.6	m
Width	6.6	m
Height	0.5	m
Infiltration surface	50.19	m^2
Return period	25	years
Rainfall duration	6h50'	/
Elevation	289.5	m

Table 4.9: Parameter for reservoir

FIGURE 4.29 shows a cross section of the reservoir, and FIGURE 4.28 presents the modules used in the WSC model.

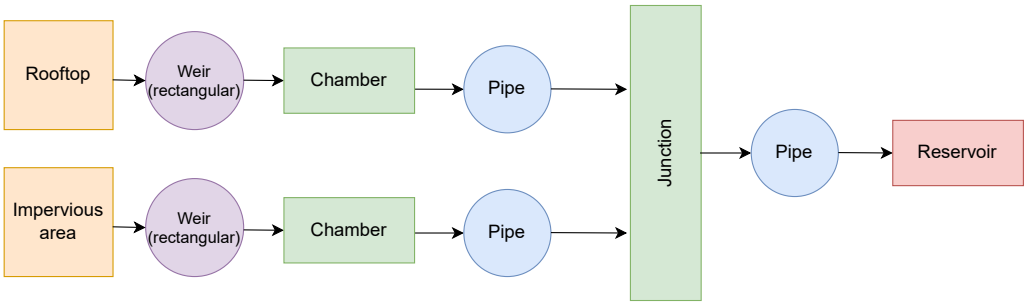

Figure 4.28: Flow diagram

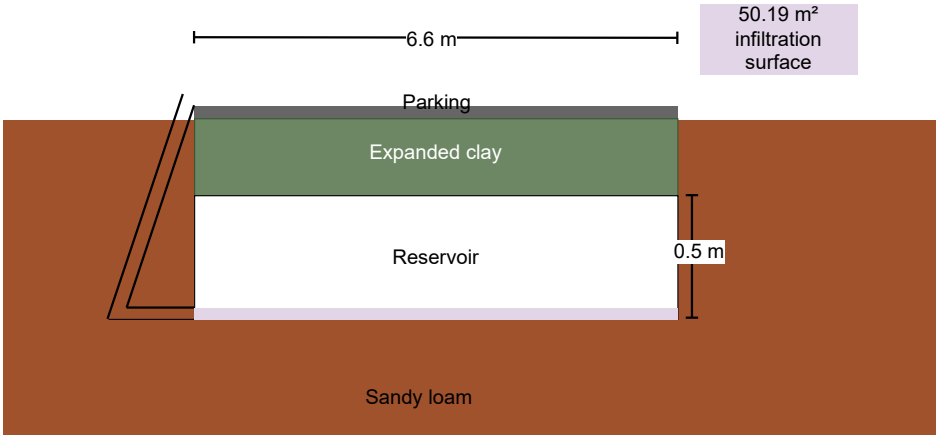

Figure 4.29: Cross section of Example 2

4.3.2 Comparison Excel Sheet and WSC Solver

Figure 4.30a shows that the water level in the reservoir never exceeded 0.5 [m] (the reservoir height), meaning the reservoir did not overflow during the simulation.
Figure 4.30b and Table 4.10 compare the peak volume and drainage time obtained from the SPW Technical Guide Excel sheet and the WSC solver. The Excel sheet predicts a peak volume at 9.8 [m³], whereas the solver finds 7.2 [m³], with the drainage time reduced by approximately one hour. The Excel sheet provides a useful first estimate but tends to overdesign the system in terms of both capacity and drainage time.

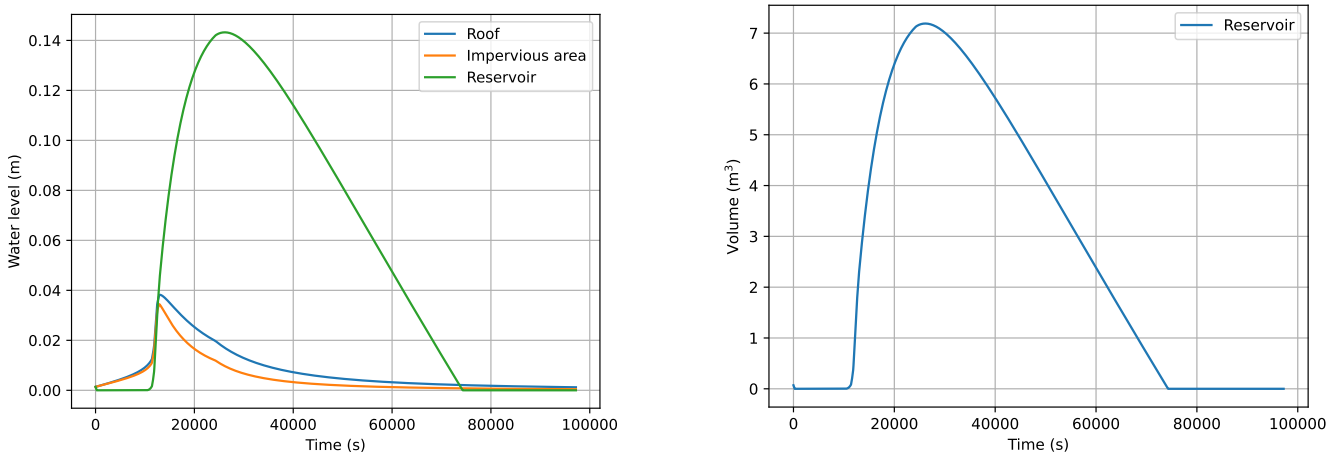

(a) Water levels

(b) Volume in reservoir

Figure 4.30: Results from solver

Method	V_{peak} (m^3)	$t_{drainage}$ (s)
Excel sheet (SPW)	9.8	21h42’
WSC solver	7.2	20h38’

Table 4.10: Results comparison between the SPW Excel sheet and the WSC solver

4.4 Example 3

4.4.1 Context

This example is located in Dinant, Belgium, and consists of a swale with an area of 80 [m²]. FIGURE 4.31 represents the location plan from the SPW Technical Guide.
The SPW Technical Guide also provides the areas to consider for the swale runoff zones. The values are listed in the following table:

Type of area	Runoff coefficient	Gross area [m²]	Runoff area [m²]	Elevation[1][m]	Pipe length [m]
Impervious	0.9	389	350	200	20
Rooftop	1	262	262	206	8

[1] Found on WalOnMap

Figure 4.31: Example 3 location plan

The following assumptions were made by the SPW Technical Guide:

- The pervious area (represented in green in FIGURE 4.31) directly infiltrates rainwater;
- Runoff from the impervious area and the rooftop of the building is directed to the swale.

The lack of detailed information required additional assumptions:

- All pipes have a diameter of 0.05 [m] and are made of PVC which has a Manning roughness coefficient of 0.009 [43];
- Rainwater from the rooftop is conveyed to the bottom of the building via a rectangular weir with the parameters $C = 1.69$ [$m^{1/2} \cdot s^{-1}$] and $L_{crest} = D_{pipe} = 0.05$ [m];
- Longitudinal head losses in vertical pipes (through the weir) are neglected, whereas horizontal pipe losses are fully accounted for;

- All horizontal pipes have a minimum slope of 3%;
- Soil is sandy loam to maintain comparability with the SPW Technical Guide system (see TABLE 4.4 for parameter values).

Parameter	Value	Unit
Length	20	m
Width	4	m
Height	0.48	m
Angle	30	°
Infiltration surface	80	m²
Return period	25	years
Rainfall duration	12h45'	/
Elevation	199.52	m

Table 4.11: Parameter for swale

FIGURE 4.33 is a cross section of Example 3, and FIGURE 4.32 represents the modules used in the WSC model.

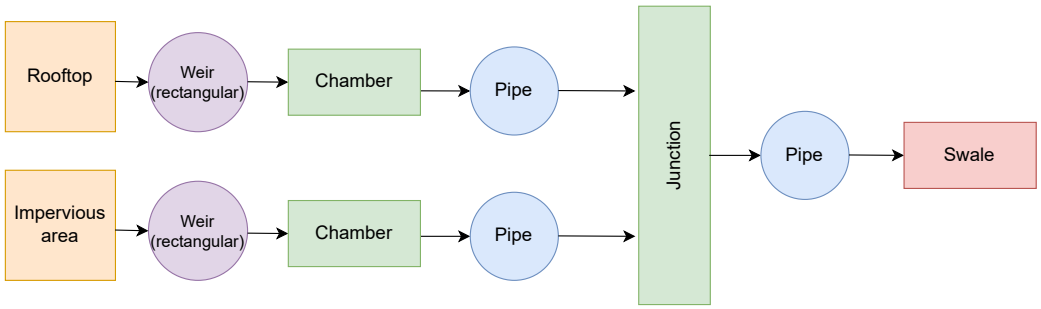

Figure 4.32: Flow diagram

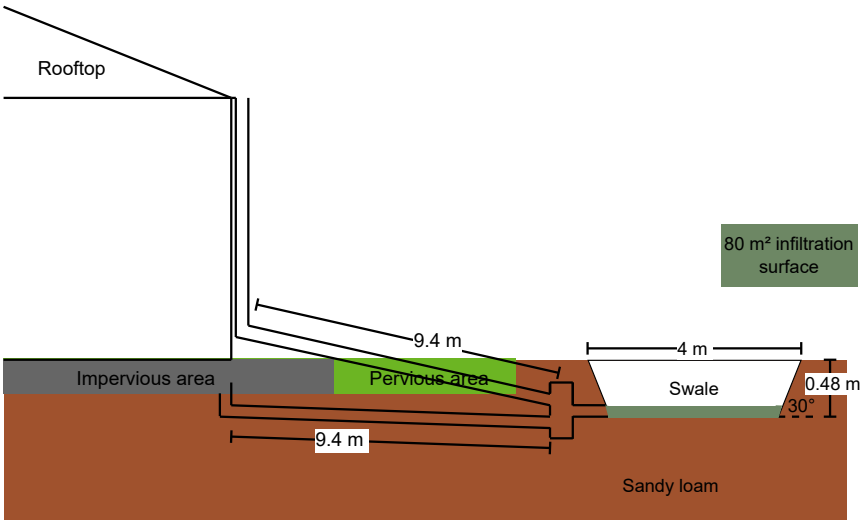

Figure 4.33: Cross section of Example 3

4.4.2 Comparison Excel Sheet and WSC Solver

Figure 4.34a shows that the water level in the swale never exceeds the swale height of 0.48 [m]. The swale appears to be over-dimensioned, as a height of 0.3 m would have sufficed for a 25-year return period rainfall. Moreover, Figure 4.34b and Table 4.12 confirm that the swale is over-dimensioned: the peak volume predicted by the Excel sheet is 1.75 times higher than that obtained by the solver. The drainage time was reduced by 3 hours using the solver.

It can be concluded that the larger the surface area of the site, the greater the difference between the Excel sheet and the solver. The Excel sheet tends to over-design the system, especially for larger swales.

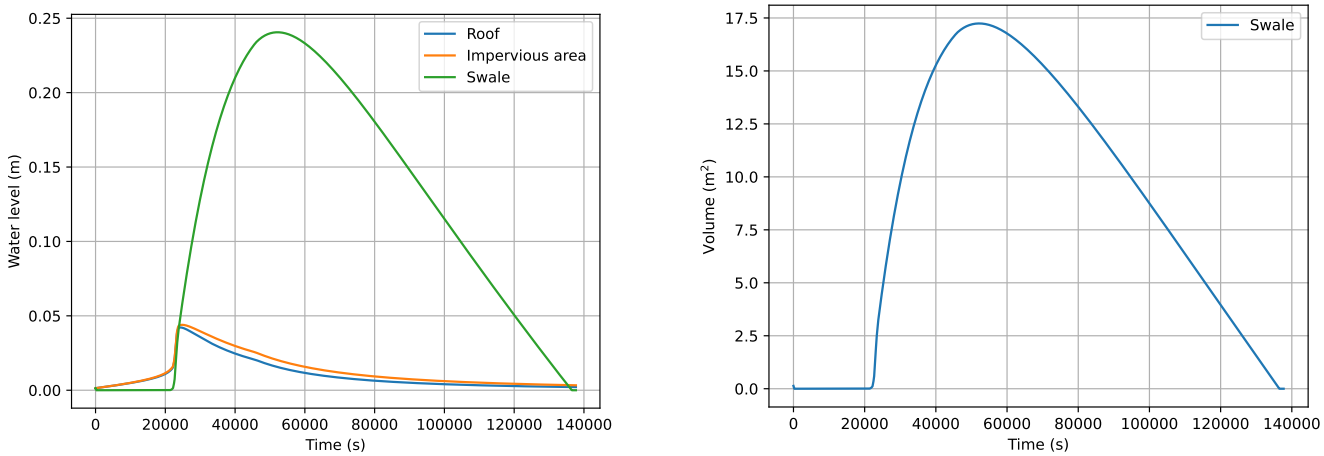

(a) Water levels

(b) Volume in swale

Figure 4.34: Results from solver

Method	V_{peak} (m^3)	$t_{drainage}$ (s)
Excel sheet (SPW)	30.1	41h48'
WSC solver	17.2	37h55'

Table 4.12: Results comparison between the SPW Excel sheet and the WSC solver

4.5 Example 4

4.5.1 General Context

Example 4 is the most complex one, as it involves spatial diversity and connections between multiple infrastructures. It is located in Coronmeuse, Liège, Belgium. This neighbourhood is under construction and may serve either as a hypothetical scenario or a potential future development.
The SPW Excel sheet is not capable of representing the full spatial complexity of this example. It aggregates multiple rooftops and other surfaces into single values, losing spatial detail. In contrast, the WSC solver allows the full representation of this spatial richness.
To illustrate the capabilities of the WSC solver, a two-step approach is used. First, a simple modelling, similar to Examples 1, 2 and 3 is performed. Second, a detailed modelling based on the actual location plan is conducted. This shows how increasing model precision in the WSC solver can lead to a more optimised design and potential economic savings by avoiding the over-design caused by the Excel sheet approach.
Table 4.13 summarises the parameters that are consistent across all models of Example 4.

Parameter	Value	Unit
Swale angle	30	°
Return period	25	years
Rainfall duration	12h30’	/

Table 4.13: Parameter for Example 4

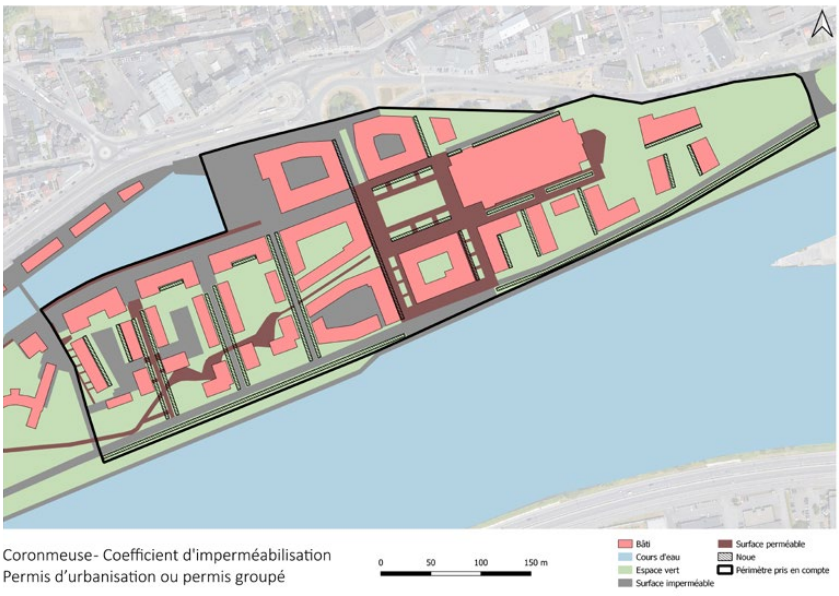

Figure 4.35: Example 4 location plan

The following assumptions were made by the SPW Technical Guide:

- The vegetated area (represented in green in Figure 4.35) directly infiltrates rainwater;
- Infiltration swales and a dry detention basin are implemented on the eastern side of the site;

- 25% of the buildings have vegetated roofs of about 10 [cm] thickness, though this is not explicitly represented in the location plan FIGURE 4.35.
- The runoff volume is proportionally distributed between the swales and the dry detention basin;
- The swale has an average height of 0.61 [m] and an average width of 3 [m].

Due to missing information in the SPW Technical Guide and publicly available data, the following assumptions were made for the WSC model:

- No soil information was available on WalOnMap. It is assumed that the soil is sandy loam or that it is reworked during swale construction (see TABLE 4.4 for soil parameter values);
- Google Earth data reflect the area under construction, so many of the buildings assumed in the SPW Technical Guide do not yet exist, and construction sites on the satellite images may cause inaccurate elevation information. Therefore, all elevations used here are estimates, while remaining close to available Google Earth data (staying in the same order of magnitude). Elevations are chosen so that upstream points are higher than downstream points, ensuring natural water flow without the need for pumps;
- The SPW Technical Guide provides only average dimensions for swales, and lengths measured on the plan may contain errors due to lack of precision. Widths and heights were chosen based on these averages and refined later;
- All pipes have a diameter of 0.05 [m] and are made of PVC which has a Manning roughness coefficient of 0.009 [43];
- Rainwater from the rooftop is conveyed to the bottom of the building via a rectangular weir with a discharge coefficient $C = 1.69$ [$m^{1/2} \cdot s^{-1}$] and a crest length $L_{crest} = D_{pipe} = 0.05$ [m];
- Longitudinal head losses in vertical pipes (through the weir) are neglected, whereas horizontal pipe losses are fully accounted for;
- All horizontal pipes have a minimum slope of 3%;
- Original lengths and areas were scaled down, divided by 10 and 100, respectively, to match the solver's limitations. The Excel sheet was re-run using these revised values;
- Vegetated roofs, although present in the SPW Technical Guide, are neglected in the WSC model due to uncertainties in their location, and stratification
- Although a dry detention basin is mentioned in the SPW Technical Guide, it is not explicitly represented nor analysed in the Excel sheet, and no information is available regarding its geometry or capacity. It is therefore neglected in the WSC model;
- When an orifice is used as the outflow control for a swale, its diameter is set to 0.1 [m], its discharge coefficient to 3.54 [$m^{1/2} \cdot s^{-1}$], and its elevation to the swale height minus half the orifice diameter. When a triangular weir is used instead, its angle is set to 45 [°], its discharge coefficient to 1.27 [$m^{1/2} \cdot s^{-1}$], and an elevation equal to the swale height minus 0.05.

4.5.2 Comparison Excel Sheet and WSC Solver - Basic Modelling

A simplified representation of Example 4, similar to Examples 1, 2 and 3, is first modelled to compare results between the Excel sheet and the solver. This "basic modelling" aggregates all areas into a single general swale, without capturing spatial diversity.
The table below summarises the characteristics of each type of areas contributing runoff to the single general swale:

Type of area	Runoff coefficient	Gross area [m²]	Runoff area [m²]	Elevation [m]	Pipe length [m]
Pervious	0.7	127	88.9	61	10
Impervious	0.9	242	217.8	61	10
Rooftop	1	291	291	69	10

Table 4.14 presents the parameters of the "single" general swale, which in reality corresponds to multiple swales as shown in Figure 4.35.

Parameter	Value	Unit
Length	25	m
Width	4	m
Height	0.61	m
Infiltration surface	75	m²
Elevation	59	m

Table 4.14: Parameter for swale

Even in this simplified case, Figure 4.37 and Table 4.15 show that WSC solver predicts a lower peak volume than the Excel sheet, although the drainage time is slightly longer. However, the drainage time remains below 48 hours for a rainfall exceeding 10 hours. This difference may be due to the soil properties used or calibration issues, but the results are still within the same order of magnitude as the Excel sheet and can be considered reasonable.
The end reservoir remains empty and the outflow discharge is zero, indicating the swale does not overflow. Both methods predict relatively large peak volumes, exceeding 20 [m³]. Despite this, the dimensions of the swale are sufficient to manage a 25-year return period rainfall.

Method	V_{peak} (m^3)	$t_{drainage}$ (s)
Excel sheet (SPW)	28.1	41h38’
WSC solver	20.8	43h41’

Table 4.15: Results comparison between the SPW Excel sheet and the WSC solver for the basic WSC modelling

FIGURE 4.36 shows the flow diagram for the basic modelling of Example 4.

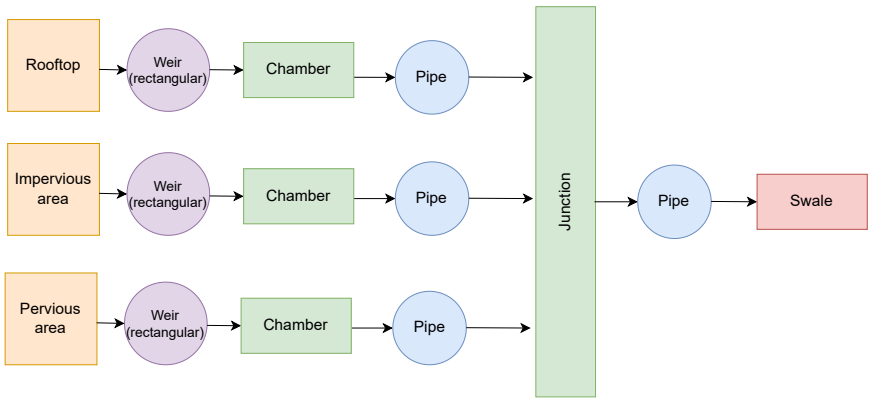

Figure 4.36: Flow diagram for basic case of Example 4

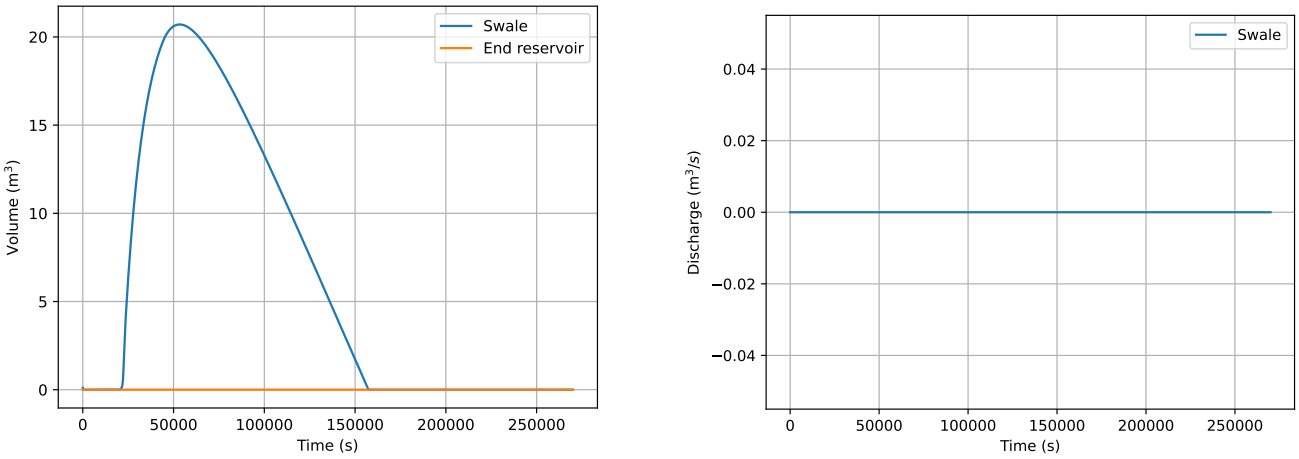

(a) Volume

(b) Discharge

Figure 4.37: Results from solver

4.5.3 Comparison Excel Sheet and WSC Solver - Precise Modelling

In the appendix, all necessary data to model Example 4 precisely are gathered in TABLES 5.19, 5.20, 5.21, 5.22, 5.23, 5.24 and 5.25. The mean width is about 2.34 [m] and the mean height of the swales is about 0.38 [m], so they are slightly smaller than those assumed in the SPW Technical Guide.
Each element in the system is numbered for clarity in FIGURE 5.43 in the appendix.
Since no explicit information was provided about the connections between elements several general assumptions were made:

- Small swales adjacent to buildings are linked to the linked to the nearest rooftops;
- Small swales feed into larger nearby swales, which in turn connect to the two main swales at the bottom of the site, referred to as the east and west swales. The east swale is linked to the west swale (see FIGURE 4.38);

- Swale 11 (called S11) is considered a secondary main swale due to its great length and its connections with multiple smaller swales;
- The east and west swales are divided into four segments each to better observe the flow evolution within each segment (see Figure 4.38);
- The last swale, S32, is connected to an end reservoir which only serves to monitor potential overflow. Any overflow would indicate that swale dimensions are insufficient and that either the swales must be enlarged or additional storage added.

The connections are complex, and for this reason, these connections are illustrated in flow diagrams in the appendix Figures 5.45, 5.46, 5.47, 5.48, 5.49, 5.50 and Section 5.1.

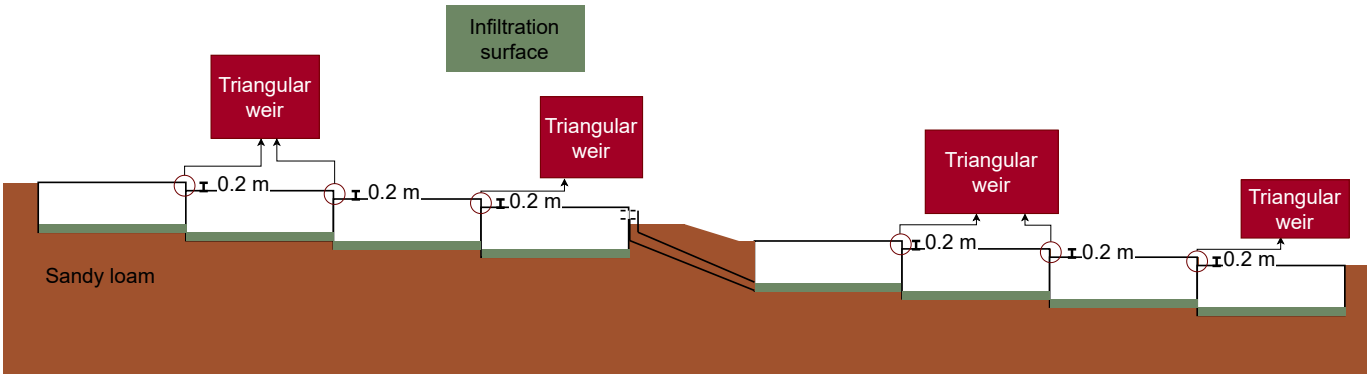

Figure 4.38: Cross section west and east swales

Figure 4.39a shows that S11 is the critical swale in terms of design. It exhibits the highest peak volume and the longest drainage time, as it is connected to 4 other swales, 5 rooftops, 4 impervious zones and 5 pervious zones. However, even in this case, these peak volume and drainage time are significantly lower than those obtained from the basic solver modelling (see Table 4.15) and those obtained from the SPW Technique Guide seen in Table 4.16. The volume peak is reduced by half and the drainage time decreases by almost 20 hours.
This increased spatial precision in the WSC solver greatly improves prediction accuracy and allows for a more optimised swale design. Economically, this can reduce costs by requiring fewer swales or shallower excavations.

Figure 4.39b shows that the outflow between the main swales is close to zero. This indicates that the connections are not utilised between main swales, and the swales are not operating at their full capacity to distribute runoff, reduce peak volumes, and possibly shorten drainage times.

Method	V_{peak} (m^3)	$t_{drainage}$ (s)
Excel sheet (SPW)	28.1	41h38’
WSC solver (S11)	10.2	25h15’

Table 4.16: Results comparison between the SPW Excel sheet and the WSC solver for the initial case

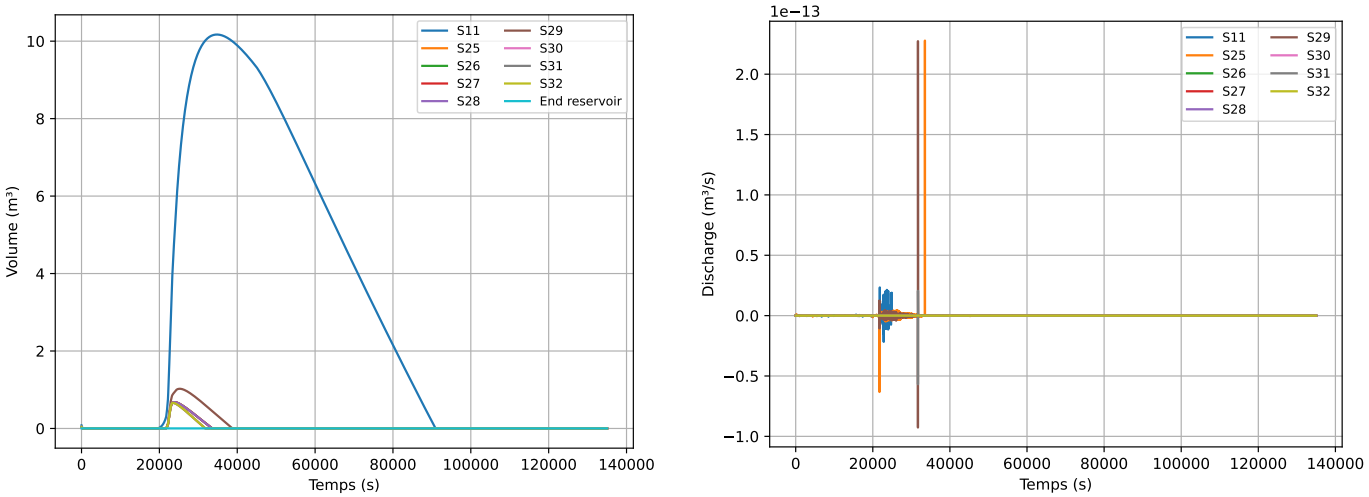

(a) Volume in main swales

(b) Discharge in main swales

Figure 4.39: Results from solver

4.5.4 Re-design with the WSC Solver

The previous results showed that the swales are largely over-dimensioned. A re-design was therefore carried out, reducing most swales' width and height. The new values used in the solver are summarised in Tables 5.26 and 5.27 in the appendix. Swale lengths, the number of swales, and their relative placement remain unchanged, as these are the only parameters that are certain; elevations are also kept unchanged.

Figure 4.40a and Table 4.17 show that the re-design reduces the peak volume compared to the precise modelling. All swales contribute to handling runoff, not just S11. The load is shared between S11 and the east swale, as S11 drains into it, reducing both peak volume and its drainage time. Most swales now have a shorter drainage times compared to S11 in the precise modelling case, except for the end of the east swale (S29), which shows a slightly longer drainage time of about one hour.
The mean swale height is now 1.81 [m] and the mean width is 0.23 [m], representing a reduction from the previous design.

The recommended maximum leakage discharge is the maximum between 0.1 [L/s] and 5 [L/s/ha] as mentioned previously. For a total surface area of 798.96 [m²] = 0.0799 [ha], this gives a maximum discharge of $5 \cdot 0.0799 = 0.3995$ [L/s] = $3.995 \cdot 10^{-4}$ [m³/s] $\approx 4 \cdot 10^{-4}$ [m³/s]. Figure 4.40b shows that S11 and S29 exceed the threshold of $4 \cdot 10^{-4}$ [m³/s].

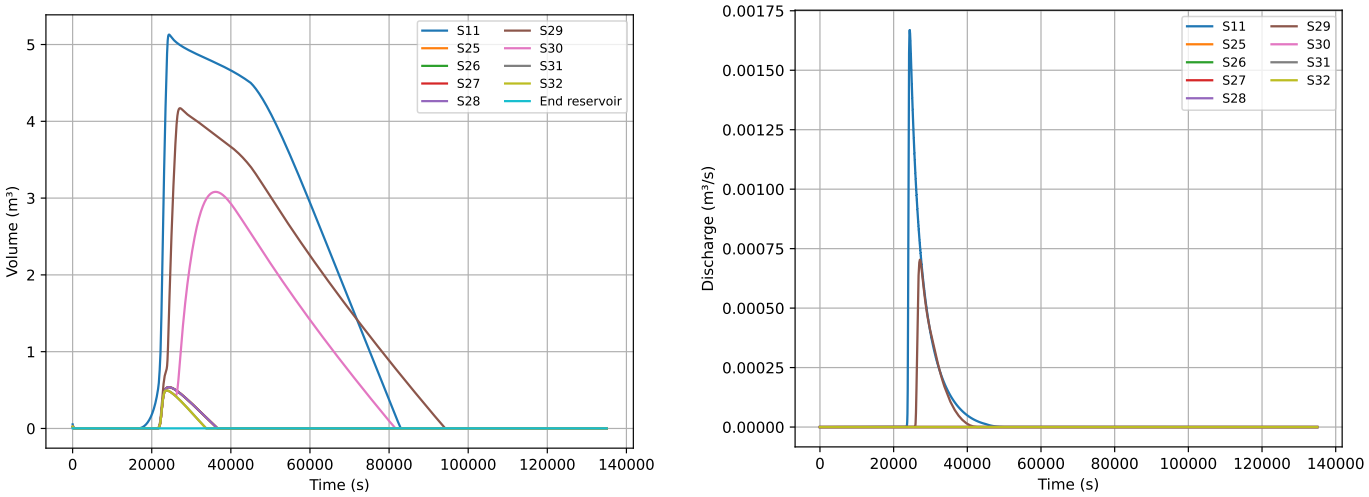

(a) Volume in main swales

(b) Discharge in main swales

Figure 4.40: Results from solver

Method	V_{peak} (m^3)	$t_{drainage}$ (s)
Excel sheet (SPW)	28.1	41h38'
WSC solver	5.1 (S11)	26h10' (S29)

Table 4.17: Results comparison between the SPW Excel sheet and the WSC solver for the redesign WSC modelling

4.5.5 Return Periods of 50-year and 100-year

Since the Excel sheet tends to overestimate, the system designed using it is likely to remain safe for higher return periods. Therefore, the re-design was also tested for 50-year and 100-year events.

Figures 4.41a and 4.42a, along with Table 4.18, show that the re-design is sufficient for both return periods. As expected, peak volumes and drainage times increase with rainfall intensity, but no additional storage is needed, and drainage times remain well below the recommended 48 hours for rainfall durations of 10 hours or more.

Figures 4.41b and 4.42b show that, for these higher return periods, S11, S29, and S30 (with S31 exceeding the threshold only for the 100-year return period) exceed the recommended maximum leakage discharge. This highlights that, despite the re-design, certain swales may still be critical in terms of flow capacity and could require further attention.

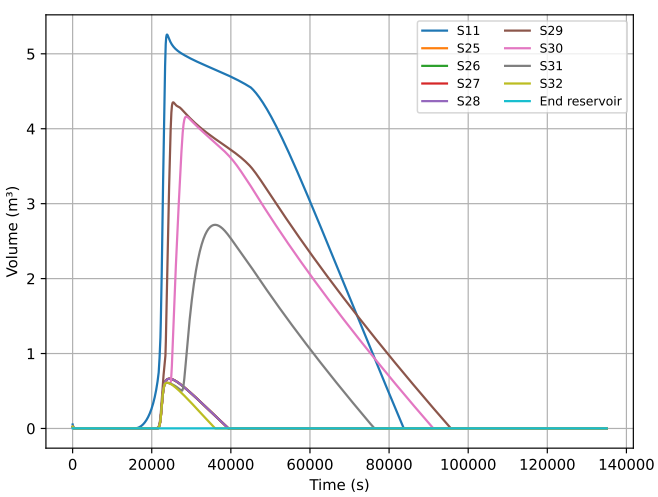

(a) Volume in main swales

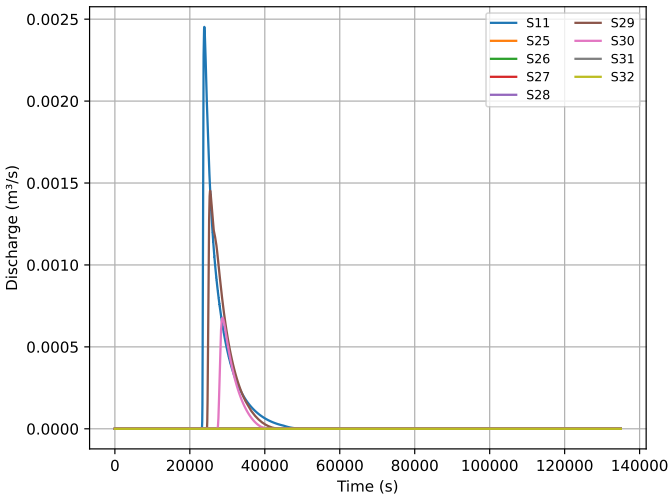

(b) Discharge in main swales

Figure 4.41: Results from solver

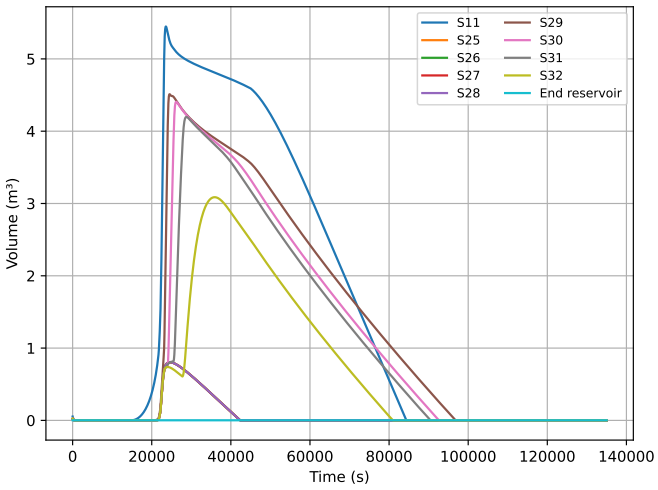

(a) Volume in main swales for 50-year return period

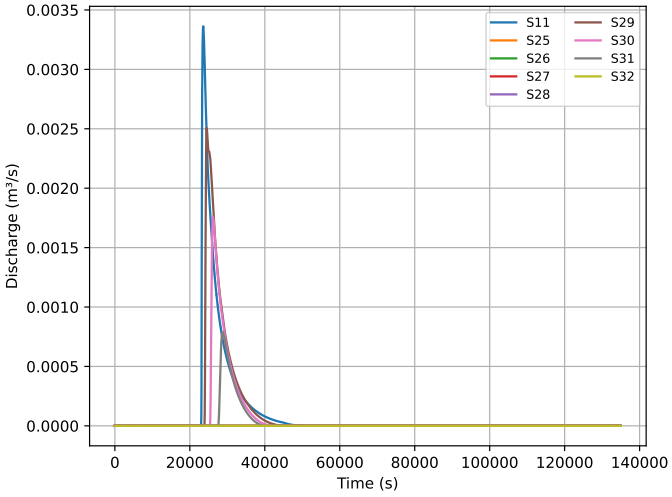

(b) Discharge in main swales for 100-year return period

Figure 4.42: Results from solver

Method	V_{peak} (m^3)	$t_{drainage}$ (s)
WSC solver (50-year)	5.3 (S11)	26h34' (S29)
WSC solver (100-year)	5.4 (S11)	26h54' (S29)

Table 4.18: Results with WSC solver for 50-year and 100-year return period

The solutions presented in this example are strongly dependent on the connections defined between swales and on elevations. It is likely that alternative configurations could further optimise the system. Swale lengths and the total number of swales were not modified, even though adjusting these parameters could potentially improve the design from an economic standpoint. They were kept unchanged because they are the only parameters for which reliable and precise information was provided by the SPW Technique Guide (implicitly). Consequently, the current results should be seen as a feasible solution rather than the unique or necessarily optimal one.

Conclusion and Perspectives

The review of previous work helped to understand how NbS projects operate and the mindset required to model such systems effectively. It also highlighted the extent of existing research, the tools commonly used, and the possible sequences of NbS interventions, providing a solid foundation for the development of the WSC solver modules presented in the report.
Building upon these insights, the main objective was to expand the library of modules to model a variety of real-life NbS examples. Flow control structures (including weirs, orifices, and perforated risers) were implemented to enhance the connections between modules. These modules were first verified against expected results through simple tests to ensure their proper functioning. They were then applied to more concrete examples from the SPW Referential, confirming the capability of the WSC solver to model different configurations. These applications also validated the correct functioning of the swale, reservoir, and pipe modules alongside the flow control structures.

The first applications were quite simple and at a small scale. However, they confirmed the capability of the WSC solver to model different configurations and produce convincing results. Example 4 represented the most complex and largest-scale case studied, corresponding to a neighbourhood-scale project, likely the upper limit of the solver's applicability. This example demonstrated the solver's ability to model complex solutions with multiple connections while requiring only a limited set of input parameters, often publicly available, producing reasonably accurate results.
Unlike simpler tools, the WSC solver requires the user to have a preliminary idea of the project's dimensioning before application. In addition, the solver captures the dynamics of water transfers between modules, enabling more precise dimensioning and avoiding potential oversizing. These observations highlight the practical value of the solver in modelling real-life NbS interventions at the urban scale.
While this study focused on hydraulic aspects, previous research has shown that NbS projects also involve water quality, pollutant removal, and multiple ecosystem services, aspects that the WSC solver already integrates, providing a more comprehensive representation than simpler tools.

At this stage, the `softplus` function was used to overcome continuity issues encountered in some definitions, providing stable convergence. While this solution proved effective, further refinements could be explored to enhance the evolution of the L2 norm of residuals.
Ideally, the WSC solver should be validated against a monitored existing project, allowing direct comparison with real-world data. However, it is expected that results would not perfectly match reality, as the tool is designed to remain relatively simple; for instance, it relies on the Green-Ampt approach for infiltration, which, although more informative than a simple constant infiltration rate, is not the most accurate infiltration model. This approach was chosen so that the user can still obtain the necessary information without being

obliged to perform in-situ measurements. Another way to describe infiltration could be by using the Philip equation. It is a more complex alternative, that requires more detailed information, such as sorptivity, which represents capillary diffusion, and hydraulic conductivity. This model is accurate, but these parameters are more difficult to obtain. However, it assumes a homogeneous soil and one-dimensional vertical infiltration, which may limit its accuracy in heterogeneous or layered soils.
During this research, a major limitation was the order of magnitude of the runoff areas, swale areas, and pipe lengths, which required scaling down Examples 2 and 4. Once these limitations are addressed, these examples should be tested again with their actual values to confirm the solver's functioning and to further study the outcomes. Addressing these aspects will improve the robustness and reliability of the WSC model for practical applications.

In the future, a graphical user interface (GUI) is planned to allow users to directly delimit on a map the NbS structures to be implemented. This will enable them to visualise how their project could take shape. Example 4 could serve as an interesting test case for this GUI, as it involves a high level of spatial diversity. Moreover, it will allow users to represent non-prismatic NbS structures, which is not currently possible in Example 2.
Ongoing monitoring of the rain garden at Gembloux, equipped with hydrological sensors to record water levels and flows during rainfall events, offers a valuable opportunity to validate the WSC solver against real-world measurements. These data will provide insights into the model's accuracy and guide further improvements. Such real-world validation represents a concrete step towards applying the solver reliably in future urban NbS projects.
From working on Example 4, it became clear that, for large-scale projects, it is crucial to break down the system into smaller, manageable blocks. By first modelling each block separately and then progressively integrating them, the overall system can be assembled in a more controlled and optimised manner. This approach not only facilitates debugging and validation but also ensures that complex connections are correctly represented, providing a more reliable and insightful simulation.

Overall, the WSC solver offers a practical, flexible tool to model NbS interventions at the urban scale. It enables the representation of complex connections and system dynamics, requires only a limited set of input parameters, and integrates hydraulic processes alongside water quality, pollutant removal, and ecosystem services. By providing insights not captured by simpler approaches, the solver supports more informed design, dimensioning, and planning of urban NbS projects, highlighting its value for both research and practical applications.

Appendix

5.1 Applications: Example 4

Figure 5.43: Numeration of each elements in Example 4

Figure 5.44: Numeration of each blocks in Example 4

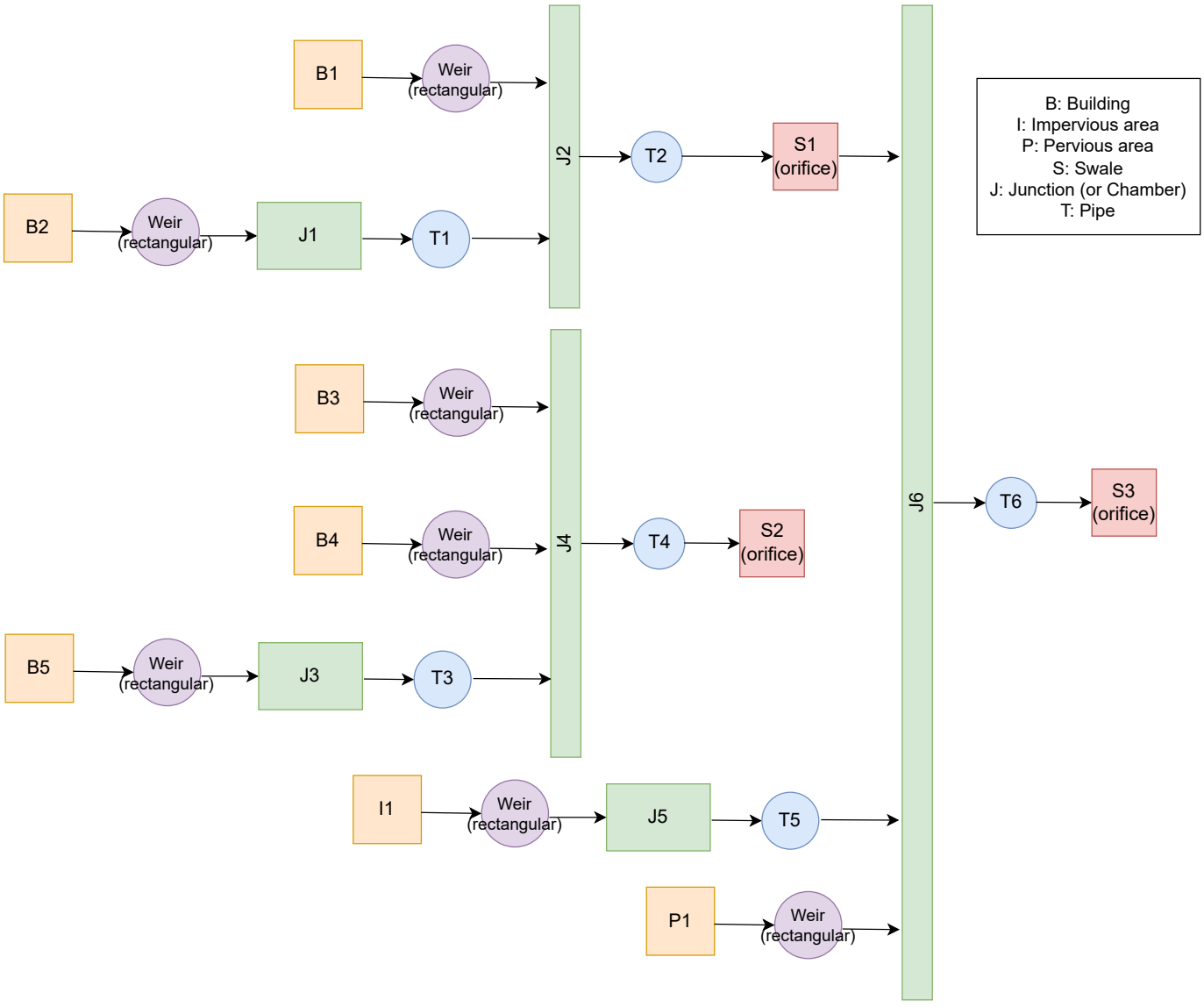

Figure 5.45: Flow diagram block 1

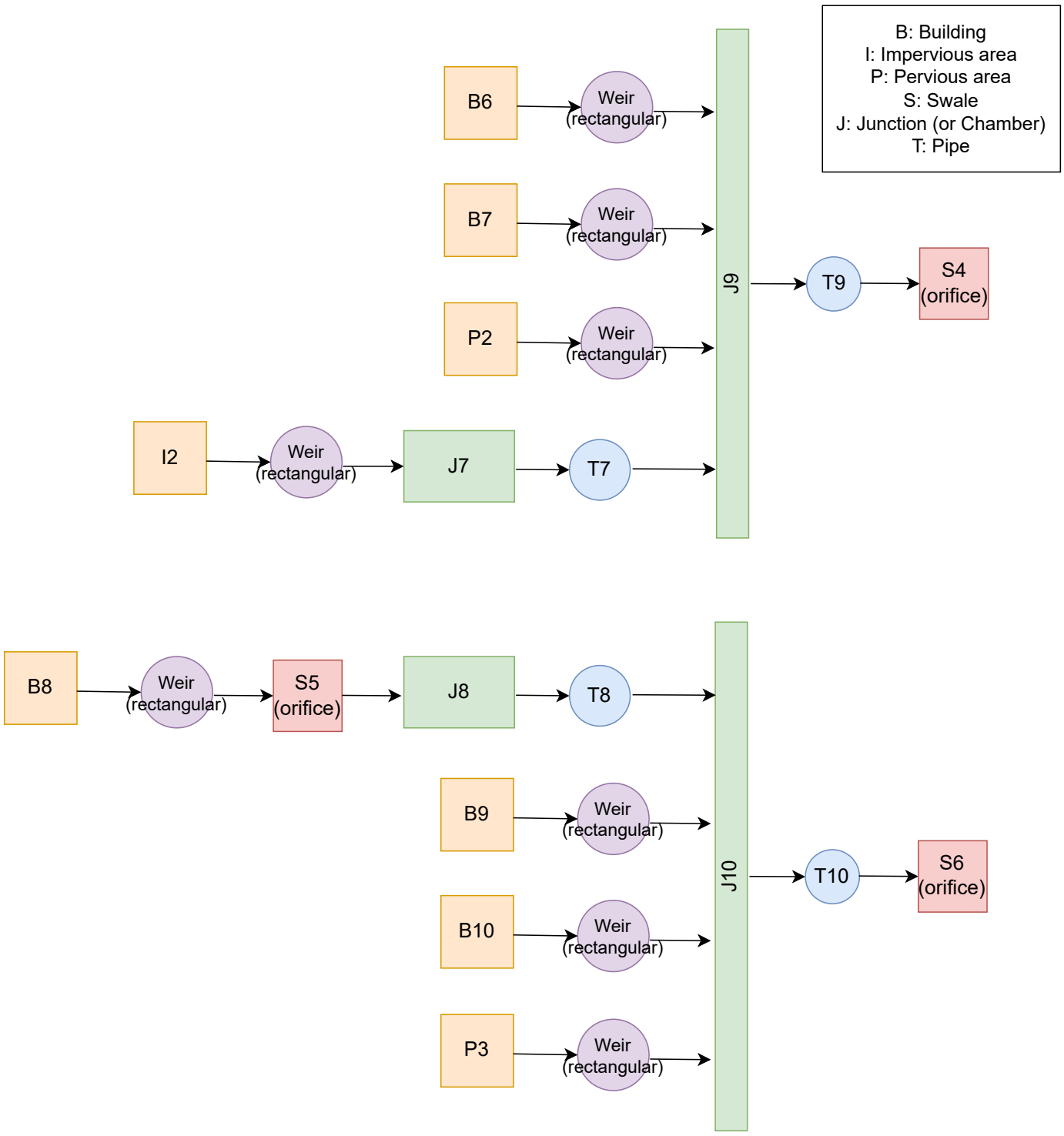

Figure 5.46: Flow diagram block 2

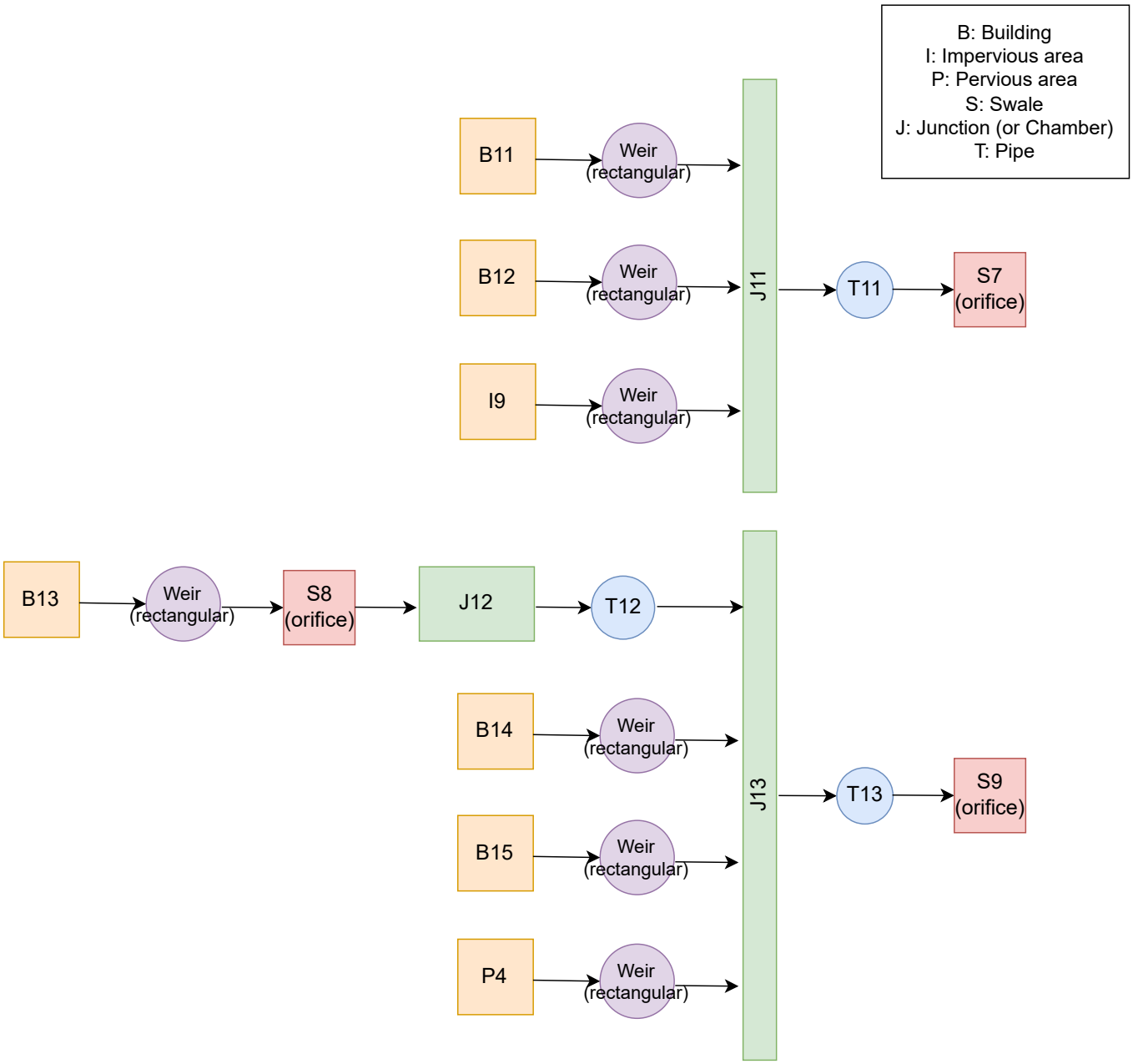

Figure 5.47: Flow diagram block 3

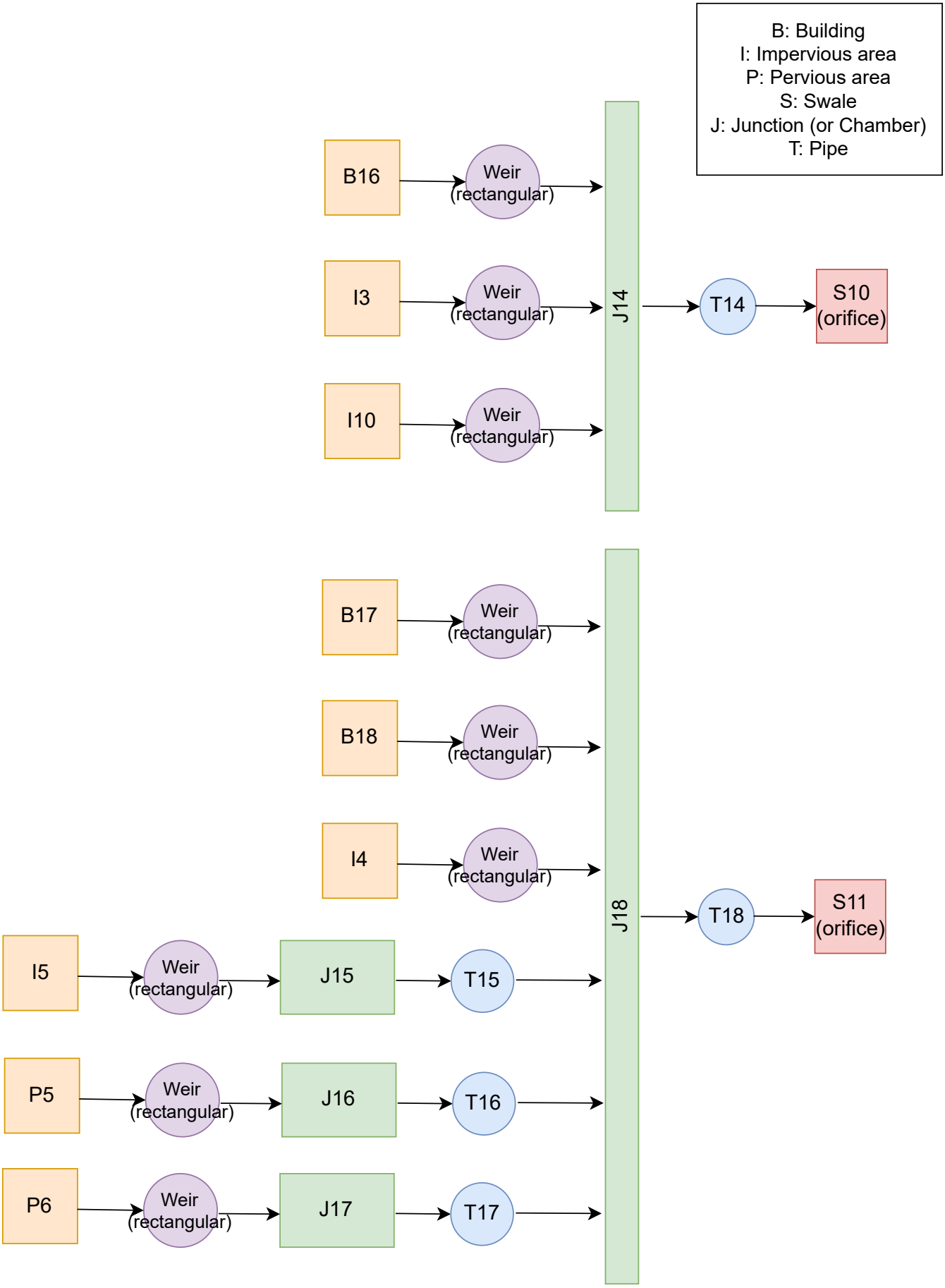

Figure 5.48: Flow diagram block 4

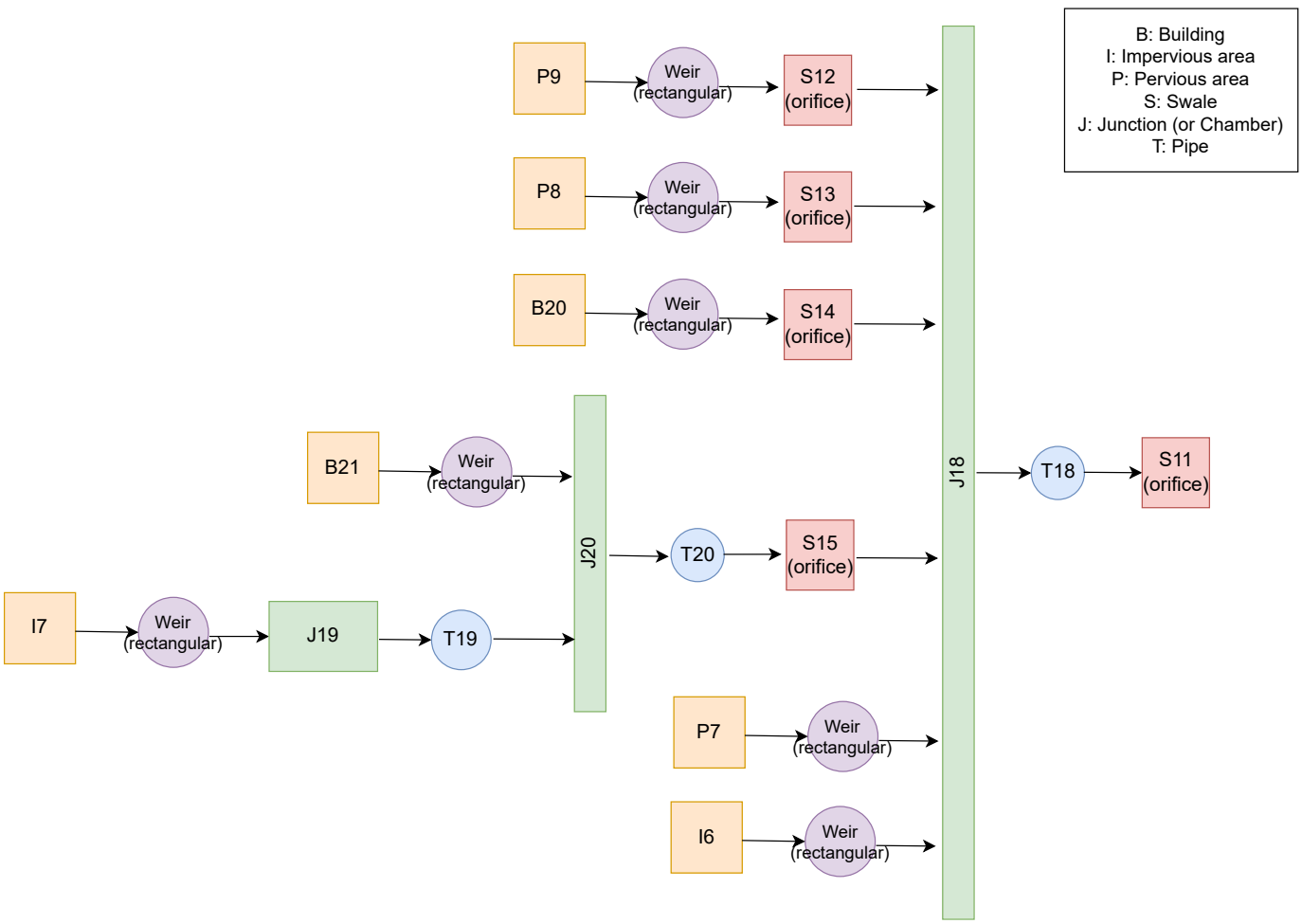

Figure 5.49: Flow diagram block 5

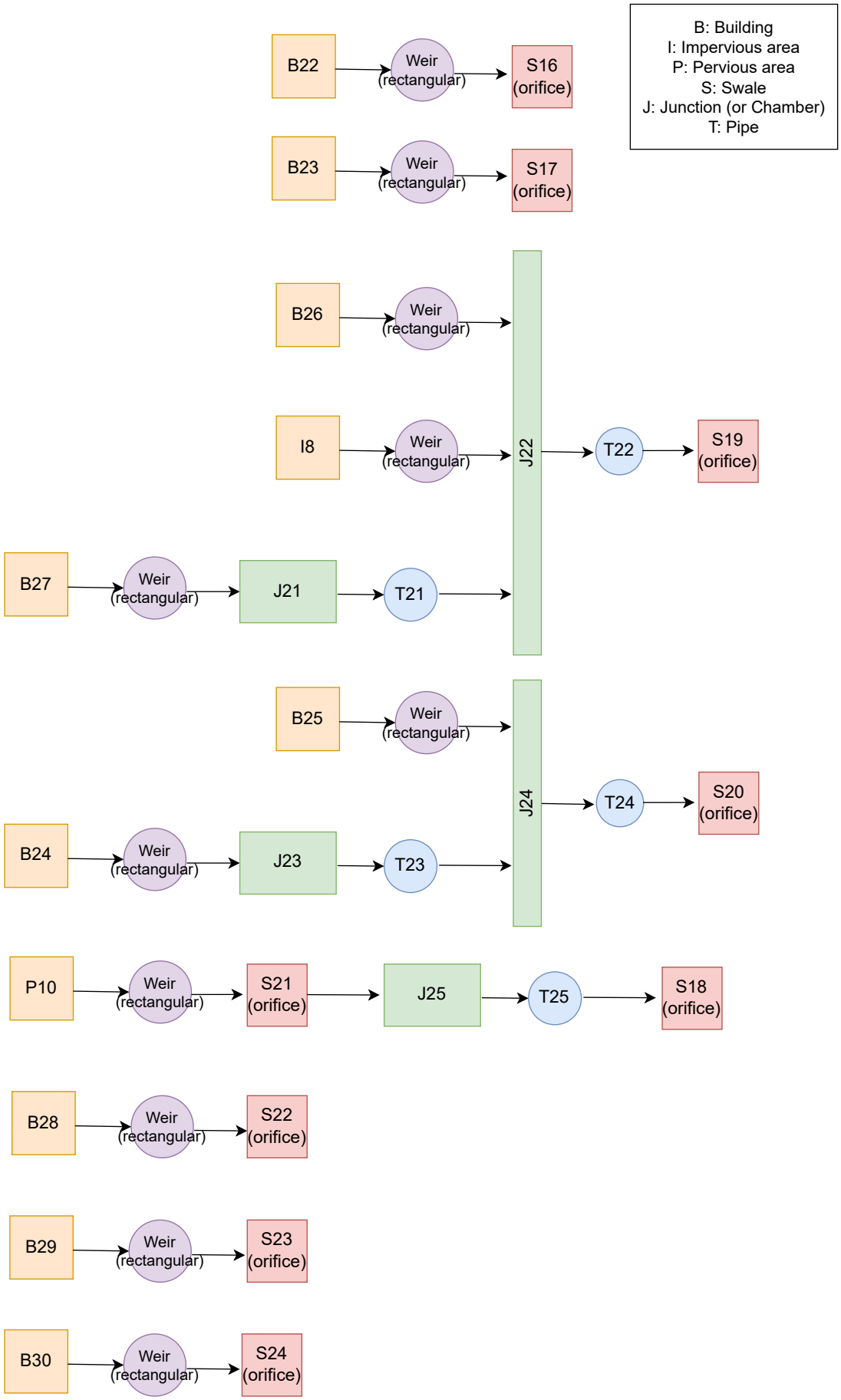

Figure 5.50: Flow diagram block 6

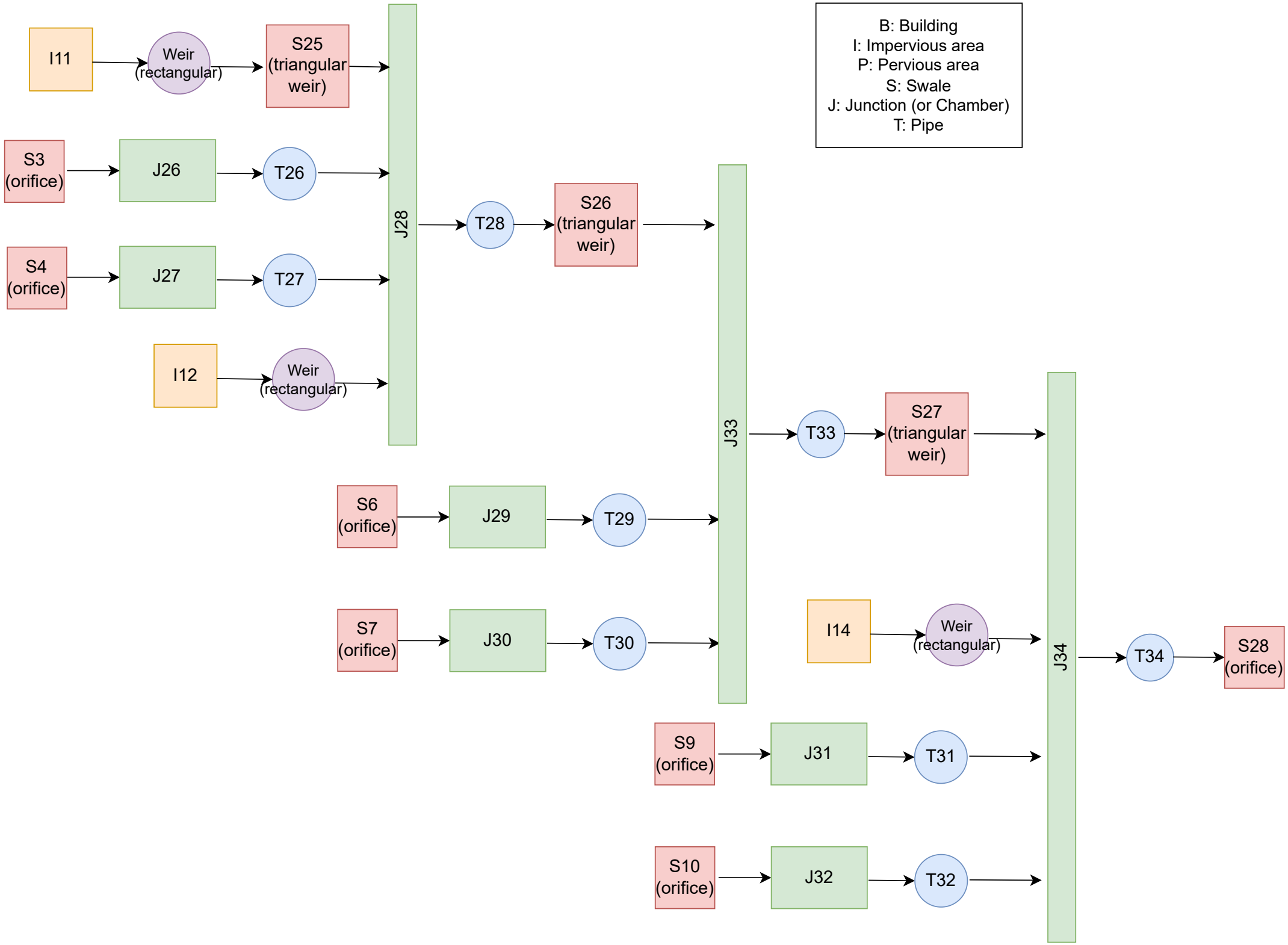

Flow diagram west swale

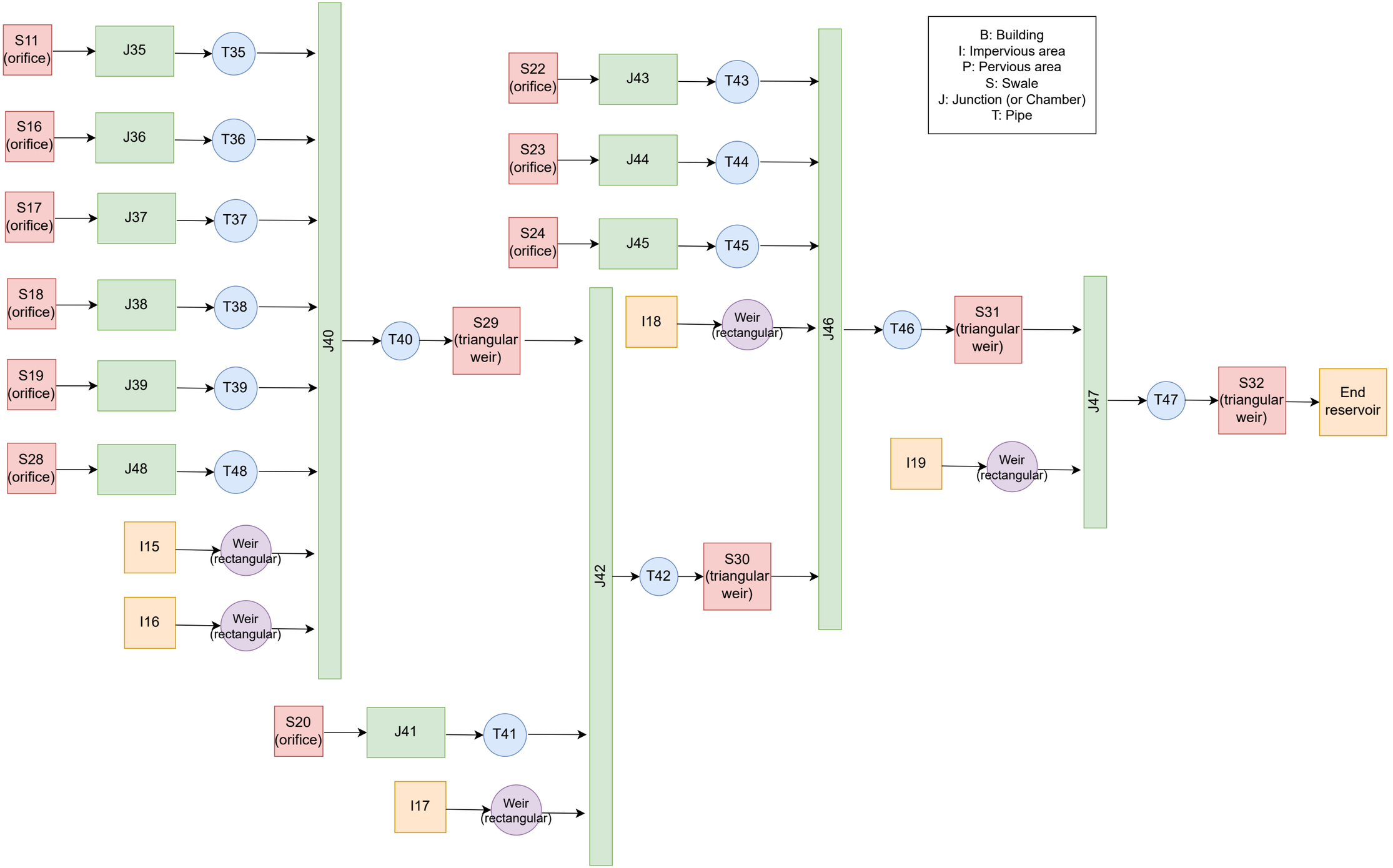

Flow diagram west east

5.1.1 Values for Initial Case

Building	Surface [m^2]	Building	Surface [m^2]	Building	Surface [m^2]	Building	Surface [m^2]
B1	706	B9	575	B17	498	B25	1131
B2	1027	B10	607	B18	2993	B26	7656
B3	459	B11	372	B19	3313	B27	466
B4	348	B12	591	B20	2560	B28	556
B5	244	B13	1086	B21	3954	B29	588
B6	357	B14	325	B22	1102	B30	1245
B7	487	B15	605	B23	771		
B8	1078	B16	1037	B24	349		

Table 5.19: Surfaces of rooftops as measured in the plan location

Impervious	Surface [m^2]	Impervious	Surface [m^2]	Impervious	Surface [m^2]
I1	1423	I8	614	I15	413
I2	1211	I9	1347	I16	413
I3	1756	I10	1491	I17	413
I4	10125	I11	696		
I5	1073	I12	696		
I6	1275	I13	1119		
I7	560	I14	413		

Table 5.20: Surfaces of impervious area as measured in the plan location

Pervious	Surface [m^2]	Pervious	Surface [m^2]
P1	415	P8	540
P2	672	P9	850
P3	758	P10	1988
P4	607		
P5	498		
P6	1064		
P7	5885		

Table 5.21: Surfaces of pervious area as measured in the plan location

Swale	Length [m]	Swale	Length [m]	Swale	Length [m]	Swale	Length [m]
S1	56	S9	133	S17	49	S25	82
S2	39	S10	132	S18	48	S26	82
S3	106	S11	193	S19	119	S27	82
S4	110	S12	64	S20	50	S28	82
S5	25	S13	63	S21	48	S29	90
S6	102	S14	53	S22	34	S30	90
S7	106	S15	42	S23	32	S31	90
S8	23	S16	34	S24	61	S32	90

Table 5.22: Lengths of swales as measured in the plan location

Swale	Width [m]	Elevation [m]	Height [m]	Swale	Width [m]	Elevation [m]	Height [m]
S1	2	63.0	0.3	S14	2	61.4	0.3
S2	1	63.0	0.2	S15	2	61.4	0.2
S3	3	62.8	0.6	S16	1	61.2	0.2
S4	3	62.6	0.6	S17	2	61.2	0.3
S5	1	62.4	0.1	S18	2	61.2	0.3
S6	3	62.2	0.6	S19	3	61.2	0.6
S7	3	62.0	0.6	S20	2	61.2	0.3
S8	1	61.8	0.1	S21	2	61.2	0.2
S9	3	61.6	0.6	S22	1	61.0	0.2
S10	3	61.4	0.6	S23	1	61.0	0.2
S11	3	61.0	0.6	S24	3	60.0	0.4
S12	2	61.2	0.3	S28	3	59.2	0.4
S13	2	61.2	0.3				

Table 5.23: Geometric characteristics of swales with orifice

Swale	Width [m]	Elevation [m]	Height [m]	Swale	Width [m]	Elevation [m]	Height [m]
S25	3	59.8	0.4	S30	3	58.8	0.5
S26	3	59.6	0.4	S31	3	58.6	0.5
S27	3	59.4	0.4	S32	3	58.4	0.5
S29	3	59.0	0.5				

Table 5.24: Geometric characteristics of triangular swales

Pipe	Length [m]	Pipe	Length [m]	Pipe	Length [m]
T1	1.25	T17	6.00	T33	0.01
T2	0.01	T18	0.01	T34	0.01
T3	3.15	T19	3.75	T35	6.00
T4	0.01	T20	0.01	T36	1.25
T5	1.25	T21	1.25	T37	1.25
T6	0.01	T22	0.01	T38	6.875
T7	0.625	T23	1.25	T39	6.00
T8	3.75	T24	0.01	T40	0.01
T9	0.01	T25	1.25	T41	1.25
T10	0.01	T26	1.25	T42	0.01
T11	0.01	T27	1.25	T43	1.875
T12	1.875	T28	0.01	T44	1.875
T13	0.01	T29	1.25	T45	6.25
T14	0.01	T30	1.25	T46	0.01
T15	3.125	T31	1.25	T47	0.01
T16	1.25	T32	1.25	T48	6.00

Table 5.25: Pipe lengths

5.1.2 Reduction of Swale Width and Height (Re-Design)

Swale	Width [m]	Elevation [m]	Height [m]	Swale	Width [m]	Elevation [m]	Height [m]
S1	2	63.0	0.2	S14	2	61.4	0.2
S2	1	63.0	0.2	S15	2	61.4	0.2
S3	2	62.8	0.2	S16	1	61.2	0.2
S4	2	62.6	0.2	S17	2	61.2	0.2
S5	1	62.4	0.2	S18	2	61.2	0.2
S6	2	62.2	0.2	S19	2	61.2	0.2
S7	2	62.0	0.2	S20	2	61.2	0.2
S8	1	61.8	0.2	S21	2	61.2	0.2
S9	2	61.6	0.2	S22	1	61.0	0.2
S10	2	61.4	0.2	S23	1	61.0	0.2
S11	2	61.0	0.2	S24	2	60.0	0.2
S12	2	61.2	0.2	S28	2	59.2	0.3
S13	2	61.2	0.2				

Table 5.26: Geometric characteristics of swales with orifice

Swale	Width [m]	Elevation [m]	Height [m]	Swale	Width [m]	Elevation [m]	Height [m]
S25	2	59.8	0.3	S30	2	58.8	0.3
S26	2	59.6	0.3	S31	2	58.6	0.3
S27	2	59.4	0.3	S32	2	58.4	0.3
S29	2	59.0	0.3				

Table 5.27: Geometric characteristics of triangular swales

Bibliography

[1] Urban Interweaving. Swiss alps green roof. https://urbaninterweaving.wordpress.com/2013/10/18/swiss-alps-green-roof/, October 2013. Accessed: 2025-11-24.

[2] Geosyntec Consultants. Bioretention areas & rain gardens. https://megamanual.geosyntec.com/npsmanual/bioretentionareasandraingardens.aspx, n.d. Accessed: 2025-11-24.

[3] Jared Green. Kongjian yu defends his sponge city campaign. https://dirt.asla.org/2021/08/04/kongjian-yu-defends-his-sponge-city-campaign/, August 2021. Accessed: 2025-11-24.

[4] © Shutterstock / Contributor. Vertical forest, milan - bosco verticale. https://www.shutterstock.com/fr/image-photo/bosco-verticale-vertical-forest-milan-city-1440165473, 2019. Accessed: 2025-11-24; licensed via Shutterstock.

[5] Zhonghao Zhang and Caterina Valeo. Low impact development technologies for mitigating climate change: Summary and prospects. *National Science Open*, 3(1), 2024. All Open Access, Gold Open Access.

[6] H.S. Hasibuan, B.N. Elizandri, F.W. Asrofani, and G.A.Y. Putra. Potential application of rain water harvesting technology as an alternative clean water source to mitigate land subsidence. *Global Journal of Environmental Science and Management*, 11(1):277 – 294, 2025.

[7] Xuan Wu and Patrick Willems. Assessing blue-green infrastructures for urban flood and drought mitigation under changing climate scenarios. *Journal of Hydrology: Regional Studies*, 62, 2025. All Open Access, Gold Open Access.

[8] Endah Lestari, Wati A. Pranoto, and Chaidir A. Makarim. Utilization of rainwater harvesting installation to fulfil water needs in educational buildings. volume 852, 2020. All Open Access, Gold Open Access.

[9] S. Sirait, H. Suhardiyanto, S.K. Saptomo, and Liyantono. Enhancing water sustainability in greenhouses: A study on rainwater harvesting potential for crop water supply. volume 1386, 2024. All Open Access, Gold Open Access.

[10] Afiya Narzis and Jessica Eisma. Developing green stormwater infrastructure strategies to reduce flood runoff and improve water quality for the vulnerable coastal communities of houston. page 675 – 687, 2023.

[11] Sarah E. Waickowski, Rebecca A. Purvis, Carmen C. Tormey, Ryan M. Mullins, Brian Jacobson, Andrew H. McDaniel, and William F. Hunt. Quantifying the water quality and hydrologic benefits of two bioswales receiving highway runoff in north carolina. *Journal of Sustainable Water in the Built Environment*, 11(3), 2025.

[12] Lea Rosenberger, Jorge Leandro, and Brigitte Helmreich. Enhancing swmm-urbaneva for continuous long-term water balance analysis of green infrastructure. *Sustainable Cities and Society*, 128, 2025. All Open Access, Hybrid Gold Open Access.

[13] Camillo Bosco, Elhadi Mohsen Hassan Abdalla, Tone Merete Muthanna, Knut Alfredsen, Britt Rasten, Heidi Kjennbakken, and Edvard Sivertsen. Evaluating the stormwater management model for hydrological simulation of infiltration swales in cold climates. *Blue-Green Systems*, 5(2):306 – 320, 2023. All Open Access, Gold Open Access.

[14] K. Bagheri and H. Davani. An integrated framework for stormwater management and life cycle assessment of rainwater harvesting: A comparative study of two underserved communities. *Science of the Total Environment*, 956, 2024.

[15] Rocco Pace, Theodore A. Endreny, Marco Ciolfi, Marcel Gangwisch, Somidh Saha, Nadine K. Ruehr, and Rüdiger Grote. Mitigation potential of urban greening during heatwaves and stormwater events: a modeling study for karlsruhe, germany. *Scientific Reports*, 15(1), 2025. All Open Access, Gold Open Access, Green Open Access.

[16] Valentina Cerda, Osheen, and Jorge Gironás. Evaluating the long-term performance and economic benefits of suds using continuous simulation. *Water Resources Management*, 39(11):5391 – 5413, 2025.

[17] Mayra Rodriguez, Guangtao Fu, David Butler, Zhiguo Yuan, and Lauren Cook. The effect of green infrastructure on resilience performance in combined sewer systems under climate change. *Journal of Environmental Management*, 353, 2024. All Open Access, Hybrid Gold Open Access.

[18] Joanna Boguniewicz-Zabłocka and Ewelina Łukasiewicz. Blue–green infrastructure effectiveness for urban stormwater management: A multi-scale residential case study. *Land*, 14(7), 2025.

[19] Wenhui Wu, Behzad Jamali, Lucy Marshall, Ana Deletic, and Kefeng Zhang. A water sensitive urban design (wsud) planning framework for catchment-scale urban pluvial flood mitigation targets. *Water Research*, 285, 2025. All Open Access, Hybrid Gold Open Access.

[20] Carlotta Quagliolo, Peter Roebeling, Alessandro Pezzoli, Fábio André Matos, Max López-Maciel, and Elena Comino. Valuing the contribution of green roofs to pluvial flood risk mitigation: A cost-benefit analysis. *Cities*, 168, 2026. All Open Access, Hybrid Gold Open Access.

[21] Lea Rosenberger, Jorge Leandro, Stephan Pauleit, and Sabrina Erlwein. Sustainable stormwater management under the impact of climate change and urban densification. *Journal of Hydrology*, 596, 2021.

[22] Stefano Cascone and Serena Vitaliano. Innovative green roof technologies in mediterranean climate: Implications for sustainable design of the built environment. *Building and Environment*, 273, 2025. All Open Access, Hybrid Gold Open Access.

[23] Nayeon Kwak, Virginia Smith, and Kelly D. Good. Assessing the influence of green stormwater infrastructure implemented for combined sewer overflow control on urban streamflows. *Journal of Hydrology*, 640, 2024. All Open Access, Hybrid Gold Open Access.

[24] M.W. McGauley, G. Zaremba, and B.M. Wadzuk. A complete water balance of a constructed stormwater wetland. *Water Resources Research*, 61(7), 2025. All Open Access, Gold Open Access.

[25] Jun Zhai, Jing Ren, Miao Xi, Xiaonan Tang, and Yixin Zhang. Multiscale watershed landscape infrastructure: Integrated system design for sponge city development. *Urban Forestry and Urban Greening*, 60, 2021.

[26] Rajati Dahal and Suresh Sharma. Green infrastructure for storm water management with stakeholder participation in the town of willoughby-chagrin river huc 12 watershed. *Urban Water Journal*, 2025.

[27] Villanova University. Constructed stormwater wetland (csw). `https://www1.villanova.edu/university/engineering/faculty-research/Resilient-Water-Systems/Constructed-Stormwater-Wetland.html`, 2025. Consulted on: 2026-01-04.

[28] Mariana Marchioni, Franco Raimondi, Gianfranco Becciu, and Claudia Dresti. Nature-based solutions for watershed management: An investigation on water-related ecosystem services delivery at multiple spatial scales. *Ecosystem Services*, 73, 2025.

[29] Line Johanne Barkved and NbS Guide. Rain garden in bjørstjerne gate in drammen (photo). `https://nbsguide.org/Urban/Rain-gardens-and-swales`, 2025. Photo by Line Barkved (NIVA). Consulted on: 2026-01-04.

[30] Comune di Milano. La vasca di laminazione delle piene del seveso. `https://www.comune.milano.it/aree-tematiche/ambiente/acqua/vasca-contenimento-seveso`, 2025. Consulted on: 2026-01-04.

[31] Mojtaba Moravej, Cassady Swinbourne, Rebecca Hall, and Steven Kenway. Vertical green systems (vgss) and on-site storage for stormwater management. *Water Research*, 281, 2025. All Open Access, Hybrid Gold Open Access.

[32] North Carolina Department of Transportation. Evaluating the hydrologic and water quality benefits associated with retrofitting vegetated swales with check dams. Technical Report NCDOT 2014-17-1, North Carolina Department of Transportation, Research and Development Unit, 2016. Final Report.

[33] Boris Van Zanten, Gonzalo Gutierrez Goizueta, Luke Mckinnon Brander, Borja Gonzalez Reguero, Robert Griffin, Kavita Kapur Macleod, Alida Ivana Alves Beloqui, Amelia Midgley, Luis Diego Herrera Garcia, and Brenden Jongman. Assessing the benefits and costs of nature-based solutions for climate resilience: A guideline for project developers. Technical report, The World Bank and Global Facility for Disaster Reduction and Recovery, Washington, DC, 2023. Guideline for assessing NBS costs and benefits.

[34] WASABI – Gembloux Agro-Bio Tech, Université de Liège. Jardin de pluie – rain garden in gembloux. `https://www.wasabi.uliege.be/cms/c_9088497/fr/wasabi-jardin-de-pluie`, 2025. Accessed: 2025-01-06.

[35] City of Melbourne. Swales. `https://www.melbourne.vic.gov.au/swales`, n.d. Accessed: 2025-11-24.

[36] CIRIA. *The SuDS Manual*. CIRIA, London, UK, 1 edition, 2015. Report C753.

[37] Bosiger. Rivière serrière. https://commons.wikimedia.org/wiki/File:Rivi%C3%A8re_serri%C3%A8re.jpg, 2009. Photograph, Wikimedia Commons. Licensed under CC BY-SA 3.0.

[38] Federal Highway Administration. Hydraulic design of highway culverts. https://www.fhwa.dot.gov/engineering/hydraulics/pubs/hif24006.pdf, 2006. Accessed: 2025-10-16.

[39] C.D. Smith. Hydraulic structures, 1995.

[40] Ministère du Développement durable, de l'Environnement, de la Faune et des Parcs and Ministère des Affaires municipales, des Régions et de l'Occupation du territoire. *Guide de gestion des eaux pluviales: stratégies d'aménagement, principes de conception et pratiques de gestion optimales pour les réseaux de drainage en milieu urbain.* Gouvernement du Québec, 2025. Consulté le 4 janvier 2026.

[41] jaxoplanet Documentation. A brief introduction to jax. https://jax.exoplanet.codes/en/latest/tutorials/introduction-to-jax/, 2025. Accessed: 2025-10-16.

[42] Référentiel : Gestion durable des eaux pluviales. Référentiel technique, Service public de Wallonie (SPW), Wallonie, Belgique, jun 2023.

[43] IPEX Inc. Caractéristiques hydrauliques du pvc / the hydraulics of pvc pipe. PDF document, August 2022. Bulletin d'information technique.

[44] U.S. Army Corps of Engineers, Hydrologic Engineering Center. Green-ampt. https://www.hec.usace.army.mil/confluence/rasdocs/ras1dtechref/6.5/overview-of-optional-capabilities/modeling-precipitation-and-infiltration/green-ampt, 2025. Accessed: 2025-12-25.

[45] Guide technique pour le dimensionnement des ouvrages de rétention. Technical guide, Public Service of Wallonia (SPW), Permanent Centre for Territorial Programming (CPDT), Wallonia, Belgium, apr 2017.

[46] H. W. Vogel and R. E. Brown. Laboratory studies of v-notch weirs. url = https://pubs.usgs.gov/wsp/1617b/report.pdf, 1966.